

IceHEP

High Energy Physics at the South Pole

Luis Anchordoqui¹ and Francis Halzen²

¹ *Department of Physics, Northeastern University,
Boston, MA 02115, USA*

²*Department of Physics, University of Wisconsin,
Madison, WI 53706, USA*

(Dated: October 2005)

Abstract

With the solar and SN87 neutrino observations as proofs of concepts, the kilometer-scale neutrino experiment IceCube will scrutinize its data for new particle physics. In this paper we review the prospects for the realization of such a program. We begin with a short overview of the detector response and discuss the reach of “beam” luminosity. After that we discuss the potential of IceCube to probe deviations of neutrino-nucleon cross sections from the Standard Model predictions at center-of-mass energies well beyond those accessible in man-made accelerators. Then we review the prospects for extremely long-baseline analyses and discuss the sensitivity to measure tiny deviations of the flavor mixing angle, expected to be induced by quantum gravity effects. Finally we discuss the potential to uncover annihilation of dark matter particles gravitationally trapped at the center of the Sun, as well as processes occurring in the early Universe at energies close to the Grand Unification scale.

Contents

I. Introduction	3
II. Overall Detector Performance	5
A. Muon Tracks	6
B. Electromagnetic Showers	9
C. Shower-Track Combo	10
III. Luminosity	11
A. Atmospheric Neutrinos	11
B. Extraterrestrial Neutrinos	13
C. Directional Signals	16
IV. Neutrino Interactions beyond the Weak Scale	19
V. Flavor Metamorphosis	25
A. Neutrino Oscillations	25
B. Quantum Decoherence	31
VI. Dark Matter	39
VII. Topological Defects and Superheavy Relics	45
VIII. Outlook	50
Acknowledgments	50
References	51

I. INTRODUCTION

Conventional astronomy spans 60 octaves in photon frequency, from 10^4 cm radio-waves to 10^{-14} cm γ -rays of GeV energy. This is an amazing expansion of the power of our eyes which scan the sky over less than a single octave just above 10^{-5} cm wavelength. In recent years, detection and data handling techniques of particle physics have been reborn in instrumentation to probe the Universe at new wavelengths, smaller than 10^{-14} cm. In addition to the traditional photon signals, neutrinos and very high-energy protons (that are only weakly deflected by the magnetic field of our galaxy) have become astronomical messengers from the Universe. As exemplified time and again, the development of novel ways of looking into the cosmos invariably results in the discovery of unanticipated phenomena. For particle physicists, the sexiest astrophysical problem is undoubtedly how Nature manages to impart an energy of more than one Joule to a single elementary particle.

Although cosmic rays were discovered almost a century ago, we do not know how and where they are accelerated. This may be the oldest mystery in astronomy and solving it is challenging as can be seen by the following argument. It is reasonable to assume that, in order to accelerate a proton to energy E in a magnetic field B , the size R of the accelerator must encompass the gyro radius of the particle: $R > R_{\text{gyro}} = E/B$, i.e. the accelerating magnetic field must contain the particle's orbit. By dimensional analysis, this condition yields a maximum energy $E = \Gamma B R$. The Γ -factor has been included to allow for the possibility that we may not be at rest in the frame of the cosmic accelerator, resulting in the observation of boosted particle energies. Opportunity for particle acceleration to the highest energies is limited to dense regions where exceptional gravitational forces create relativistic particle flows. All speculations involve collapsed objects and we can therefore replace R by the Schwarzschild radius $R \sim GM/c^2$ to obtain $E < \Gamma B M$.

Cosmic accelerators are also cosmic beam dumps producing secondary photons and neutrino beams. Particles accelerated near black holes pass through intense radiation fields or dense clouds of gas leading to production of secondary photons and neutrinos that accompany the primary cosmic ray beam. The target material, whether a gas or photons, is likely to be sufficiently tenuous so that the primary beam and the photon beam are only partially attenuated.

At this point a reality check is in order. Such a dimensional analysis applies to the Fermilab accelerator: 10 kilogauss fields over several kilometers (covered with a repetition rate of 10^5 revolutions per second) yield 1 TeV. The argument holds because, with optimized design and perfect alignment of magnets, the accelerator reaches efficiencies matching the dimensional limit. It is highly questionable that nature can achieve this feat. Theorists can imagine acceleration in shocks with an efficiency of perhaps 1 – 10%.

Given the microgauss magnetic field of our galaxy, no structures are large or massive enough to reach the energies of the highest energy cosmic rays. Dimensional analysis therefore limits their sources to extragalactic objects. A common speculation is that they may be relatively nearby active galactic nuclei powered by a billion solar mass black holes. With kilo-Gauss fields we reach 10^{11} GeV. The jets (blazars) emitted by the central black hole could reach similar energies in accelerating sub-structures boosted in our direction by a Γ -factor of 10, possible higher. The neutron star or black hole remnant of a collapsing supermassive star could support magnetic fields of 10^{12} G, possible larger. Shocks emanating from the collapse black hole could be the origin of gamma ray bursts and, possibly, the source of the highest energy cosmic rays.

The astrophysics problem is so daunting that many believe that cosmic rays are not the beam of cosmic accelerators but the decay products of remnants from the early Universe, for instance topological defects associated with phase transitions (near 10^{16} GeV) in Grand Unified Theories (GUT's). A topological defect will suffer a chain decay into GUT particles X that subsequently decay to familiar weak bosons, leptons, quarks- or gluon-jets. Cosmic rays are the fragmentation products of these jets.

All in all, where the highest energy cosmic rays are concerned, both the accelerator mechanism and the particle physics are enigmatic. There is a realistic hope that the oldest problem in astronomy will be resolved soon by ambitious experimentation. One such experiment is the IceCube neutrino telescope, which is required to be sensitive to the best estimates of potential cosmic ray neutrino fluxes. Though this telescope is primarily motivated by these astronomical goals, it has also appeared in the U.S. Roadmap to Particle Physics, and as we will argue in this review, deservedly so.

As the lightest of fermions and the most weakly interacting of particles, neutrinos occupy a fragile corner of the Standard Model and one can realistically hope that they will reveal the first and most dramatic signatures of new physics. IceCube's opportunities for particle physics are only limited by imagination; they include

- The search for theories where particle interactions, including gravity, unify at the TeV scale. Neutrinos with energies approaching this scale will interact gravitationally with large cross sections, similar to those of quarks and leptons, and this increase should yield dramatic signatures in a neutrino telescope including, possibly, the production of black holes.
- The search for deviations from the neutrino's established oscillatory behavior that result from non-standard interactions, for instance neutrino decay or quantum decoherence.
- The search for a breakdown of the equivalence principle as a result of non-universal interactions with the gravitational field of neutrinos with different flavors. Similarly, the search for breakdown of Lorentz invariance resulting from different limiting velocities of neutrinos of different flavors.
- The search for neutrinos from the annihilation of dark matter particles gravitationally trapped at the center of the Sun.
- The search from particle emission from cosmic strings or other topological defects and heavy cosmological remnants created in the early Universe.
- The search for magnetic monopoles.

Alternatively, it is possible that we may be guessing the future while holding too small deck of cards and IceCube will open a new world that we did not anticipate.

The case for doing particle physics with cosmic neutrinos is compelling, the challenge has been to deliver the technology to build the instrumentation for a neutrino detector with the largest possible effective telescope area to overcome the small neutrino cross section with matter, and the best possible angular and energy resolution to address the wide diversity of possible signals. We discuss this next.

II. OVERALL DETECTOR PERFORMANCE

In deep ice neutrinos are detected by observation of the Čerenkov light emitted by charged particles produced in charged current (CC) and neutral current (NC) interactions. To a first approximation, a neutrino (of energy E_ν) incident on a side of area L^2 will be detected provided it interacts within the lattice of photomultiplier tubes (PMT's) constituting the sensitive volume $\sim L^3$ of the detector. That probability is

$$P(E_\nu) = 1 - \exp[-L/l_\nu(E_\nu)] \simeq L/l_\nu(E_\nu), \quad (1)$$

where $l_\nu(E_\nu) = [\rho_{\text{ice}} N_A \sigma_{\nu N}(E_\nu)]^{-1}$ is the mean free path. Here $\rho_{\text{ice}} = 0.9 \text{ g cm}^{-3}$ is the density of the ice, $N_A = 6.022 \times 10^{23}$ is Avogadro's number and $\sigma_{\nu N}(E_\nu)$ is the neutrino nucleon cross section. A neutrino flux dF/dE_ν (neutrinos per GeV per cm^2 per s) crossing a detector with energy threshold E_ν^{th} and cross sectional area A ($\simeq L^2$) facing the incident beam will produce

$$\mathcal{N} = T \int_{E_\nu^{\text{th}}} A(E_\nu) P(E_\nu) \frac{dF}{dE_\nu} dE_\nu \quad (2)$$

events after a time T . In practice, the "effective" detector area A is not strictly equal to the geometric cross section of the instrumented volume facing the incoming neutrino because even neutrinos interacting outside the instrumented volume, may produce a sufficient amount of light inside the detector to be detected. Therefore, A is determined as a function of the incident neutrino direction by simulation of the full detector, including the trigger. To be realistic such a simulation must account for all of the detector properties that we discuss next.

The Antarctic Muon And Neutrino Detector Array (AMANDA) [1] is located below the surface of the Antarctic ice sheet at the geographic South pole. During 1993 and 1994, in an exploratory phase project, the four-string AMANDA-A array was deployed and instrumented with 80 PMT's spaced at 10 m intervals from 810 to 1000 m. A deeper array of 10 strings, referred to as AMANDA-B10, was deployed during the austral summers between 1995 and 1997, to depths between 1500 and 2000 m. The instrument volume of AMANDA-B10 forms a cylinder with diameter 120 m, overlooked by 302 PMT's. During December 1997 and January 2000, the detector was expanded by adding nine strings of PMT's. The composite array of 19 strings and 677 PMT's forms the AMANDA-II array.

Overall, AMANDA represents a proof of concept for the kilometer-scale neutrino observatory, IceCube [2], now under construction. IceCube will consist of 80 kilometer-length strings, each instrumented with 60 10-inch photomultipliers spaced by 17 m. The deepest module is 2.4 km below the surface. The strings are arranged at the apexes of equilateral triangles 125 m on a side. The instrumented (not effective!) detector volume is a cubic kilometer. A surface air shower detector, IceTop, consisting of 160 Auger-style [3] Čerenkov detectors deployed over 1 km^2 above IceCube, augments the deep-ice component by providing a tool for calibration, background rejection and air-shower physics. The expected energy resolution is ± 0.1 on a \log_{10} scale. Construction of the detector started in the Austral summer of 2004/2005 and will continue for 6 years, possibly less. At the time of writing, data collection by the first string has begun.

The event signatures are grouped as tracks, showers, or a combination of the two. Tracks include muons resulting from both cosmic ray showers and from CC interaction of muon neutrinos. Tracks can also be produced by τ leptons arising in ultra-high energy ν_τ CC

interactions. Showers are generated by neutrino collisions (ν_e or low energy ν_τ CC interactions, and all NC interactions) inside or near the detector, and by muon bremsstrahlung radiation near the detector.

A. Muon Tracks

In a CC event a ν_μ produces a muon traveling in nearly the same direction as the neutrino. Secondary muons range out over kilometers at $E_\mu \sim 10^3$ GeV, to tens of kilometers at $E_\mu \sim 10^9$ GeV, generating showers along their track by bremsstrahlung, pair production and photonuclear interactions. All of these are sources of blue Čerenkov light. As the energy of the muon degrades along its track, the energy of the secondary showers diminishes and the distance from the track over which the associated Čerenkov light can trigger a PMT becomes smaller. The geometry of the lightpool surrounding the muon track over which single photo-electron are produced is therefore a kilometer-long cone with gradually decreasing radius. The orientation of the Čerenkov cone reveals the neutrino direction, with an angular resolution $\approx 0.7^\circ$ [2]. Muons created by cosmic ray interactions in the atmosphere constitute the main background. Full event reconstruction, with quality cuts applied for the rejection of cosmic ray muon background, is referred to as “level 2” [2]. Down-going atmospheric neutrinos at level 2 are highly suppressed because low energy muons need to be rejected with energy cuts.

High energy muons lose energy catastrophically according to

$$\frac{dE_\mu}{dl} = -\alpha - \beta_\mu E_\mu, \quad (3)$$

where $\alpha = 2.0 \times 10^{-6}$ TeV cm² g⁻¹ (characterizes the ionization process) and $\beta_\mu = 4.2 \times 10^{-6}$ cm² g⁻¹ (takes into account bremsstrahlung, e^+e^- pair production and nuclear interactions) [4]. The distance a muon travels before its energy drops below some energy threshold E_μ^{th} , called the muon range, is then given by

$$l_\mu^{\text{min}} = \frac{1}{\beta_\mu} \ln \left[\frac{\alpha + \beta_\mu E_\mu}{\alpha + \beta_\mu E_\mu^{\text{th}}} \right]. \quad (4)$$

In the first kilometer a high energy muon typically loses energy in a couple of showers of one tenth its energy. So the initial size of the cone is the radius of a shower with 10% of the muon energy, e.g. 130 m for a 100 TeV muon. Near the end of its range the muon becomes minimum ionizing emitting light that creates single photoelectron signals at a distance of just over 10 m from the track. For 0.3 photoelectrons, the standard PMT threshold setting, this distance reaches 45 m.

The expected ν_μ event rate at IceCube can be estimated through semi-analytical calculations [5],

$$\begin{aligned} \mathcal{N}_{\nu_\mu} = & T \int_{-1}^1 d\cos\theta \int_{l_\mu^{\text{min}}}^{\infty} dl_\mu \int_{m_\mu}^{\infty} dE_\mu^{\text{fin}} \int_{E_\mu^{\text{fin}}}^{\infty} dE_\mu^0 \int_{E_\mu^0}^{\infty} dE_\nu \\ & \frac{dF^{\nu_\mu}}{dE_\nu d\cos\theta}(E_\nu, \cos\theta) \frac{d\sigma_{\text{CC}}}{dE_\mu^0}(E_\nu, E_\mu^0) n_T F(E_\mu^0, E_\mu^{\text{fin}}, l_\mu) A_{\text{eff}}^0, \end{aligned} \quad (5)$$

where $dF^{\nu_\mu}/dE_\nu d\cos\theta$ is the differential muon neutrino neutrino flux, $d\sigma_{\text{CC}}/dE_\mu^0$ is the differential CC interaction cross section producing a muon of energy E_μ^0 and n_T is the

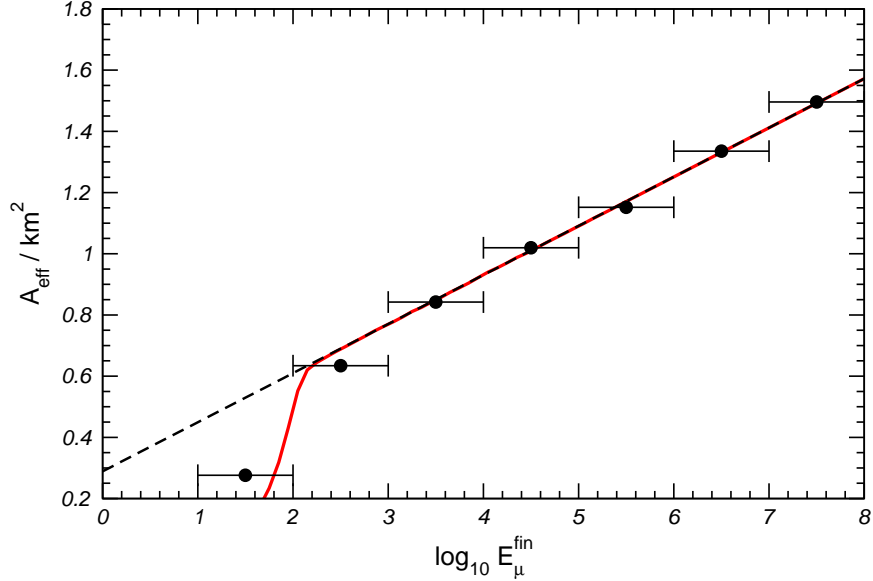


FIG. 1: Effective area as a function of the final muon energy after level 2 cuts. The full line indicates the result from the semi-analytical calculation [5], whereas the data points are from Monte Carlo simulation [6]. For comparison, also shown by a dashed line is $A_0(E_\mu^{\text{fin}})$.

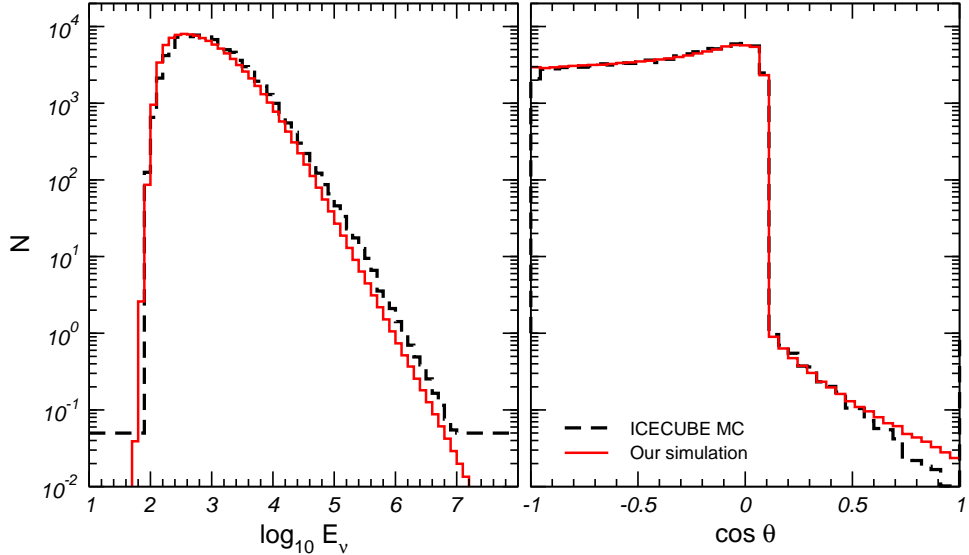


FIG. 2: Expected \mathcal{N}_{ν_μ} event rate after level 2 cuts for one year exposure obtained with the semianalytical calculation (full lines) [5] and with Monte Carlo simulations (dashed lines) [6]. The left panel shows the energy spectrum and the right panel the zenith angular distribution.

number density of nucleons in the matter surrounding the detector. After production with energy E_μ^0 , the muon ranges out in the rock and in the ice surrounding the detector and loses energy. Here, $F(E_\mu^0, E_\mu^{\text{fin}}, l_\mu)$ is the function that describes the energy spectrum of the muons arriving at the detector. Hence, $F(E_\mu^0, E_\mu^{\text{fin}}, l_\mu)$ represents the probability that a muon produced with energy E_μ^0 arrives at the detector with energy E_μ^{fin} after traveling

a distance l_μ . The function $F(E_\mu^0, E_\mu^{\text{fin}}, l_\mu)$ is computed by propagating the muons to the detector taking into account energy losses as given in Eq. (4). The possibility of fluctuations around the average muon energy loss (using the average energy loss would equalize l_μ to the average muon range distance) is included in $F(E_\mu^0, E_\mu^{\text{fin}}, l_\mu)$. Thus, E_μ^0 , E_μ^{fin} , and, l_μ are kept as independent variables. For simplicity, n_T and $F(E_\mu^0, E_\mu^{\text{fin}}, l_\mu)$ in ice are used and the effect of the rock bed below the ice is accounted for in the form of an additional angular dependence of the effective area for upward going events. The details of the detector response are encoded in the effective area A_{eff}^0 . A phenomenological parametrization has been used to simulate the response of the IceCube detector after events that are not neutrinos have been rejected (i.e., level 2 cuts [6])

$$A_{\text{eff}}^0 = A_0(E_\mu^{\text{fin}}) \times R(\cos \theta, E_\mu^{\text{fin}}) \times R(l_\mu^{\text{min}}), \quad (6)$$

where $A_0(E_\mu^{\text{fin}})$ includes the energy dependence of the effective area due to trigger requirements [6]. Here $R(l_\mu^{\text{min}})$ represents the smearing in the minimum track length cut, $l_\mu^{\text{min}} = 300$ m, due to the uncertainty in the track length reconstruction which can be parametrized by a Gaussian

$$R(l_\mu^{\text{min}}) = \frac{1}{\sqrt{2\pi}\sigma_l} \int_0^\infty dl'_\mu \exp -\frac{(l_\mu^{\text{min}} - l'^{\text{min}})^2}{2\sigma_l^2}, \quad (7)$$

with $\sigma_l = 50$ m. Introduction of a simple straight line dependence on $\log_{10}(E_\mu^{\text{fin}})$

$$A_0(E_\mu^{\text{fin}}) = \mathcal{A}_0 \left[1 + 0.55 \log_{10} \left(\frac{E_\mu^{\text{fin}}}{\text{GeV}} \right) \right], \quad (8)$$

leads to a good agreement with the results of Monte Carlo simulations [6]. Here \mathcal{A}_0 is an overall normalization constant, which is calibrated using the flux of atmospheric neutrinos as seen by AMANDA [7]. After level 2 cuts are applied the atmospheric neutrino flux yields 91000 events/yr at IceCube. Next, one has to “simulate” the cuts in the muon tracklength l_μ^{min} and the number of PMT’s reporting signals in an event $N_{\text{CH}}^{\text{min}}$ [6]. The angular dependence of the effective area for downgoing events ($\theta < 80^\circ$) is determined by the level 2 cut on the minimum number of channels $N_{\text{CH}} > N_{\text{CH}}^{\text{min}}(\cos \theta) = 150 + 250 \cos \theta$. This requirement leads to an E_μ^{fin} -dependent angular constraint

$$R(\cos \theta, E_\mu^{\text{fin}}) = \frac{1}{\sqrt{2\pi}\sigma_{N_{\text{CH}}}} \int_{N_{\text{CH}}^{\text{min}}}^\infty dN_{\text{CH}} \exp -\frac{(N_{\text{CH}} - \langle N_{\text{CH}} \rangle_{E_\mu^{\text{fin}}})^2}{2\sigma_{N_{\text{CH}}}^2}, \quad (9)$$

where $\langle N_{\text{CH}} \rangle_{E_\mu^{\text{fin}}}$ is the average channel multiplicity produced by a muon which reaches the detector with energy E_μ^{fin} and $\sigma_{N_{\text{CH}}}^2$ is the spread on the distribution. The parametrization

$$\log_{10} \left(\langle N_{\text{CH}} \rangle_{E_\mu^{\text{fin}}} \right) = 2.0 + 0.88 \frac{X}{\sqrt{1 + X^2}}, \quad (10)$$

with

$$X = 0.47 \left(\log_{10} \left(\frac{E_\mu^{\text{fin}}}{\text{GeV}} \right) - 4.6 \right) \quad (11)$$

and

$$\sigma_{N_{\text{CH}}} = 0.4 \langle N_{\text{CH}} \rangle_{E_{\mu}^{\text{fin}}} \quad (12)$$

shows good agreement with the charged multiplicity obtained through Monte Carlo simulations [6]. Finally, to account for the presence of the rock bed below the detector, one can introduce a phenomenological angular dependence of the effective area for upward going muons

$$R(\cos \theta) = 0.70 - 0.48 \cos \theta \quad \text{for } \theta > 85^\circ, \quad (13)$$

independent of the muon energy. Figure 1 shows the effective area A_{eff} , defined as the ratio of the number of upgoing muon events, with/without the inclusion of $A_0(E_{\mu}^{\text{fin}}) \times R(l_{\mu}^{\text{min}})$ and the level 2 cuts on l_{μ}^{min} , and compare the results of the semi-analytical calculation with Monte Carlo simulations of the detector response [6]. Figure 2 compares the energy spectrum and the zenith angular distribution of the events (after level 2 cuts are applied) obtained with the semi-analytical calculation and with Monte Carlo simulations.

B. Electromagnetic Showers

Showers are generated by neutrino collisions — ν_e or ν_{τ} CC interactions, and all NC interactions — inside of or near the detector, and by muon bremsstrahlung radiation near the detector. Normally, a reduction of the muon bremsstrahlung background is effected by placing a cut of 4×10^4 GeV on the minimum reconstructed energy [8].

Electron neutrinos deposit 0.5-0.8% of their energy into an electromagnetic shower initiated by the leading final state electron. The rest of the energy goes into the fragments of the target that produce a second subdominant shower. Because the size of the shower, of order meters in ice, is small compared to the spacing of the PMT's, it represents, to a good approximation, a point source of Čerenkov photons radiated by the shower particles. These trigger the PMT at the single photoelectron level over a spherical volume whose radius scales linearly with the shower energy. For ice, the radius is 130 m at 10⁴ GeV and 460 m at 10¹⁰ GeV, i.e. the shower radius grows by just over 50 m per decade in energy.

The measurement of the radius of the sphere in the lattice of PMT determines the energy and turns neutrino-detection-experiments into total energy calorimeters. Note that a contained “direct hit” by a 10¹⁰ GeV neutrino will not saturate a km³ detector volume. Because the shower and its accompanying Čerenkov lightpool are not totally symmetric but elongated in the direction of the leading electron (and incident neutrino), its direction can be reconstructed. Pointing is however far inferior to what can be achieved for muon neutrinos and estimated to be precise to $\sim 10^\circ$ only.

The expected shower event rate at IceCube can also be estimated through semi-analytical calculations [9],

$$\mathcal{N}_{\text{sh}} = \mathcal{N}_{\text{sh,CC}} + \mathcal{N}_{\text{sh,NC}}, \quad (14)$$

where

$$\mathcal{N}_{\text{sh,CC}} = T n_{\text{T}} \int_{E_{\text{sh}}^{\text{min}}}^{\infty} dE_{\nu} \sum_{\alpha=e,\tau} \frac{dF^{\nu\alpha}}{dE_{\nu}}(E_{\nu}) \sigma_{\text{CC}}(E_{\nu}) \mathcal{V}_{\text{eff}}(E_{\nu}), \quad (15)$$

and

$$\mathcal{N}_{\text{sh,NC}} = T n_{\text{T}} \int_{E_{\nu}-E_{\text{sh}}^{\text{min}}}^{\infty} dE'_{\nu} \int_{E_{\text{sh}}^{\text{min}}}^{\infty} dE_{\nu} \sum_{\alpha=e,\mu,\tau} \frac{dF^{\nu\alpha}}{dE_{\nu}}(E_{\nu}) \frac{d\sigma_{\text{NC}}}{dE'_{\nu}}(E_{\nu}, E'_{\nu}) \mathcal{V}_{\text{eff}}(E_{\nu}). \quad (16)$$

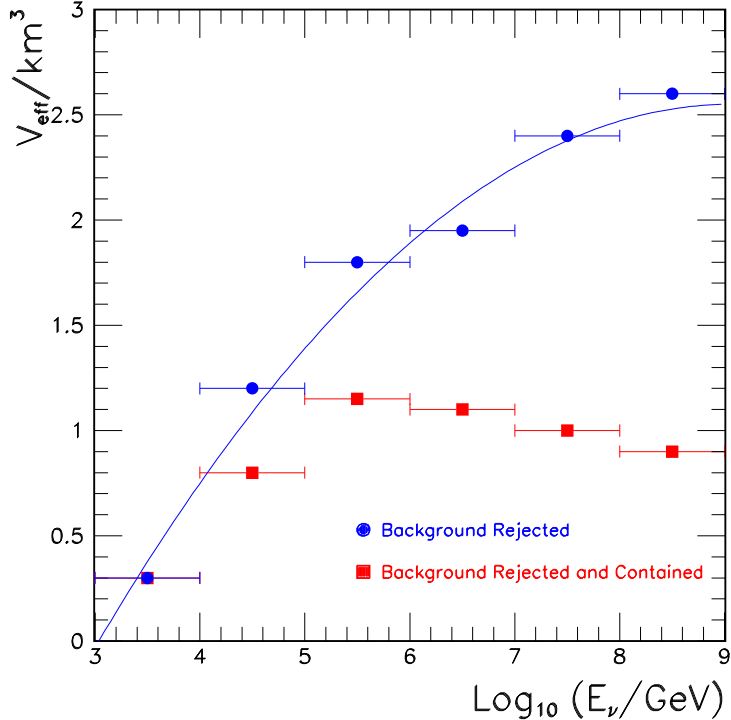


FIG. 3: Effective volume of IceCube for showers initiated by neutrinos. The parametrization shown by a solid curve corresponds to $\mathcal{V}_{\text{eff}}(E_{\nu}) \approx -0.07 \log_{10}^2 E_{\nu} + 1.27 \log_{10} E_{\nu} - 3.21$.

Here, $d\sigma_{\text{NC}}/dE'_{\nu}$ is the differential NC interaction cross section producing a secondary neutrino of energy E'_{ν} , and $\mathcal{V}_{\text{eff}}(E_{\nu})$ is the effective volume shown in Fig. 3. In writing Eqs. (15) and (16) we are assuming that for contained events the shower energy corresponds with the interacting ν_e or ν_{τ} neutrino energy ($E_{\text{sh}} = E_{\nu}$) in a CC interaction, while for NC the shower energy corresponds to the energy in the hadronic shower $E_{\text{sh}} = E_{\nu} - E'_{\nu} \equiv E_{\nu} y$, where y is the usual inelasticity parameter in deep inelastic scattering [10].

C. Shower-Track Combo

For ν_{τ} 's, CC current interactions have different signals depending on the energy. The τ has a decay length

$$l_{\tau} \approx 50 \text{ m} \times (E_{\tau}/10^6 \text{ GeV}), \quad (17)$$

and loses energy in the Earth according to

$$\frac{dE_{\tau}}{dl} = -\alpha - \beta_{\tau} E_{\tau}, \quad (18)$$

where $\beta_{\tau} = 8 \times 10^{-7} \text{ cm}^2 \text{ g}^{-1}$ [4]. From Eqs. (17) and (18) it is easily seen that for energies above about 10^8 GeV the τ is more likely to interact electromagnetically than to decay, whereas for $E_{\tau} < 10^{7.5}$ GeV the energy loss before decay is negligible.

For τ leptons less energetic than 10^6 GeV, the shower (hadronic or electromagnetic) from the tau decay cannot be separated from the hadronic shower of the initial ν_{τ} interaction. At a few times 10^6 GeV, the range of the tau becomes a few hundred meters and the two

showers produced may be easily separated and be identify as a double bang event. At energies between $10^7 - 10^{7.5}$ GeV, the tau decay length is comparable to the instrumented volume. In such cases, one may observe a τ track followed by the τ -decay shower (“lollipop topology”), or a hadronic shower followed by a τ track which leaves the detector (“popillol topology”). At energies $> 10^{7.5}$ GeV, $l_\tau \gg 1$ km and τ ’s leave only a track like muons. However, a τ going through the detector at high energies without decaying will not deposit as much energy in the detector as a comparable-energy muon, due to the mass difference. (The direct-pair production process scales inversely with mass, so it dominates tau-lepton energy loss [11] resulting in $1/20^{\text{th}}$ the light produced by a muon.) Such a tau might then be indistinguishable from a low energy muon track, and thus might not be flagged as an interesting event. In summary, the energy range from $10^6 - 10^{7.5}$ GeV is the “sweet spot” for τ detection in IceCube, since here one can observe all the distinctive topologies.

Although neutrino “telescopes” are designed as discovery instruments, be it for particle or astrophysics, their conceptual design is very much anchored to the observational fact that Nature produces protons and photons with energies in excess of 10^{11} GeV and 10^4 GeV, respectively. The cosmic ray connection sets the scale of cosmic neutrino fluxes. We discuss this next.

III. LUMINOSITY

IceCube is unique among high energy neutrino experiments in being sensitive to ten decades in energy. Unlike terrestrial experiments with a man-made beam, the luminosity varies significantly with the center-of-mass energy [12]. In what follows we discuss the different energy regimes accesible to IceCube.

A. Atmospheric Neutrinos

A guaranteed beam of high energy neutrinos originates in the atmospheric cascades initiated by cosmic rays [13]. When protons and nuclei enter the atmosphere, they collide with the air molecules and produce all kind of secondary particles, which in turn interact or decay or propagate to the ground, depending on their intrinsic properties and energies. In the GeV range, the most abundant particles are neutrinos. The production mechanism is the decay chains of mesons created in these cascades.

Pion decay dominates the atmospheric neutrino production: $\pi^+ \rightarrow \mu^+ \nu_\mu \rightarrow e^+ \nu_e \nu_\mu \bar{\nu}_\mu$ and the conjugate process. This decay chain determines the neutrino energy spectra up to about 100 GeV above which they become increasingly modified by the kaon contribution, which asymptotically reaches 90%. In the atmosphere mesons encounter the interaction–decay competition. Therefore, neutrinos from meson decay will have a spectrum one power of energy steeper than the primary cosmic ray spectrum. The muon daughter neutrinos will have a spectrum steeper by two powers of energy, because the muon spectrum itself is steeper by $1/E$. Electron neutrinos have a differential spectrum (approximately) $\propto E_\nu^{-4.7}$. The muon neutrino spectrum is flatter,

$$dF_{\text{atm}}^{\nu_\mu}/dE_\nu \equiv \phi_{\text{atm}}^{\nu_\mu} \approx \begin{cases} 1.6 \times 10^{-16} E_\nu^{-3.7} \text{ GeV cm}^{-2} \text{ s}^{-1} \text{ sr}^{-1} & E_\nu < 10^5 \text{ GeV} \\ 5.0 \times 10^{-18} E_\nu^{-4.0} \text{ GeV cm}^{-2} \text{ s}^{-1} \text{ sr}^{-1} & E_\nu > 10^5 \text{ GeV} \end{cases} . \quad (19)$$

In this energy window, the flavor ratios are $w_e : w_\mu : w_\tau \approx 1/20 : 19/20 : 0$ [14] and, as can be seen in Fig. 4, the energy spectra are a function of the zenith angle of the atmospheric cascades. This is because mesons in inclined showers spend more time in tenuous atmosphere where they are more likely to decay rather than interact. For this reason the spectra of highly inclined neutrinos are flatter than those of almost vertical neutrinos. In the sub-GeV energy range the spectra are significantly flatter (parallel to the primary cosmic ray spectrum) as all mesons and muons decay. Thus, one can immediately predict that the flavor ratios at production are $1/3 : 2/3 : 0$. Above about 10^5 GeV, kaons are also significantly attenuated before decaying and the “prompt” component, arising mainly from very short-live charmed mesons (D^\pm, D^0, D_s and Λ_c) dominates the spectrum [18]. Such a “prompt” neutrino flux is isotropic with flavor ratios $12/25 : 12/25 : 1/25$.

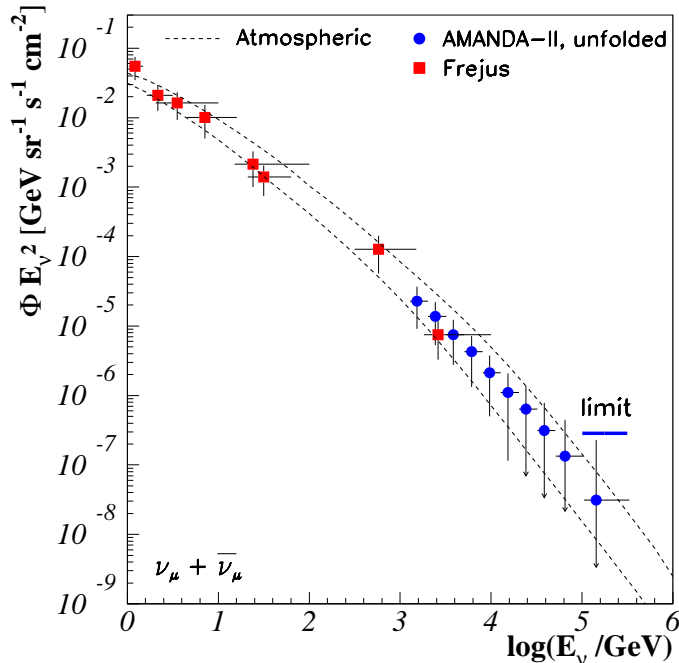


FIG. 4: Energy spectrum of atmospheric neutrinos as seen by the AMANDA II [15] and Frejus [16] experiments. The two dotted curves indicates model predictions [17] for the horizontal (upper) and vertical (lower) flux.

The neutrino flux arising from pion and kaon decay is reasonably well understood, with an uncertainty in the range 10% – 20% [13]. The prompt atmospheric neutrino flux, however, is much less understood, because of uncertainty about cosmic ray composition and relatively poor knowledge of small- x QCD processes [19]. For numerical estimates, throughout this review we have chosen to use the 3-dimensional estimates of conventional atmospheric neutrino flux given in [20], which we extrapolate to match at higher energies the 1-dimensional calculations of Volkova [17]. We also incorporate “prompt” neutrinos from charm decay as calculated in [21].

In 10 yr of operation IceCube will collect more than 7×10^5 atmospheric neutrino events with $E_\mu^{\text{fin}} > 100$ GeV. These events are generated by neutrinos with large enough energy for standard mass-induced oscillations to be very much suppressed so they should behave as

flavor eigenstates. As we discuss in Sec. V A, this high-statistics high-energy event sample offers a unique opportunity to probe new physics mechanisms for leptonic flavor mixing.

B. Extraterrestrial Neutrinos

Interactions of ultra-high energy cosmic ray protons propagating over cosmological distances with the cosmic microwave background (CMB) generates a nearly guaranteed cosmogenic flux of neutrinos [22] through the decay of charged pions produced in $p\gamma$ interactions, which should also result in a suppression of the cosmic ray spectrum above the “GZK cutoff”: $E_{\text{GZK}} \sim 10^{10.7}$ GeV [23]. The intermediate state of the reaction $p\gamma_{\text{CMB}} \rightarrow N\pi$ is dominated by the Δ^+ resonance, because the n decay length is smaller than the nucleon mean free path on the relic photons. Hence, there is roughly an equal number of π^+ and π^0 . Gamma rays, produced via π^0 decay, subsequently cascade electromagnetically on the cosmic radiation fields through e^+e^- pair production followed by inverse Compton scattering. The net result is a pile up of γ rays at GeV energies, just below the threshold for further pair production. On the other hand, each π^+ decays to 3 neutrinos and a positron. The e^+ readily loses its energy through synchrotron radiation in the cosmic magnetic fields. The neutrinos carry away about 3/4 of the π^+ energy, and therefore the energy in cosmogenic neutrinos is about 3/4 of the one produced in γ -rays.

The normalization of the neutrino flux depends critically on the cosmological evolution of the cosmic ray sources and on their proton injection spectra [24, 25]. It also depends on the assumed spatial distribution of sources; for example, relatively local objects, such as sources in the Virgo cluster [26], would dominate the high energy tail of the neutrino spectrum. Another source of uncertainty in the cosmogenic neutrino flux is the energy at which there is a transition from Galactic to extragalactic cosmic rays as inferred from a change in the spectral slope [27]. A fourth source of uncertainty in the cosmogenic flux is the chemical composition — if ultra-high energy cosmic rays are heavy nuclei rather than protons the corresponding cosmogenic neutrino flux may be somewhat reduced [28].

In addition to being produced in the propagation of ultra-high energy cosmic rays, neutrinos are also expected to be generated in their sources. How many neutrinos are produced in association with the cosmic ray beam? The answer to this question, among many others, provides the rationale for building kilometer-scale neutrino detectors. We first consider a neutrino beam produced at an accelerator laboratory. The accelerator beam is “dumped” into a large target, for instance a hundred meters of steel. The target absorbs all parent protons as well as the secondary electromagnetic and hadronic showers. Only neutrinos, the decay products of charged pions, exit the dump. If Nature constructed such a “hidden source” in the heavens, conventional astronomy will not reveal it. It cannot be the source of the cosmic rays, however, because in this case the dump must be transparent to protons.

A more generic “transparent” source can be imagined as follows: protons are accelerated in a region of high magnetic fields near a black hole or neutron star. They inevitably interact with the radiation surrounding collapsed objects via the processes $p + \gamma \rightarrow \Delta \rightarrow \pi^0 + p$ and $p + \gamma \rightarrow \Delta \rightarrow \pi^+ + n$. While the secondary protons may remain trapped in the acceleration region, equal numbers of neutrons, neutral and charged pions escape/decay. The energies escaping the source in the form of cosmic rays, gamma rays and neutrinos produced by the decay of neutrons and neutral and charged pions, are related by the physics of photoproduction. The neutrino flux from a generic transparent cosmic ray source is often referred to as the Waxman-Bahcall (WB) flux [29]. It is easy to calculate and the derivation

is revealing.

We will concentrate on the population of extragalactic cosmic rays with energies in excess of $10^{9.9}$ GeV, i.e., beyond the “ankle” in the spectrum. The flux above the ankle is often summarized as ”one 10^{10} GeV particle per kilometer square per year per steradian”. This can be translated into an energy flux

$$\begin{aligned} E \left\{ E \frac{dN_{\text{CR}}}{dE} \right\} &= \frac{10^{10} \text{ GeV}}{(10^{10} \text{ cm}^2)(3 \times 10^7 \text{ s}) \text{ sr}} \\ &= 3 \times 10^{-8} \text{ GeV cm}^{-2} \text{ s}^{-1} \text{ sr}^{-1}. \end{aligned} \quad (20)$$

From this we can derive the energy density ρ_E in cosmic rays using flux = velocity \times density, or

$$4\pi \int dE \left\{ E \frac{dN_{\text{CR}}}{dE} \right\} = c\rho_E. \quad (21)$$

We obtain

$$\rho_E = \frac{4\pi}{c} \int_{E_{\text{min}}}^{E_{\text{max}}} \frac{3 \times 10^{-8}}{E} dE \frac{\text{GeV}}{\text{cm}^3} \simeq 10^{-19} \frac{\text{TeV}}{\text{cm}^3}, \quad (22)$$

taking the extreme energies of the accelerator(s) to be $E_{\text{max}}/E_{\text{min}} \simeq 10^3$.

This energy density derived professionally by integrating the spectrum beyond the “ankle” assuming an E^{-2} energy spectrum with a GZK cutoff is closer to $\sim 3 \times 10^{-19} \text{ erg cm}^{-3}$ [30]. The power required for a population of sources to generate this energy density over the Hubble time of 10^{10} years is $\sim 3 \times 10^{37} \text{ erg s}^{-1}$ per $(\text{Mpc})^3$ or, as often quoted in the literature, $\sim 5 \times 10^{44} \text{ TeV}$ per year per $(\text{Mpc})^3$. This works out to [31]

- $\sim 3 \times 10^{39} \text{ erg s}^{-1}$ per galaxy,
- $\sim 3 \times 10^{42} \text{ erg s}^{-1}$ per cluster of galaxies,
- $\sim 2 \times 10^{44} \text{ erg s}^{-1}$ per active galaxy, or
- $\sim 2 \times 10^{52} \text{ erg}$ per cosmological gamma ray burst.

The coincidence between these numbers and the observed output in electromagnetic energy of these sources explains why they have emerged as the leading candidates for the cosmic ray accelerators. The coincidence is consistent with the relationship between cosmic rays and photons built into the ”transparent” source. In the photoproduction processes roughly equal energy goes into the secondary neutrons, neutral and charged pions whose energy ends up in cosmic rays, gamma rays and neutrinos, respectively. For $E_{\text{max}} = 10^{12} \text{ GeV}$, the generic source of the highest energy cosmic rays produces a flux of $E_{\nu}^2 dN_{\nu}/dE_{\nu} \sim 4 \times 10^{-8} \text{ GeV cm}^{-2} \text{ s}^{-1} \text{ sr}^{-1}$, close to the back-of-the-envelope calculation performed first.

There are several ways to modify this simple prediction:

- The derivation fails to take into account the fact that there are more cosmic rays in the Universe producing neutrinos than observed at Earth because of the GZK-effect and neglects evolution of the sources with redshift. This increases the neutrino flux by a factor d_H/d_{CMB} , the ratio of the Hubble to the attenuation length radius over which cosmic rays above the ankle penetrate the cosmic microwave background.

- For proton- γ interactions muon neutrinos (and muon antineutrinos receive only 1/2 of the energy of the charged pion in the decay chain $\pi^+ \rightarrow \mu^+ + \nu_\mu \rightarrow e^+ + \nu_e + \bar{\nu}_\mu + \nu_\mu$ assuming that the energy is equally shared between the 4 leptons. Furthermore half the muon neutrinos oscillate into tau neutrinos by over cosmic distances.

In summary,

$$E_\nu \frac{dN_\nu}{dE_\nu} = \frac{1}{2} \times \frac{1}{2} \times E \frac{dN_{\text{CR}}}{dE} \times \frac{d_H}{d_{\text{CMB}}} \simeq E \frac{dN_{\text{CR}}}{dE} \quad (23)$$

The corrections approximately cancel. The transition from galactic to extragalactic sources is debated; a transition at lower energy significantly increases the energy in the extragalactic component. This raises the possibility of an increase in the associated neutrino flux [32]. Waxman and Bahcall referred to this as a bound because in reality more energy is transferred to the neutron than to the charged pion in the source; in the case of the photoproduction reaction $p + \gamma \rightarrow \Delta \rightarrow \pi^+ + n$ four times more. Therefore

$$E_\nu \frac{dN_\nu}{dE_\nu} = \frac{1}{4} E \frac{dN_{\text{CR}}}{dE}. \quad (24)$$

This is, for instance, the diffuse flux expected from all gamma ray bursts.

In the end we estimate that for each neutrino flavor the flux associated with the sources of the highest energy cosmic rays is loosely confined to the range,

$$E_\nu^2 \phi_{\text{WB}}^\nu \simeq 1.3 \times 10^{-8} \text{ GeV cm}^{-2} \text{ s}^{-1} \text{ sr}^{-1}, \quad (25)$$

yielding $10 \sim 50$ detected muon neutrinos per km^2 per year. This number depends weakly on E_{max} and the spectral slope. The observed event rate is obtained by folding the predicted flux with the probability that the neutrino is actually detected in a high energy neutrino telescope; only one in a million is at TeV energy. As we discussed in Sec. II A, this probability is given by the ratio of the muon and neutrino interaction lengths in the detector medium, l_μ/l_ν .

This flux has to be compared with the sensitivity of $\sim 10^{-7} \text{ GeV cm}^{-2} \text{ s}^{-1} \text{ sr}^{-1}$ reached during the first 4 years of operation of the completed AMANDA detector in 2000–2003 [33]. The analysis of the data has not been completed, but a preliminary limit of $2.9 \times 10^{-7} \text{ GeV cm}^{-2} \text{ s}^{-1} \text{ sr}^{-1}$ has been obtained with a single year of data [34]. On the other hand, after three years of operation IceCube will reach a diffuse flux limit of $E_\nu^2 \phi_{\text{IceCube}}^{\nu_\mu} \sim 2 - 7 \times 10^{-9} \text{ GeV cm}^{-2} \text{ s}^{-1} \text{ sr}^{-1}$. The exact value depends on the magnitude of the dominant high energy atmospheric neutrino background from the prompt decay of atmospheric charmed particles [6]. As noted in the previous section, the level of this background is difficult to anticipate. A cosmic flux at the "Waxman-Bahcall" level will result in the observation of several hundred neutrinos in IceCube [6].

In Fig. 5, we plot the expected spectrum of ultra-high energy cosmic neutrinos in the models discussed above. For comparison we show the upper limits on neutrino fluxes reported by the AMANDA Collaboration [36] and the cascade limit.¹ Hidden sources must have a steeper spectrum than transparent sources in order to be consistent with data. In

¹ The cascade limit arises from the requirement that the diffuse γ -ray fluxes initiated by photons and electrons from pion decays should not exceed measurements. The cascade limit from Ref. [37] exploits the measurement of the diffuse γ -ray background by EGRET [38]. A lower extragalactic contribution

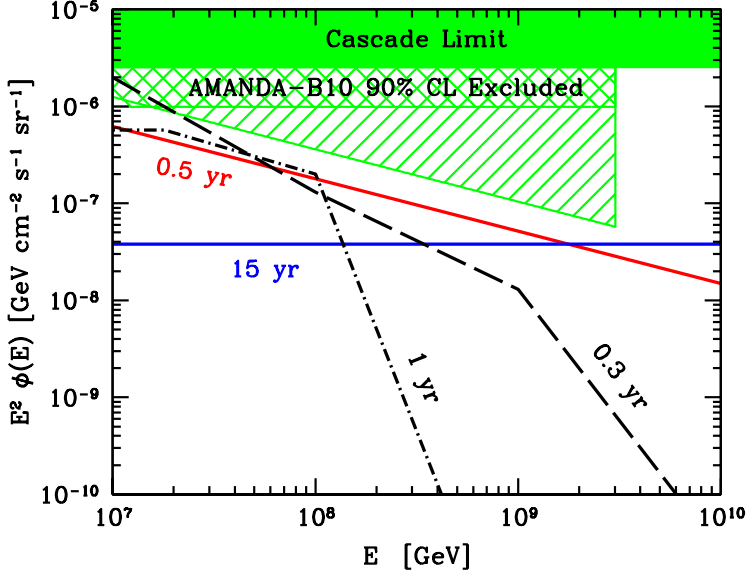


FIG. 5: Neutrino fluxes from transparent and hidden sources. The horizontal solid line indicates the WB prediction (summed over all flavors) which corresponds to a Galactic/extra-galactic crossover energy $\sim 10^{10}$ GeV [29]. The falling solid line indicates the expected neutrino flux from transparent sources, if one assumes the onset of dominance by the extra-galactic component is at $10^{8.6}$ GeV [32]. The dash and dashed-dotted lines indicate neutrino flux estimates from hidden sources [35]. The label on each curve indicates the time required for IceCube to achieve an integrated luminosity $\mathcal{L} \approx 30 \text{ nb}^{-1}$ at $\sqrt{s} \simeq 6$ TeV. The cross-hatched region excludes an E_ν^{-2} spectrum at the 90% CL by measurements of AMANDA-B10 [36]. The single hatched region, obtained by rescaling the AMANDA integrated bolometric flux limit to an $E_\nu^{-2.54}$ power law, is the exclusion region for the low crossover model. The shaded region indicates the cascade limit.

particular, the flux could be enhanced by more than an order of magnitude in the energy decade between 10^{7-8} GeV. Therefore, the energy region $E_\nu \simeq 10^{7-7.5}$ GeV is particularly amenable to probe high energy neutrino interactions: commonly proposed non-atmospheric neutrino fluxes are still sizeable, while the anisotropic background from atmospheric neutrinos has become insignificant. This insures a statistically significant sample of neutrino collisions with center-of-mass energy $\sqrt{s} \simeq 6$ TeV. It should be noted that this energy is well above the HERA domain ($\sqrt{s} \simeq 500$ GeV), the highest accelerator energy at which even indirect tests of the Standard Model cross sections are possible.

C. Directional Signals

MeV neutrino astronomy have been existing for about 40 years. Thus far two sources have been identified: the Sun [41] and supernova 1987A (SN87) [42]. During the next decade, the

to the γ -ray background than that inferred in above reference, by roughly a factor of two, has been proposed recently [39]. The cascade limit may therefore be stronger by a corresponding factor. Note that logarithmic corrections to the spectrum $\propto E_\nu^{-2}$ could result in sizeable deviations of the cascade limit at very high energy [40].

large sensitivity of IceCube to extraterrestrial neutrino fluxes gives a hope to open a new era in neutrino astronomy through detection of high energy neutrinos.

One of the key features of high energy neutrinos is that they are unique carriers of unambiguous information about hadronic process in cosmic accelerators [43]. Since generally these processes also result in TeV gamma-rays of comparable fluxes [44], the best candidates to be discovered by neutrino telescopes are sources of gamma-rays with fluxes above 1 TeV around $(3 - 10) \times 10^{-12} \text{ ph cm}^{-2} \text{ s}^{-1}$. Presently several TeV gamma-ray sources, in particular persistant galactic sources like Crab Nebula [45], shell type SNRs RXJ1713 [46] and Vela Jr [47], as well as strongly variable Active Galactic Nuclei Mrk 421, Mkn 501, and 1ES 1959 [48] do show fluxes of TeV gamma-rays above $10^{-11} \text{ ph cm}^{-2} \text{ s}^{-1}$. Therefore, if significant fractions of these gamma-ray fluxes are of hadronic origin IceCube should be able to detect the neutrino counterparts of TeV gamma-rays. Moreover, in the case of sources with heavily absorbed TeV gamma-ray emission, the chances of detection of counterpart neutrino emission could be quite high even for relatively weak TeV sources with a flux well below the level 0.1 Crab [49].

Antineutrinos are also produced through the β -decay process, but since cosmic neutrino production is dominated by π^\pm decay, the search for the $\bar{\nu}_e$ channel is not straightforward. A potential way is to identify neutron-emitting-sources. However, the decay mean free path of a neutron is $c \Gamma_n \bar{\tau}_n = 9.15 (E_n/10^9 \text{ GeV}) \text{ kpc}$ (the lifetime being boosted from its rest-frame value, $\bar{\tau}_n = 886$ seconds, to its lab value by $\Gamma_n = E_n/m_n$), and so only neutrons with energy $\gtrsim 10^9 \text{ GeV}$ have a boosted $c\tau_n$ sufficiently large to serve as Galactic messengers.

Air shower arrays have observed a “directional” flux of cosmic rays from the galactic plane [50], unlikely to be protons whose directions are scrambled in the magnetic field. The flux appears only in a narrow energy range from $10^{8.9}$ to $10^{9.5} \text{ GeV}$, the energy where neutrons reach typical galactic kiloparsec distances within their lifetime of minutes. Both the directionality and the characteristic energy make a compelling case for electrically neutral neutron primaries. The galactic plane excess, which is roughly 4% of the diffuse flux, is mostly concentrated in the direction of the Cygnus region [51].

Independent evidence may be emerging for a cosmic accelerator in the Cygnus spiral arm. The HEGRA experiment has detected an extended TeV γ -ray source, J2032+4130, in the Cygnus region with no clear counterpart and a spectrum not easily accommodated with synchrotron radiation by electrons [52]. The difficulty to accommodate the spectrum by conventional electromagnetic mechanisms has been exacerbated by the failure of CHANDRA and VLA to detect X-rays or radiowaves signaling acceleration of any electrons [53]. The model proposed is that of a proton beam, accelerated by a nearby mini-quasar or possibly Cygnus X-3, interacting with a molecular cloud to produce pions that are the source of the gamma rays. Especially intriguing is the possible association of this source with Cygnus OB2, a cluster of more than 2700 (identified) young, hot stars with a total mass of $\sim 10^4$ solar masses [54]. Proton acceleration to explain the TeV photon signal requires only 0.1% efficiency for the conversion of the energy in the stellar wind into cosmic ray acceleration. Also, the stars in Cygnus OB2 could be the origin of time-correlated, clustered supernova remnants forming a source of cosmic ray nuclei. By cooperative acceleration their energies may even exceed the $\sim 10^6 \text{ GeV}$ cutoff of individual remnants and accommodate cosmic rays up to the ankle, where the steeply falling ($\propto E^{-3.16 \pm 0.08}$) cosmic ray spectrum flattens to $E^{-2.8 \pm 0.3}$ [55]. An immediate consequence of this nucleus-dominance picture is the creation of free neutrons via nuclei photodisintegration on background photon fields. These liberated neutrons are presumably responsible for the observed directional signals.

The observed spectrum from the Cygnus region can be described by single power law reflecting the average shape of the diffuse cosmic ray spectrum between 10^6 and $10^{8.5}$ GeV,

$$\begin{aligned} \frac{dF_n}{dE_n} &= \frac{dF_n}{dE_n} \Big|_{\text{source}} e^{-D/(c\Gamma_n \bar{\tau}_n)} \\ &= C E_n^{-3.1} e^{-D/(c\Gamma_n \bar{\tau}_n)}, \end{aligned} \quad (26)$$

where $D \approx 1.7$ kpc is the distance to Cygnus OB2. By integrating the spectrum between $E_1 = 10^{8.9}$ GeV and $E_2 = 10^{9.5}$ GeV [51], normalization to the observed integrated flux [51],

$$\int_{E_1}^{E_2} C E_n^{-3.1} e^{-D/(c\Gamma_n \bar{\tau}_n)} dE_n \approx 9 \text{ km}^{-2} \text{yr}^{-1}, \quad (27)$$

leads to $C = 1.15 \times 10^{20} \text{ km}^{-2} \text{yr}^{-1}$.

For every surviving neutron at $\sim 10^9$ GeV, there are many neutrons at lower energies that do decay via $n \rightarrow p + e^- + \bar{\nu}_e$. The proton is bent by the Galactic magnetic field and the electron quickly loses energy via synchrotron radiation, but the $\bar{\nu}_e$ travels along the initial neutron direction, producing a directed TeV energy beam which is potentially observable.

The basic formula that relates the neutron flux at the source to the antineutrino flux observed at Earth is [56]:

$$\begin{aligned} \frac{dF_{\bar{\nu}}}{dE_{\bar{\nu}}}(E_{\bar{\nu}}) &= \int dE_n \frac{dF_n}{dE_n}(E_n) \Big|_{\text{source}} \left(1 - e^{-\frac{D m_n}{E_n \bar{\tau}_n}}\right) \int_0^Q d\epsilon_{\bar{\nu}} \frac{dP}{d\epsilon_{\bar{\nu}}}(\epsilon_{\bar{\nu}}) \\ &\times \int_{-1}^1 \frac{d \cos \bar{\theta}_{\bar{\nu}}}{2} \delta \left[E_{\bar{\nu}} - E_n \epsilon_{\bar{\nu}} (1 + \cos \bar{\theta}_{\bar{\nu}}) / m_n \right]. \end{aligned} \quad (28)$$

The variables appearing in Eq. (28) are the antineutrino and neutron energies in the lab ($E_{\bar{\nu}}$, E_n), the antineutrino angle with respect to the direction of the neutron momentum in the neutron rest-frame ($\bar{\theta}_{\bar{\nu}}$), and the antineutrino energy in the neutron rest-frame ($\epsilon_{\bar{\nu}}$). The last three variables are not observed by a laboratory neutrino-detector, and so are integrated over. The observable $E_{\bar{\nu}}$ is held fixed. The delta-function relates the neutrino energy in the lab to the three integration variables. The parameters appearing in Eq. (28) are the neutron mass and rest-frame lifetime (m_n and $\bar{\tau}_n$). Finally, $dP/d\epsilon_{\bar{\nu}}$ is the normalized probability that the decaying neutron produces an antineutrino with energy $\epsilon_{\bar{\nu}}$ in the neutron rest-frame. Note that the maximum antineutrino energy in the neutron rest frame is very nearly $Q \equiv m_n - m_p - m_e = 0.71$ MeV.

The integral neutrino flux, $F_{\bar{\nu}}(> E_{\bar{\nu}}) \equiv \int_{E_{\bar{\nu}}} dE_{\bar{\nu}} dF_{\bar{\nu}}/dE_{\bar{\nu}}$, is particularly useful for experiments having a neutrino detection-efficiency that is independent of neutrino energy, or nearly so. The integral flux, normalized to the integrated neutron flux in Eq. (27), is shown in Fig. 6. Note that the nuclear photodisintegration threshold implies an infrared cutoff on the primary neutron energy at the source, which in turn leads to a low energy cutoff of $\mathcal{O}(\text{TeV})$ on the integral flux.

In summary, the AMANDA experiment using natural 1 mile-deep Antarctic ice as a Čerenkov detector is in steady operation collecting roughly 7 to 10 neutrinos per day. Expansion into the IceCube kilometer scale neutrino telescope will increase the event rate at least to 250 events per day. Because of this high-statistics data sample IceCube will be a powerful high-energy physics laboratory. We explore the science reach next.

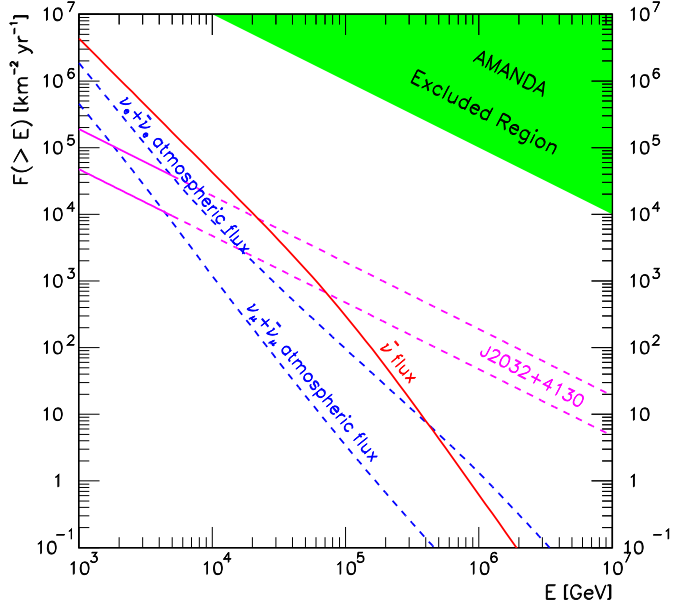


FIG. 6: Integrated flux of $\bar{\nu}_\mu + \bar{\nu}_e + \bar{\nu}_\tau$ (solid line) predicted to arrive at Earth from the direction of the Cygnus region. Also shown are the integrated $\nu_\mu + \bar{\nu}_\mu$ and $\nu_e + \bar{\nu}_e$ atmospheric fluxes for an angular bins of $1^\circ \times 1^\circ$ and $10^\circ \times 10^\circ$, respectively. The shaded band indicates the region excluded by the AMANDA experiment [57]. The fluxes of neutrinos inferred from HEGRA measurements of the γ -ray flux are also shown: the lower line is based on the assumption of $p\gamma$ interactions, whereas the upper line is based on pp interactions (the charged/neutral pion-production ratio depends on the interaction). In each case the solid portion of the line indicates the region where HEGRA data is available and the dashed part is an extrapolation to unobserved energies [9].

IV. NEUTRINO INTERACTIONS BEYOND THE WEAK SCALE

The saga of the Standard Model [58] is still exhilarating because it leaves all questions of consequence unanswered. The most evident of unanswered questions is why the weak interactions are weak. Though electromagnetism and weak interactions are unified, electromagnetism is apparent in day life while the weak interactions are not. Already in 1934 Fermi [59] provided an answer with a theory that prescribed a quantitative relation between the fine structure constant and the weak coupling, $G_F \sim \alpha/M_W^2$. Although Fermi adjusted M_W to accommodate the strength and range of nuclear radioactive decays, one can readily obtain a value of M_W of 40 GeV from the observed decay rate of the muon for which the proportionality factor is $\pi/\sqrt{2}$. The answer is of by a factor of 2 because the discovery of parity violation and neutral currents was in the future and introduces an additional factor $1 - M_W^2/M_Z^2$,

$$G_F = \left[\frac{\pi\alpha}{\sqrt{2}M_W^2} \right] \left[\frac{1}{1 - M_W^2/M_Z^2} \right] (1 + \Delta r). \quad (29)$$

Fermi could certainly not have anticipated that we now have a renormalizable gauge theory that allows us to calculate the radiative correction Δr to his formula. Besides regular higher order diagrams, loops associated with the top quark and the Higgs boson contribute.

If one calculates the radiative corrections to the mass M_H appearing in the Higgs potential, the same theory that withstood the onslaught of precision experiments at LEP/SLC and the Tevatron yields a result that grows quadratically

$$\delta M_H^2 = \frac{3}{16\pi v^2} (2M_W^2 + M_Z^2 + M_H^2 - 4M_t^2) \Lambda^2 , \quad (30)$$

where $M_H^2 = 2\lambda v^2$, λ is the quadratic Higgs coupling, $v = 246$ GeV, and Λ is a cutoff. Upon minimization of the potential, this translates into a dangerous contribution to the Higgs vacuum expectation value which destabilizes the electroweak scale [60]. The Standard Model works amazingly well by fixing Λ at the electroweak scale M_W . It is generally assumed that this indicates the existence of new physics beyond the Standard Model. Following Weinberg,

$$\mathcal{L}(M_W) = \frac{1}{2} M_H^2 H^\dagger H + \frac{1}{4} \Lambda (H^\dagger H)^2 + \mathcal{L}_{\text{SM}}^{\text{gauge}} + \mathcal{L}_{\text{SM}}^{\text{Yukawa}} + \frac{1}{\Lambda} \mathcal{L}^5 + \frac{1}{\Lambda^2} \mathcal{L}^6 + \dots , \quad (31)$$

where the operators of higher dimension parametrized physics beyond the Standard Model. The optimistic interpretation of all this is that, just like Fermi anticipated particle physics at 100 GeV in 1934, the electroweak gauge theory requires new physics to tame the divergences associated with the Higgs potential. By the most conservative estimates this new physics is within our reach. Avoiding fine tuning requires $\Lambda \lesssim 2 - 3$ TeV to be revealed by the CERN Large Hadron Collider (LHC), possibly by the Tevatron. For instance, for $M_H = 115 - 200$ GeV,

$$\left| \frac{\delta M_H^2}{M_H^2} \right| = \frac{\delta v^2}{v^2} \leq 10 \Rightarrow \Lambda = 2 - 3 \text{ TeV} . \quad (32)$$

Any physics which may turn on beyond the electroweak scale can easily enhance weak interaction cross sections beyond Standard Model predictions. In this context, neutrino telescopes provide an important probe of new ideas in particle physics. One caveat for the realization of such a program is that the event rates depend on the as yet unknown extraterrestrial neutrino flux, generating an ambiguity in obtaining cross sections from event rates. However, the event rates for up-coming and down-going neutrinos have different responses to the inelastic cross section [61]. Therefore, a full study in the two-dimensional parameter space (cross section and flux) can serve as a powerful testbed for probing anomalous neutrino interactions [62, 63]. Bounds (or discovery potential) of neutrino fluxes emerge in a correlated fashion with the cross section probes.

Physics at the high energy frontier is the physics of partons. We master this physics with unforseen precision because of a decade of steadily improving HERA measurements of the nucleon structure [64]. These now includes experiments using targets of polarized protons and neutrons. HERA is our nucleon microscope, tunable by the wavelength and the fluctuation time of the virtual photon exchanged in the electron proton collision. The wavelength of the virtual photons probing the nucleon is reduced with increased momentum transfer Q . The proton has now been probed to 10^{-3} fm, about one-thousandth of its size. In the interaction, the fluctuations of the virtual photons survive over distances $ct \sim 1/x$, where x is the relative momentum of the parton. HERA now studies the production of chains of gluons as long as 10 fm, an order of magnitude larger than and probably insensitive to the proton target. These are novel QCD structures, the understanding of which has been

challenging. The xQ region probed by cosmic neutrinos lies in this challenging region, beyond the reach of the HERA experiments. It is therefore necessary to think of reliable methods for extrapolating the structure functions to very low x . For the purpose of phenomenological studies, we have chosen to use the parametrizations of the CC

$$\sigma_{\text{CC}} = 5.53 \left(\frac{E_\nu}{\text{GeV}} \right)^{0.363} \text{ pb}, \quad (33)$$

and NC

$$\sigma_{\text{NC}} = 2.31 \left(\frac{E_\nu}{\text{GeV}} \right)^{0.363} \text{ pb}, \quad (34)$$

neutrino-nucleon cross sections, as derived in [65] using the CTEQ4 parton distribution functions [66].

Deviations of the neutrino-nucleon cross sections from the simple parton model can result from more sophisticated treatments of QCD or from new physics beyond the Standard Model. Included in the former are saturation effects which can substantially modify simple parton results at small x [67]. These effects can significantly alter the total cross section at high energies [68], softening the power law behavior predicted by the simple parton model toward compliance with the Froissart bound [69]. At the forefront of the new physics category are scenarios based on TeV-scale quantum gravity [70]. Enhancements of the neutrino cross section in this framework may come from exchange of towers of Kaluza-Klein gravitons [71] and black hole production [72]. Similar enhancements may originate from TeV-scale string excitations [73], electroweak instanton processes [74], or in some supersymmetric models through direct channel production of superpartner resonances [75].

In what follows we discuss the potential of IceCube to reveal deviations of the neutrino-nucleon cross section from Standard Model predictions or to set limits on such deviations, without assuming particular neutrino fluxes or cross sections. It will be convenient, however, to present results relative to standard reference values. For the reference cross section, we adopt σ_{SM} the neutrino-nucleon cross section of the simple parton model given in Eq. (33).² For the reference flux, we adopt the WB flux ϕ_{WB}^ν given in Eq. (25). Altogether, in the energy range $10^{7-7.5}$ GeV, after applying selection criteria necessary for good energy resolution, we estimate an effective integrated luminosity (over the lifetime of the experiment) $\mathcal{L} \approx 30 \text{ nb}^{-1}$. At an average energy $\langle E \rangle = 10^{7.25}$ GeV, $\phi_{\text{WB}}^\nu \simeq 4 \times 10^{-23} \text{ GeV}^{-1} \text{ cm}^{-2} \text{ s}^{-1} \text{ sr}^{-1}$ per flavor and $\sigma_{\text{SM}}(\langle E \rangle) \simeq 2 \times 10^{-33} \text{ cm}^2$. In order to separate the flux and cross section contributions to the event rate, we require two independent pieces of data, which hereafter we identify as up-coming and down-going events.

For down-going events, the probability of neutrino conversion is always small, barring extraordinary enhancements to neutrino cross sections. Letting $\sigma_{\nu N}$ denote the total (NC + CC) neutrino-nucleon cross section, the down-going event rate is therefore

$$\mathcal{N}_{\text{down}} = C_{\text{down}} \frac{\phi^\nu}{\phi_{\text{WB}}^\nu} \frac{\sigma_{\nu N}}{\sigma_{\text{SM}}}, \quad (35)$$

where ϕ^ν indicates the average extraterrestrial $\nu + \bar{\nu}$ flux per flavor in the energy bin of interest. The constant C_{down} depends on exposure and varies according to neutrino flavor

² We neglect NC interactions, which at these energies serve only to reduce the neutrino energy by approximately 20%.

from experiment to experiment. Here, $\sigma_{\nu N}$ indicates any enhancement of the cross section which will increase the event rate for down-going neutrinos, but because of absorption will suppress the up-coming events. The latter can be achieved through cuts on shower energy fraction greater than or equal to that characterizing the CC Standard Model process.

For up-going events, the dependence on cross section is completely different. At energies above 10^6 GeV, neutrino interaction lengths become smaller than the radius of the Earth, $R_{\oplus} \approx 6371$ km. This implies that most upward-going neutrinos are shadowed by the Earth, and only those that are traveling at large nadir angles along chords, $\ell = 2R_{\oplus} \cos \theta$, with lengths of order their interaction length, $l_{\nu}(E_{\nu}) = [\rho_{\text{crust}} N_A \sigma_{\nu N}(E_{\nu})]^{-1}$, can produce a visible signal ($\rho_{\text{crust}} \simeq 2.65$ g cm $^{-3}$ is the Earth's crust density) [76].

The dependence of upward-going event rates on anomalous neutrino cross sections depends on the source of the anomaly. We consider two prominent cases. First, in many new physics cases, the Standard Model CC cross section σ_{SM} is not altered, but there are new neutrino interactions that produce showers. For $E_{\nu} > 10^7$ GeV, the neutrino interaction length satisfies $l_l \ll l_{\nu} < R_{\oplus}$, and so the up-going event rate is [62]

$$\mathcal{N}_{\text{up}} = C_{\text{up}} \frac{\phi_{\text{WB}}^{\nu}}{\phi_{\text{WB}}^{\nu}} \frac{\sigma_{\text{SM}}^2}{\sigma_{\nu N}^2} \left(\frac{\sigma_{\nu N}}{\sigma_{\text{SM}}} > 1 \right), \quad (36)$$

where l_l is the typical lepton path length in Earth. Extreme enhancements to $\sigma_{\nu N}$ may reduce l_{ν} to l_l , leading to a different parametric dependence in Eq. (36), but such cases are neglected here. Next we consider the possibility of screening. In order to probe deviations from the unscreened parton model calculations of the cross section, it is necessary to note that the screening correction affects CC and NC equally. In this case one finds [61, 62],

$$\mathcal{N}_{\text{up}} = C_{\text{up}}^{\text{screen}} \frac{\phi_{\text{WB}}^{\nu}}{\phi_{\text{WB}}^{\nu}} \frac{\sigma_{\text{SM}}}{\sigma_{\nu N}}, \quad (37)$$

where $\sigma_{\nu N}$ and σ_{SM} are CC cross sections with and without screening, respectively.

Constraints on the two-parameter space can be obtained using AMANDA data. To see this, we note that the 90% CL upper bound on the diffuse neutrino flux

$$E_{\nu}^2 \phi_{\text{max}}^{\nu} = 3.3 \times 10^{-7} \text{ GeV cm}^{-2} \text{ s}^{-1} \text{ sr}^{-1} \quad (38)$$

(per flavor) reported by the AMANDA Collaboration [36] was derived on the basis of CC neutrino interactions within Standard Model physics, assuming an E_{ν}^{-2} dependence of the flux, valid for 10^6 GeV to $10^{9.5}$ GeV neutrinos. In full generality, the stated quantity ϕ_{max}^{ν} constitutes two joint constraints on *two* unknowns: the diffuse neutrino flux and any deviation of the simple parton model neutrino-nucleon cross sections. Since the energy distribution of the AMANDA data peaks in the energy bin of interest, it is reasonable to use $\phi_{\text{max}}^{\nu}(\langle E \rangle)$ as the upper limit in the bin. Applied to down-going events, the constraint implies

$$\phi^{\nu} \frac{\sigma_{\nu N}}{\sigma_{\text{SM}}} < \phi_{\text{max}}^{\nu}. \quad (39)$$

Dividing Eq. (39) by ϕ_{WB}^{ν} gives

$$\frac{\phi^{\nu}}{\phi_{\text{WB}}^{\nu}} \frac{\sigma_{\nu N}}{\sigma_{\text{SM}}} < 26 \quad (40)$$

at 90% CL. A similar analysis for up-going events yields

$$\frac{\phi^{\nu}}{\phi_{\text{WB}}^{\nu}} \frac{\sigma_{\text{SM}}^2}{\sigma_{\nu N}^2} < 26 \quad (41)$$

for the case of new physics contributions, and

$$\frac{\phi^\nu}{\phi_{\text{WB}}^\nu} \frac{\sigma_{\text{SM}}}{\sigma_{\nu N}} < 26 \quad (42)$$

for the case of screening. These constraints exclude the shaded and cross-hatched regions of Fig. 7. The shaded region is excluded by down-going data, and the cross-hatched region is excluded by the up-going data, assuming screening. The shaded and cross-hatched regions meet at $\sigma_{\nu N}/\sigma_{\text{SM}} = 1$. As a result, irrespective of cross section assumptions, one finds an upper bound on the neutrino flux in the energy range 10^7 GeV to $10^{7.5}$ GeV of $\phi^\nu < 26\phi_{\text{WB}}^\nu$.

How will these results improve in the near future? To evaluate the prospects for IceCube, one must determine C_{down} and C_{up} . We focus on the case in which new neutrino interactions modify the NC cross sections, but leave the CC cross sections invariant. In NC processes most of the energy is carried off by pions. At TeV energies, the interaction mean free path of π^\pm in ice is orders of magnitude smaller than the pion decay length, and so nearly all energy is channeled into electromagnetic modes through π^0 decay. To estimate the efficiencies for down-going events in the NC channel, we therefore adopt as our basis of comparison the electromagnetic showers induced by ν_e . With this in mind,

$$\begin{aligned} C_{\text{down}} &= 2\pi T \int \phi_{\text{WB}}^\nu \sigma_{\text{SM}} n_T dE_\nu \\ &\approx 2\pi \phi_{\text{WB}}^\nu(\langle E \rangle) \sigma_{\text{SM}}(\langle E \rangle) n_T(\langle E \rangle) T \Delta E, \end{aligned} \quad (43)$$

where $n_T(\langle E \rangle) \simeq 6 \times 10^{38}$. Inserting these numbers into Eq. (43), along with a lifetime of the experiment $T = 15$ yr and $\Delta E = 2.2 \times 10^7$ GeV, one obtains $C_{\text{down}} \simeq 3$. The ν_e atmospheric background is taken to be zero, (the potential “prompt” component can be eliminated by taking advantage of the isotropic ν_μ -channel). To determine the corresponding quantity for up-going events C_{up} , we first note that the absence of oscillation precludes a ν_τ atmospheric background. For this reason the detection prospects for up-going neutrinos (with 10^7 GeV $< E_\nu < 10^{7.5}$ GeV) are brighter for ν_τ than the other flavors, and we focus on them below. From Figs. 1 and 3, after correcting for the Earth’s absorption effects, one obtains the ν_τ effective aperture, $(A\Omega)_{\text{eff}} \sim \pi \text{ km}^2 \text{ sr}$. Thus, the normalization constant for τ ’s showering in IceCube is found to be

$$C_{\text{up}} = (A\Omega)_{\text{eff}} T \int \phi^\tau(E) dE \approx 25, \quad (44)$$

where [77]

$$\begin{aligned} \int \phi^\tau(E) dE &\approx \int 2 \times 10^{-3} \phi_{\text{WB}}^\nu(E_\nu) dE_\nu \\ &\approx 5.5 \times 10^{-1} \text{ km}^{-2} \text{ yr}^{-1} \text{ sr}^{-1} \end{aligned} \quad (45)$$

is the τ -lepton flux produced in ν_τ interactions inside the Earth for $\sigma_{\nu N} = \sigma_{\text{SM}}$.

Given these estimates of C_{down} and C_{up} , one can now determine projected sensitivities of IceCube to neutrino fluxes and cross sections. The quantities \mathcal{N}_{up} and $\mathcal{N}_{\text{down}}$ as defined in Eqs. (35) and (36) can be regarded as the theoretical values of these events, corresponding to different points in the $\sigma_{\nu N}/\sigma_{\text{SM}}$, $\phi^\nu/\phi_{\text{WB}}^\nu$ parameter space. For a given set of observed rates $\mathcal{N}_{\text{up}}^{\text{obs}}$ and $\mathcal{N}_{\text{down}}^{\text{obs}}$, two curves are obtained in the two-dimensional parameter space by

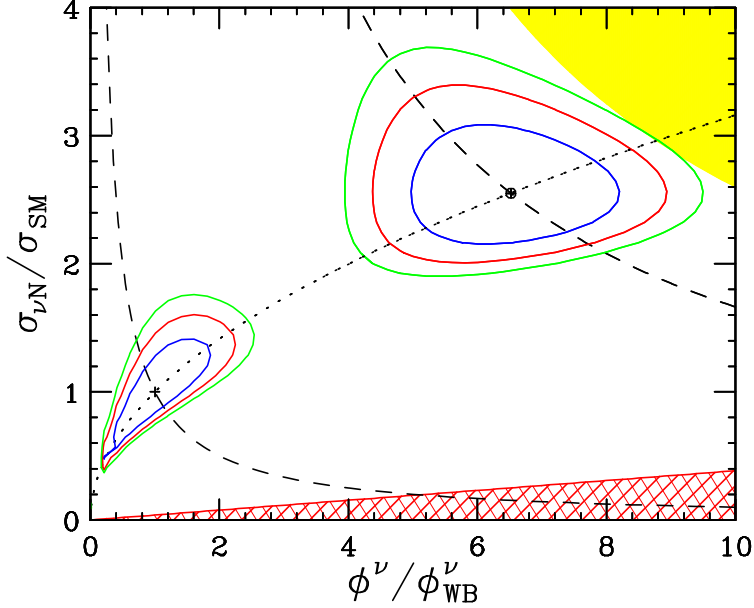


FIG. 7: Projected determinations of neutrino fluxes and cross sections at $\sqrt{s} \approx 6$ TeV from future IceCube data. Two cases with $(\mathcal{N}_{\text{down}}^{\text{obs}}, \mathcal{N}_{\text{up}}^{\text{obs}}) = (3, 25)$ and $(50, 25)$ are considered. In both cases, the best fit flux and cross sections are shown, along with the 90%, 99%, and 99.9% CL exclusion contours. Contours of constant $\mathcal{N}_{\text{up}}^{\text{obs}} = 25$ (dotted), $\mathcal{N}_{\text{down}}^{\text{obs}} = 3$ (left dashed), and $\mathcal{N}_{\text{down}}^{\text{obs}} = 50$ (right dashed) are also shown. Neutrino fluxes and cross sections excluded by AMANDA at 90%CL [36] are also indicated: The shaded (cross-hatched) region is excluded by null results for down-going (up-going) events [63].

setting $\mathcal{N}_{\text{up}}^{\text{obs}} = \mathcal{N}_{\text{up}}$ and $\mathcal{N}_{\text{down}}^{\text{obs}} = \mathcal{N}_{\text{down}}$. These curves intersect at a point, yielding the most probable values of flux and cross section for the given observations. Fluctuations about this point define contours of constant χ^2 in an approximation to a multi-Poisson likelihood analysis. The contours are defined by

$$\chi^2 = \sum_i 2 [\mathcal{N}_i - \mathcal{N}_i^{\text{obs}}] + 2 \mathcal{N}_i^{\text{obs}} \ln [\mathcal{N}_i^{\text{obs}} / \mathcal{N}_i] , \quad (46)$$

where $i = \text{up, down}$ [78].

In Fig. 7, we show results for two representative cases that are consistent with the AMANDA bounds derived above. In the first case, we assume $\sigma_{\nu N} = \sigma_{\text{SM}}$ and $\phi^{\nu} = \phi^{\nu}_{\text{WB}}$, leading to 3 down-going and 25 up-going events. The 90%, 99%, and 99.9% CL contours are those given in the lower left of the figure. (These contours will be slightly distorted for $\sigma_{\nu N} / \sigma_{\text{SM}} < 1$, where Eq. (36) receives corrections, but we neglect this effect.) We see that, even in the case that event rates are in accord with standard assumptions, the neutrino-nucleon cross section is bounded to be within 40% of the Standard Model prediction at 90% CL. This is at a center-of-mass energy $\sqrt{s} \simeq 6$ TeV, far beyond the reach of any future man-made accelerator.³ In the second case, we consider a scenario in which the number of

³ For small x physics, Standard Model predictions for neutrino-nucleon collisions at $\sqrt{s} \simeq 6$ TeV probe x down to $M_W^2/s \sim 2 \times 10^{-4}$ [79]; LHC will probe parton center-of-mass energies $\sqrt{\hat{s}} \gtrsim 50$ GeV (twice

observed upcoming events remains at 25, but the number of down-going events is 50. In the second case, clearly one has discovered new physics at well beyond 5σ .

The analysis discussed in this section is very general as the technique to extract the cross section is model independent and can be readily extended to probe higher energy bins. From Fig. 5 one can see that, if there are hidden sources in the heavens, we expect C_{down} and C_{up} to be about a factor of 15 higher, making it possible for IceCube to probe 40% (70%) enhancements from Standard Model predictions at the 90% (99.9%) CL after only 1 year of observation.

V. FLAVOR METAMORPHOSIS

A. Neutrino Oscillations

The Standard Model is based on the gauge group

$$G_{\text{SM}}^{\text{gauge}} = SU(3)_C \times SU(2)_L \times U(1)_Y, \quad (47)$$

with three fermion generations. A single generation consists of five different representations of the gauge group: $Q_L(3, 2, 1/6)$, $U_R(3, 1, 2/3)$, $D_R(3, 1, -1/3)$, $L_L(1, 2, -1/2)$, $E_R(1, 1, -1)$; where the numbers in parenthesis represent the corresponding charges under $G_{\text{SM}}^{\text{gauge}}$. The left handed fermions belong to $SU_L(2)$ doublets while the right handed chiralities to $SU_L(2)$ singlets. The model contains a single Higgs boson doublet, $H(1, 2, 1/2)$, whose vacuum expectation value breaks the gauge symmetry $G_{\text{SM}}^{\text{gauge}}$ into $SU(3)_C \times U(1)_{\text{EM}}$. The Standard Model also comprises an accidental global symmetry

$$G_{\text{SM}}^{\text{global}} = U(1)_B \times U(1)_e \times U(1)_\mu \times U(1)_\tau, \quad (48)$$

where $U(1)_B$ is the baryon number symmetry, and $U(1)_{e,\mu,\tau}$ are three lepton flavor symmetries, with total lepton number given by $L = L_e + L_\mu + L_\tau$. It is an accidental symmetry because we do not impose it. It is a consequence of the gauge symmetries and the low energy particle content. It is possible (but not necessary), however, that effective interaction operators induced by the high energy content of the underlying theory may violate sectors of the global symmetry.

In the Standard Model charged lepton (and also quark) masses arise from Yukawa interactions, which couple the right-handed fermion singlets to the left-handed fermion doublets and the Higgs doublet

$$\mathcal{L}_{\text{SM}}^{\text{Yukawa}} = \lambda_l \bar{L}_L H E_R + \text{h.c.} \quad (49)$$

After spontaneous electroweak symmetry breaking these interactions lead to charged fermion masses, $m_l = \lambda_l v/\sqrt{2}$, but leave the neutrinos massless. No Yukawa interaction can be written that would give a tree level mass to the neutrino because no right-handed neutrino field exists in the Standard Model. One could think that neutrino masses could arise from loop corrections. This, however, cannot be the case, because any neutrino mass term that can be constructed with the Standard Model fields would violate the total lepton symmetry.

the minimum jet trigger threshold), corresponding to $x \gtrsim 50/14000 \sim 3 \times 10^{-3}$. A future hadron collider would require $\sqrt{s} \sim 200$ TeV to sample $x \approx 2 \times 10^{-4}$.

In other words, the Standard Model predicts that neutrinos are *strictly* massless, and thus there is neither mixing nor CP violation in the leptonic sector.

In recent years, stronger and stronger experimental evidence for nonzero neutrino masses has been accumulating [80]. The weak interaction coupling the W boson to a charged lepton and a neutrino, can also couple any charged lepton mass eigenstate l_α ($\alpha = e, \mu, \tau$) to any neutrino mass eigenstate ν_j ($j = 1, 2, 3$). The superposition of neutrino mass eigenstates produced in association with the charged lepton of flavor α , $|\nu_\alpha\rangle = \sum_j U_{\alpha j}^* |\nu_j\rangle$, is the state we refer to as the neutrino of flavor alpha, where $U_{\alpha j}$'s are elements of the neutrino mass-to-flavor mixing matrix, fundamental to particle physics. The density matrix of a flavor state, ρ^α , can be expressed in terms of mass eigenstates by $\rho^\alpha = |\nu_\alpha\rangle\langle\nu_\alpha| = \sum_{i,j} U_{\alpha i}^* U_{\alpha j} |\nu_i\rangle\langle\nu_j|$. This is a pure quantum system, therefore the density matrix satisfies $\text{Tr } \rho^2 = \text{Tr } \rho = 1$. The time evolution of the density matrix

$$\frac{\partial \rho}{\partial t} = -i [H, \rho] , \quad (50)$$

is governed by the Hamiltonian H of the system, thereby after traveling a distance L an initial state ν_α becomes a superposition of all flavors, with probability of transition to flavor β given by $P_{\nu_\alpha \rightarrow \nu_\beta} = \text{Tr}[\rho_\alpha(t)\rho_\beta]$, or equivalently [4]

$$\begin{aligned} P_{\nu_\alpha \rightarrow \nu_\beta} &= \delta_{\alpha\beta} - 4 \sum_{i>j} \Re (U_{\alpha i}^* U_{\beta i} U_{\alpha j} U_{\beta j}^*) \sin^2 \Delta_{ij} \\ &\quad + 2 \sum_{i>j} \Im (U_{\alpha i}^* U_{\beta i} U_{\alpha j} U_{\beta j}^*) \sin 2\Delta_{ij} , \end{aligned} \quad (51)$$

where $\Delta_{ij} = 1.27 \delta m_{ij}^2 L / E_\nu$, with L measured in km, E_ν in GeV and $\delta m_{ij}^2 = m_i^2 - m_j^2$ in eV².

The simplest and most direct interpretation of the atmospheric data [81] is that of muon neutrino oscillations. The evidence of atmospheric ν_μ disappearing is now at $> 15\sigma$, most likely converting to ν_τ . The angular distribution of contained events shows that for $E_\nu \sim 1$ GeV, the deficit comes mainly from $L_{\text{atm}} \sim 10^2 - 10^4$ km. The corresponding oscillation phase must be maximal, $\Delta_{\text{atm}} \sim 1$, which requires $\delta m_{\text{atm}}^2 \sim 10^{-4} - 10^{-2}$ eV². Moreover, assuming that all upgoing ν_μ 's which would lead to multi-GeV events oscillate into a different flavor while none of the downgoing ones do, the observed up-down asymmetry leads to a mixing angle very close to maximal, $\sin^2 2\theta_{\text{atm}} > 0.85$. These results have been confirmed by KEK-to-Kamioka (K2K) which observes the disappearance of accelerator ν_μ 's at a distance of 250 km and find a distortion of their energy spectrum with a CL of $2.5 - 4\sigma$ [82]. The combined analysis leads to a best fit-point and 1σ ranges, $\delta m_{\text{atm}}^2 = 2.2_{-0.4}^{+0.6} \times 10^{-3}$ eV² and $\tan^2 \theta_{\text{atm}} = 1_{-0.26}^{+0.35}$ [80]. On the other hand, reactor data [83] point to $|U_{e3}|^2 \ll 1$. Thus, to simplify the discussion hereafter we use the fact that $|U_{e3}|^2$ is nearly zero to ignore CP violation and assume real matrix elements. The simple vacuum relations between the neutrino states produced by the weak interactions are then

$$\begin{aligned} |\nu_1\rangle &= \frac{1}{\sqrt{2}} \sin \theta_\odot (|\nu_\mu\rangle - |\nu_\tau\rangle) - \cos \theta_\odot |\nu_e\rangle \\ |\nu_2\rangle &= \frac{1}{\sqrt{2}} \cos \theta_\odot (|\nu_\mu\rangle - |\nu_\tau\rangle) + \sin \theta_\odot |\nu_e\rangle \\ |\nu_3\rangle &= \frac{1}{\sqrt{2}} (|\nu_\mu\rangle + |\nu_\tau\rangle) \end{aligned} \quad (52)$$

where θ_\odot is the solar mixing angle. Data collected by the SuperKamiokande (SK) [41] and the Sudbury Neutrino Observatory (SNO) [84] show that solar ν'_e 's convert to ν_μ or ν_τ with CL of more than 7σ . The KamLAND Collaboration [85] have measured the flux of $\bar{\nu}_e$ from distant reactors and find that $\bar{\nu}_e$'s disappear over distances of about 180 km. The combined analysis of solar and KamLAND data allows a region at 3σ CL with best-fit point and 1σ ranges: $\delta m_\odot^2 = 8.2_{-0.3}^{+0.3} \times 10^{-5}$ eV 2 and $\tan^2 \theta_\odot = 0.39_{-0.04}^{+0.05}$ [86].

Altogether, neutrinos are massive and therefore the Standard Model needs to be extended. The most economic way to get massive neutrinos would be to introduce the right-handed neutrino states (having no gauge interactions, these sterile states would be essentially undetectable and unproduceable) and obtain a Dirac mass term by means of Yukawa coupling. However, in order to get reasonable neutrino masses (below the eV range) the Yukawa coupling would have to be unnaturally small $\lambda_\nu < 10^{-11}$; the Yukawa couplings range from $\lambda_t \simeq 1$ for the top quark down to $\lambda_e \simeq 10^{-5}$ for the electron. All other attempts to give masses to the neutrinos require to extend the Standard Model in more radical ways. Throughout this review we will not concern ourselves with the origin of the neutrino masses (for a comprehensive discussion of this subject see e.g., [87]), we simply assume that neutrino acquire mass by some mechanism and discuss the reach of IceCube in probing physics beyond conventional neutrino mass-induced oscillations. The methods summarized in this section are readily applicable to probe speculations on other non-conventional physics associated with neutrino flavor mixing.

The only other interaction a neutrino can feel, besides the weak, is the gravitational interaction. A gravitational field, could contribute to neutrino oscillations if the different neutrino flavors would be differently affected by gravity, i.e., if the equivalence principle would be violated by gravity [88]. The deviation can be parametrized by assuming that the post-Newtonian parameters in the expansion of a given metric have a species dependent value, representing thus the effective coupling constant of the different flavors to a given geometry. In the weak field limit of a static source, to first order in the Newtonian potential $\phi = GM/r \ll 1$, one can consider the metric to be $g_{tt} = 1 - 2\gamma\phi$ and $g_{ij} = -\delta_{ij}(1 + 2\tilde{\gamma}\phi)$. The parameters γ and $\tilde{\gamma}$ are theory dependent (e.g., $\gamma = \tilde{\gamma} = 1$ in General Relativity), but for any given theory, their value is universal (the same for all kinds of particles) only if the principle of equivalence is satisfied. Otherwise their value could be different for test particles with different internal quantum numbers and or different energies.

Of particular interest here, for neutrinos and photons received from the SN87 it has been shown [89] that the value of $\tilde{\gamma}$ is the same to an accuracy of about 0.1%. Moreover, if neutrinos are light, $\tilde{\gamma}$ is the same for neutrinos (and antineutrinos [90]) of different energies (ranging from 7 to 40 MeV) up to an accuracy of one part in 10^6 . It is worthwhile to note that the above results have been obtained with the hypothesis $\gamma = 1$. This hypothesis holds with a data set containing only one type of particle, as possible deviations of γ from 1 can be absorbed by redefining the mass of the source. The hypothesis may not be justified however, if we compare different particles or particles with different energies, since the value of γ can be particle dependent or energy dependent just like $\tilde{\gamma}$. The laboratory experiments on neutrino oscillations testing the universality of the gravitational redshift provide information on the possibility that the value of γ be different for different neutrino flavors. If there are deviation from universality in the value of γ , in fact, the energy splitting induced by gravity may contribute in general to the transition probability between different flavors, even if gravity is not the primary source of oscillations, i.e., even if the energy eigenstates are unchanged by the weak gravitational field present in the laboratory.

At this stage it is worthwhile to point out that for a constant potential ϕ , a violation of the equivalence principle is phenomenologically equivalent to the breakdown of Lorentz invariance resulting from different asymptotic values of the velocity of the neutrinos, $c_1 \neq c_2$, with ν_1 and ν_2 being related to ν_μ and ν_τ by a rotation of an angle ξ_{vli} [91].

Gravity induced neutrino oscillations can also arise if the spacetime manifold has a non-symmetric Christoffel connection [92]. This is because the flavor eigenstates produce in the charged weak interactions are not, in general, the eigenstates of the torsion Hamiltonian, and then the oscillations can be strongly damped or enhanced in the presence of strong gravitational fields. The torsion eigenstates can be interpreted as different mixtures of right-handed and left-handed fields, yielding a deviation of the weak neutrino current from the standard $V - A$ form. For this vector-like interaction the gravity-induced oscillation wavelength is energy independent. Violation of CPT resulting from Lorentz-violating effects also leads to an energy independent contribution to the oscillation wavelength [93] which is a function of the eigenvalues of the Lorentz violating CPT-odd operator and the rotation angle between the corresponding neutrino eigenstates ν_i and the flavor eigenstates ν_α .

In the most general situation in which neutrinos are massive and gravity may contribute to the transition probability between different flavors, we may have $|\nu_\alpha\rangle \neq |\nu_i\rangle \neq |\nu_G\rangle$, where $|\nu_G\rangle$ denotes hypothetical gravity eigenstates. The eigenstates of the total energy are obtained by diagonalizing the matrix which includes the contributions of the mass and gravitational terms. In the case of 2 flavor mixing, the total matrix for neutrino (+) or antineutrino (-) oscillations can be written as [94]

$$H_\pm \equiv \frac{\delta m_{ij}^2}{4E_\nu} \mathbf{U}_\theta \begin{pmatrix} -1 & 0 \\ 0 & 1 \end{pmatrix} \mathbf{U}_\theta^\dagger + \sum_n \sigma_n^\pm \frac{\delta_n E_\nu^n}{2} \mathbf{U}_{\xi_n, \pm \eta_n} \begin{pmatrix} -1 & 0 \\ 0 & 1 \end{pmatrix} \mathbf{U}_{\xi_n, \pm \eta_n}^\dagger, \quad (53)$$

where σ_n^\pm accounts for a possible relative sign of the gravity effects between neutrinos and antineutrinos⁴ and δ_n parametrizes the size of the new physics terms. The matrices \mathbf{U}_θ and $\mathbf{U}_{\xi_n, \pm \eta_n}$ are given by

$$\mathbf{U}_\theta = \begin{pmatrix} \cos \theta & \sin \theta \\ -\sin \theta & \cos \theta \end{pmatrix}, \quad \mathbf{U}_{\xi_n, \pm \eta_n} = \begin{pmatrix} \cos \xi_n & \sin \xi_n e^{\pm i \eta_n} \\ -\sin \xi_n e^{\mp i \eta_n} & \cos \xi_n \end{pmatrix}; \quad (54)$$

where η_n denotes the possible non-vanishing relative phases. Note that in contrast to the conventional oscillation length, new physics predicts neutrino oscillations with wavelengths that are constant or decrease with energy. Therefore, IceCube with an energy reach in the $10^2 \text{ GeV} < E_\nu < 10^6 \text{ GeV}$ range for atmospheric neutrinos, is the ideal experiment to search for new physics. Moreover, these neutrinos have large enough energy for standard δm_{ij}^2 oscillations to be very much suppressed so ν 's should behave as flavor eigenstates. For simplicity, in what follows we concentrate on oscillations resulting from tensor-like interactions that lead to an oscillation wavelength inversely proportional to the neutrino energy. The results can be directly applied to oscillations due to violations of the equivalence principle with the identification of $\xi_1 = \xi_{\text{vep}}$ and $\delta_1 = 2|\phi|(\gamma_1 - \gamma_2) \equiv 2|\phi|\Delta\gamma$, as well as oscillations due to violations of local Lorentz invariance with the identification, $\xi_1 = \xi_{\text{vli}}$ and $\delta_1 = \Delta c/c$.

If the effects of new physics are constant along the neutrino trajectory, the survival probability for total oscillation length L_{tot} takes the form [94]

$$P_{\nu_\mu \rightarrow \nu_\mu} = 1 - P_{\nu_\mu \rightarrow \nu_\tau} = 1 - \sin^2 2\Theta \sin^2 (\Delta_{ij} \mathcal{R}), \quad (55)$$

⁴ For the CPT violating case $\sigma^+ = -\sigma^-$, otherwise $\sigma^+ = \sigma^-$.

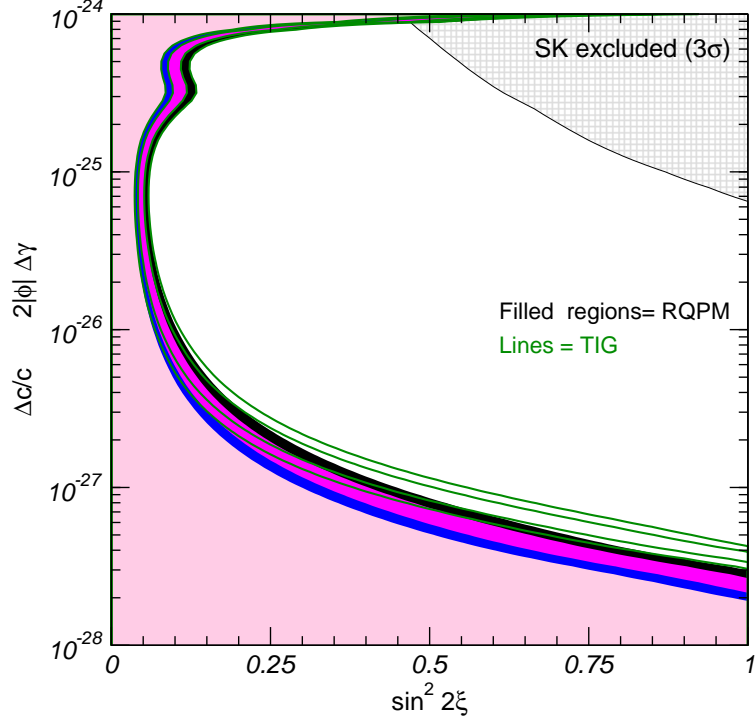


FIG. 8: Sensitivity limits in the $(\Delta c/c, \xi_{\text{vli}})$ and $(2|\phi|\Delta\gamma, \xi_{\text{vep}})$ planes at 90%, 95%, 99% and 3σ CL. To account for the uncertainty associated with the poorly known prompt neutrino fluxes results for two extreme models are shown: TIG [18] (full lines) and RQPM [21] (filled regions). The difference is about 50% in the strongest bound on δ_1 . The hatched area in the upper right corner is the present 3σ bound from the analysis of SK and K2K data [5].

where $\mathcal{R} = L_{\text{atm}}/L_{\text{tot}}$; if the contributions of mass and gravity are both non-vanishing then

$$\mathcal{R} = \sqrt{1 + R^2 + 2R(\cos 2\theta_{\text{atm}} \cos 2\xi_1 + \sin 2\theta_{\text{atm}} \sin 2\xi_1 \cos \eta_1)}. \quad (56)$$

Here, Θ is the rotation angle which diagonalizes the matrix in Eq. (53),

$$\sin^2 2\Theta = \frac{1}{\mathcal{R}^2} (\sin^2 2\theta_{\text{atm}} + R^2 \sin^2 2\xi_1 + 2R \sin 2\theta_{\text{atm}} \sin 2\xi_1 \cos \eta_1), \quad (57)$$

and

$$R \equiv \frac{L_{\text{atm}}}{L_G} = \frac{\delta_1 E_\nu}{2} \frac{4E_\nu}{\delta m_{ij}^2}, \quad (58)$$

where L_G defines the gravity oscillation length.

The experimental probes of neutrino oscillations, measuring P , provide simultaneously information on Θ and L_{tot} . In the absence of positive results, however, an upper bound on P does not fix any value for Θ and L_{tot} separately: it determines only an allow region in the (Θ, L_{tot}) plane, or equivalently in the (ξ_1, δ_1) plane. At present, the strongest limits on new physics neutrino oscillations arise from the non-observation of departure from the δm_{atm}^2 oscillation behavior in atmospheric neutrinos at SK, and the confirmation of ν_μ oscillations with the same oscillation parameters from K2K. The 3σ bounds from the up-to-date combined analysis [95] of SK and K2K data are shown in Fig. 8.

$\log_{10}(E_\mu^{\text{fin}}/\text{GeV})$	RPQM		TIG	
	$-1 \leq \cos \theta \leq -0.6$	$-0.6 \leq \cos \theta \leq -0.2$	$-1 \leq \cos \theta \leq -0.6$	$-0.6 \leq \cos \theta \leq -0.2$
2.00 – 2.20	52474	61806	51427	60920
2.20 – 2.40	46234	55598	44987	54539
2.40 – 2.60	35965	44586	34634	43422
2.60 – 2.80	26001	33588	24647	32415
2.80 – 3.00	17358	23400	16107	22294
3.00 – 3.20	10710	15126	9630	14141
3.20 – 3.40	6172	9054	5320	8250
3.40 – 3.60	3330	5099	2701	4494
3.60 – 3.80	1721	2722	1289	2291
3.80 – 4.00	856	1388	578	1098
4.00 – 4.20	410	685	242	498
4.20 – 4.40	191	330	96	215
4.40 – 4.60	86	156	36	89
4.60 – 4.80	38	74	13	36
4.80 – 5.00	16	34	5	14
5.00 – 9.00	10	28	2	8

TABLE I: Number of expected atmospheric ν_μ -induced muon events in 10 years of IceCube operation in the 16 energy bins and angular bins discuss in the text, assuming no new physics effect is observed.

For most of the neutrino energies considered here, the standard mass-induced oscillations are suppressed and the gravity effect is directly observed. As a consequence, the results will be independent of the phase η_1 and one can set the new physics parameters to be in the range $\delta_1 \geq 0$ and $0 \leq \xi_1 \leq \pi/4$.

The Hamiltonian of Eq. (53) describes the coherent evolution of the ν_μ - ν_τ ensemble for any neutrino energy. High-energy neutrinos propagating in the Earth can also interact inelastically with the Earth matter and as a consequence the neutrino flux is attenuated. For atmospheric neutrinos oscillation, attenuation, and regeneration effects occur simultaneously when the neutrino beam travels across the Earth's matter. For the phenomenological analysis of conventional neutrino oscillations this fact can be ignored because the neutrino energies covered by current experiments are low enough for attenuation and regeneration effects to be negligible. Especially for non-standard scenario oscillations, future experiments probe high-energy neutrinos for which the attenuation and regeneration effects have to be accounted for simultaneously. Attenuation effects due to CC and NC interactions can be introduced by relaxing the condition $\text{Tr}(\rho) = 1$, so that Eq (50) can be re-written as [5]

$$\frac{\partial \rho}{\partial t} = -i[H, \rho] - \sum_{\alpha} \frac{1}{2l_{\nu}} \{\Pi_{\alpha}, \rho\} , \quad (59)$$

where l_{ν} is the neutrino mean free path and $\Pi_{\alpha} = \nu_{\alpha} \otimes \nu_{\alpha}^{\dagger}$ is the ν_{α} state projector.

Neutrino oscillations introduced by new physics effects result in an energy dependent distortion of the zenith angle distribution of atmospheric muon events. This effect can be quantify by evaluating the expected angular and E_{μ}^{fin} distributions in the IceCube detector

using Eq. (6) in conjunction with ν_μ (and $\bar{\nu}_\mu$) fluxes obtained after evolution in the Earth for different sets of new physics oscillation parameters. Together with ν_μ -induced muon events, oscillations also generate μ events from the CC interactions of the ν_τ flux which reaches the detector producing a τ that subsequently decays as $\tau \rightarrow \mu\bar{\nu}_\mu\nu_\tau$ and produces a μ in the detector. Generalizing the formulae given in Sec. II it is straightforward to see that the number of ν_τ -induced muon events is

$$\mathcal{N}_{\nu_\mu}^{\nu_\tau} = T \int_{-1}^1 d\cos\theta \int_{l_\mu^{\min}}^{\infty} dl_\mu \int_{m_\mu}^{\infty} dE_\mu^{\text{fin}} \int_{E_\mu^{\text{fin}}}^{\infty} dE_\mu^0 \int_{E_\mu^0}^{\infty} dE_\tau \int_{E_\tau}^{\infty} dE_\nu \frac{dF^{\nu_\tau}}{dE_\nu d\cos\theta}(E_\nu, \cos\theta) \frac{d\sigma_{\text{CC}}}{dE_\tau}(E_\nu, E_\tau) n_T \frac{dN_{\text{dec}}}{dE_\mu^0}(E_\tau, E_\mu^0) F(E_\mu^0, E_\mu^{\text{fin}}, l_\mu) A_{\text{eff}}^0, \quad (60)$$

where dN_{dec}/dE_μ^0 is given in Ref. [96]. To quantify the energy-dependent angular distortion one defines the vertical-to-horizontal double ratio

$$R_{\text{hor/ver}}(E_\mu^{\text{fin},i}) \equiv \frac{P_{\text{hor}}}{P_{\text{ver}}}(E_\mu^{\text{fin},i}) = \frac{\frac{\mathcal{N}_\mu^{\delta_1 \neq 0}(E_\mu^{\text{fin},i}, -0.6 < \cos\theta < -0.2)}{\mathcal{N}_\mu^{\delta_1 = 0}(E_\mu^{\text{fin},i}, -0.6 < \cos\theta < -0.2)}}{\frac{\mathcal{N}_\mu^{\delta_1 \neq 0}(E_\mu^{\text{fin},i}, -1 < \cos\theta < -0.6)}{\mathcal{N}_\mu^{\delta_1 = 0}(E_\mu^{\text{fin},i}, -1 < \cos\theta < -0.6)}}, \quad (61)$$

where $E_\mu^{\text{fin},i}$ denotes integration in an energy bin of width $0.2 \log_{10}(E_\mu^{\text{fin},i})$. This leads to 16 E_μ^{fin} bins in the data sample: 15 bins between 10^2 and 10^5 GeV and one containing all events above 10^5 GeV. Note that the double ratio eliminates uncertainties associated with the overall normalization of the atmospheric fluxes at high energies. Additionally, in the definition of the double ratio we have conservatively included only events well below the horizon $\cos\theta < -0.2$ to avoid the possible contamination from missreconstructed atmospheric muons which can still survive after level 2 cuts in the angular bins closer to the horizon. In order to estimate the expected sensitivity we assume that no new physics effect is observed and define a simple $\chi^2(\delta_1, \xi_1)$ function as

$$\chi^2(\delta_1, \xi_1) = \sum_{i=1}^{16} \frac{(R_{\text{hor/ver}}(E_\mu^{\text{fin},i}) - 1)^2}{\sigma_{\text{stat},i}^2} \quad (62)$$

where $\sigma_{\text{stat},i}$ is computed from the expected number of events in the absence of new physics effects. The expected event rates are given in Table I.

Figure 8 shows the sensitivity limits in the $[\delta_1, \xi_1]$ -plane at 90%, 95%, 99% and 3σ CL obtained from the condition $\chi^2(\delta_1, \xi_1) < \chi^2_{\text{max}}(\text{CL}, 2\text{dof})$. The figure illustrates the improvement on the present bounds by more than two orders of magnitude even within the context of this very conservative analysis. The loss of sensitivity at large δ_1 is a consequence of the use of a double ratio as an observable. Such an observable is insensitive to new physics effects if δ_1 is large enough for the oscillations to be always averaged leading only to an overall suppression.

B. Quantum Decoherence

What is the meaning of quantum gravity? It means that spacetime itself is subject to quantum laws, necessitating inherent fluctuations in the fabric (metric and topology) of space

and time. These microscopic boiling bubbles force on spacetime a foam-like structure [97]. A heuristic example pictures spacetime to be filled with tiny virtual black holes that pop in and out of existence on a timescale allowed by Heisenberg's uncertainty principle [98]. These black holes conserve energy, angular momentum, and electric and color charge (unbroken gauged quantum numbers), but they *are believed* not to conserve global quantum numbers. The transition between initial and final density matrices associated with black hole formation and evaporation is not factorizable into products of S -matrix elements and their hermitian conjugates. The evolution of such a quantum system is characterized by a superscattering operator \mathbb{S} that maps initial mixed states to final mixed states, $\rho_{\text{out}} = \mathbb{S}\rho_{\text{in}}$, with $\mathbb{S} \neq S^\dagger S$ [99]. In other words, there *may be* a loss of quantum information across the black hole event horizons, providing an environment that can induce decoherence of apparently isolated matter systems [100].

Of particular interest is the question whether fast baryon decay can proceed via virtual black hole states in the spacetime foam [101]. The process is envisioned as the simultaneous absorption of two quarks into the black hole, followed without memory of the initial state by the thermal emission of an antiquark and a lepton, entailing a change in the global baryon and lepton quantum numbers $qq \rightarrow \bar{q}l$. The probability that two quarks in a proton of size $\Lambda_{\text{QCD}}^{-1}$ pass within a fundamental Planck length, within the Heisenberg lifetime uncertainty of the black hole is $\propto (\Lambda_{\text{QCD}}/M_{\text{QG}})^4$, where M_{QG} is the gravitational UV cutoff. Thus, the present limit on the proton lifetime, $\tau_p \sim 10^{33}$ yr [102], implies $M_{\text{QG}} > 10^{16}$ GeV [101].⁵

Measurements of flavor transformations in a neutrino beam can provide a clean and sensitive probe of interactions with the spacetime foam. Without interference from the gravitational sector, oscillations in the neutrino sector provide a pure quantum phenomenon in which the density matrix has the properties of a projection operator. Because black holes do conserve energy, angular momentum (helicity), color and electric charge, any neutrino interacting with the virtual black holes needs to re-emerge as a neutrino. As an example, if spacetime foam black holes do not conserve $U(1)_e \times U(1)_\mu \times U(1)_\tau$, neutrino flavor is randomized by interactions with the virtual black holes. The result of many interactions is to equally populate all three possible flavors.

The Hamiltonian evolution in Eq. (50) is a characteristic of physical systems isolated from their surroundings. The time evolution of such a quantum system is given by the continuous group of unitarity transformations, $U_t = e^{-iHt}$, where t is the time. The existence of the inverse of the infinitesimal generator, H , which is a consequence of the algebraic structure of the group, guarantees *reversibility* of the processes. For open quantum-mechanical systems, the introduction of dissipative effects lead to modifications of Eq. (50) that account for the *irreversible* nature of the evolution. The transformations responsible for the time evolution of these systems are defined by the operators of the Lindblad quantum dynamical semi-groups [104]. Since this does not admit an inverse, such a family of transformations has the property of being only forward in time.

The Lindblad approach to decoherence does not require any detailed knowledge of the environment. The corresponding time evolution equation for the density matrix takes the

⁵ Note that interactions through the higher dimensional QQQL operator can be prevented if one separates the quark and lepton fields far enough in an extra dimension, so that their wave function overlap is exponentially suppressed [103].

form

$$\frac{\partial \rho}{\partial t} = -i[H_{\text{eff}}, \rho] + \mathcal{D}[\rho] , \quad (63)$$

where the decoherence term is given by

$$\mathcal{D}[\rho] = -\frac{1}{2} \sum_j \left([b_j, \rho b_j^\dagger] + [b_j \rho, b_j^\dagger] \right) . \quad (64)$$

Here, $H_{\text{eff}} = H + H_{\text{d}}$ is the effective Hamiltonian of the system, H is its free Hamiltonian, H_{d} accounts for possible additional dissipative contributions that can be put in the Hamiltonian form, and $\{b_j\}$ is a sequence of bounded operators acting on the Hilbert space of the open quantum system, \mathcal{H} , and satisfying $\sum_j b_j^\dagger b_j \in \mathcal{B}(\mathcal{H})$, where $\mathcal{B}(\mathcal{H})$ indicates the space of bounded operators acting on \mathcal{H} .

The intrinsic coupling of a microscopic system to the space-time foam can then be interpreted as the existence of an arrow of time which in turn makes possible the connection with thermodynamics via an entropy. The monotonic increase of the von Neumann entropy, $S(\rho) = -\text{Tr}(\rho \ln \rho)$, implies the hermiticity of the Lindblad operators, $b_j = b_j^\dagger$ [105]. In addition, the conservation of the average value of the energy can be enforced by taking $[H, b_j] = 0$ [106].

In a 2-level system with mixing angle θ (relevant for atmospheric neutrinos), the ν_μ survival probability after propagation of a distance L is [107]

$$P_{\nu_\mu \rightarrow \nu_\mu} = 1 - P_{\nu_\mu \rightarrow \nu_\tau} = 1 - \sin^2 2\theta \sin^2 [e^{-\gamma L} \Delta_{ij}] , \quad (65)$$

where γ has dimension of energy, and its inverse defines the typical (coherence) length after which the system gets mixed.⁶ Thus, for $\gamma L \sim \mathcal{O}(1)$ one expects significant deviations from standard mass-induced oscillations formula $P_{\nu_\mu \rightarrow \nu_\mu} = 1 - \sin^2 2\theta \sin^2 \Delta_{ij}$. For dissipative scenarios in which decoherence effects vanish in the weak gravitational limit, $M_{\text{QG}} \rightarrow \infty$, γ can be parametrized as

$$\gamma = \tilde{\kappa} \left(\frac{E_\nu}{\text{GeV}} \right)^n \left(\frac{M_{\text{QG}}}{\text{GeV}} \right)^{-n+1} \text{GeV} , \quad (66)$$

where $\tilde{\kappa}$ is a dimensionless parameter, which by naturalness is expected to be $\mathcal{O}(1)$, and $n \geq 2$.

The energy behavior of γ depends on the dimensionality of the operators b_j . But care must be taken, since \mathcal{D} is bilinear in the b_j , and due to the hermiticity requirement, each b_j is itself at least bilinear in the neutrino fields ψ . Examples are

$$b_j \propto \int d^3x \psi^\dagger (i\partial_t)^j \psi , \quad (67)$$

where $j = 0, 1, 2, \dots$. A Fourier expansion of the fields ψ, ψ^\dagger , inserted into Eq. (67), gives the energy behavior $b_j \propto E_\nu^j$, and hence $\gamma \propto E_\nu^{2j}$. This restriction of the energy behavior

⁶ The parametrization that leads to Eq. (65) is appropriate for including dissipation as a perturbation on the standard oscillations [108]. In the most general solution of Eq. (63) [109], after propagation over extreme long-baselines (i.e., $L \rightarrow \infty$) the system evolves to an equal flavor ratio regardless of the initial flavor content and mixing angle.

to non-negative even powers of E_ν may possibly be relaxed when the dissipative term is directly calculated in the most general space-time foam background.

An interesting example is the case where the dissipative term is dominated by the dimension-4 operator b_1 , $\int d^3x \psi^\dagger i\partial_t \psi$, yielding the energy dependence $\gamma \propto E_\nu^2/M_{\text{QG}}$. This is characteristic of non-critical string theories where the space-time defects of the quantum gravitational “environment” are taken as recoiling D -branes, which generate a cellular structure in the space-time manifold [110].

A best fit to data collected by the SK atmospheric neutrino experiment [41], allowing for both oscillation and decoherence yields, for $n = 2$,

$$\tilde{\kappa} \left(\frac{M_{\text{QG}}}{\text{GeV}} \right)^{-1} < 0.9 \times 10^{-27}, \quad (68)$$

at the 90% CL [107]. A similar lower limit on M_{QG} has been obtained at Fermilab. The CCFR detector is sensitive to $\nu_\mu \leftrightarrow \nu_e$ [111] and $\nu_e \leftrightarrow \nu_\tau$ [112] flavor transitions. Neutrino energies range from 30 to 600 GeV with a mean of 140 GeV, and their flight lengths vary from 0.9 to 1.4 km. A best fit to the data allowing for both oscillation and decoherence yields

$$\tilde{\kappa} \left(\frac{M_{\text{QG}}}{\text{GeV}} \right)^{-1} < 2.0 \times 10^{-24}, \quad (69)$$

at the 99% CL [113]. It is clear that for $n = 2$ existing experiments are probing M_{QG} all the way up to the Planck scale $M_{\text{Pl}} \sim 10^{19}$ GeV. For larger n , Eq.(68) generalizes to

$$\tilde{\kappa} \left(\frac{M_{\text{QG}}}{\text{GeV}} \right)^{-n+1} < 0.9 \times 10^{-27}. \quad (70)$$

This can be seen from Eq. (66): the analysis of data places bounds on γ , and the neutrino energies are well above 1 GeV. Thus, for $n = 3$, the lower bound on $M_{\text{QG}} > 10^{13}$ GeV is comparable to the one obtained from limits on proton decay [101].⁷ Although the cubic energy dependence $\gamma \propto E_\nu^3$ is not obtainable from the simple operator analysis presented above, it may be heuristically supported by a general argument that each of the b_j must be suppressed by at least one power of M_{Pl} , giving a leading behavior

$$\gamma = \tilde{\kappa} E_\nu^3 / M_{\text{Pl}}^2. \quad (71)$$

IceCube will collect a data set of order one million atmospheric neutrinos over 10 years. Not surprisingly, because of the increased energy and statistics over present experiments, the telescope will be sensitive to effects of quantum decoherence at a level well beyond

⁷ Note that for $\tilde{\kappa} \sim 1$, the lower limit on the UV cutoff is well beyond the electroweak scale. Thus, if TeV-scale gravity is realized in nature, interactions with virtual black holes would be non-dissipative. Non-dissipative interactions are expected when gravity is embedded in string theory, so that an S -matrix description is possible. The existence of an S -matrix makes it no longer automatic that, *e.g.*, the B -violating $\bar{q}l$ and B -conserving qq outgoing channels have the same probability, as they would in thermal evaporation. Thus, the problem of avoiding rapid baryon decay is shifted to the examination of symmetries [114] in the underlying string theory which would suppress the appropriate non-renormalizable operators at low energies.

current limits. Additionally, since the loss of quantum coherence is weighted by the distance traveled by the neutrinos, IceCube data analysis of high energy extraterrestrial neutrinos can be used to probe decoherence effects arising only after long propagation lengths. Such an analysis can be carried out by measuring the ratios of neutrino flavors present in the cosmic spectrum.

Let the ratios of neutrino flavors at production in the cosmic sources be written as $w_e : w_\mu : w_\tau$ with $\sum_\alpha w_\alpha = 1$, so that the relative fluxes of each mass eigenstate are given by $w_j = \sum_\alpha w_\alpha U_{\alpha j}^2$. For $\Delta_{ij} \gg 1$, the phases in Eq. (51) will be erased by uncertainties in L and E_ν . Consequently, averaging over $\sin^2 \Delta_{ij}$ one finds the transition probability between flavor states α and β [115]

$$P(\nu_\alpha \rightarrow \nu_\beta) = \sum_i U_{\alpha i}^2 U_{\beta i}^2. \quad (72)$$

Thus, we conclude that the probability of measuring on Earth a flavor α is given by

$$P_{\nu_\alpha \text{ detected}} = \sum_j U_{\alpha j}^2 \sum_\beta w_\beta U_{\beta j}^2. \quad (73)$$

Straightforward calculation shows that any initial flavor ratio that contains $w_e = 1/3$ will arrive at Earth with equipartition on the three flavors. Since neutrinos from astrophysical sources are expected to arise dominantly from pions (and kaons) and their muon daughters, their initial flavor ratios of $1/3 : 2/3 : 0$ should arrive at Earth democratically distributed. Consequently there is a fairly robust prediction of $1/3 : 1/3 : 1/3$ flavor ratios for measurement of astrophysical neutrinos.

The prediction for the flavor population at Earth due to standard flavor-mixing (i.e. with no spacetime dynamics) of a pure $\bar{\nu}_e$ beam is $\sum_j |U_{ej}|^2 |U_{\alpha j}|^2 \sim \frac{1}{3} |U_{\alpha 2}|^2 + \frac{2}{3} |U_{\alpha 1}|^2$ for flavor α , which leads to the flavor ratios $\sim 3/5 : 1/5 : 1/5$. This is very different from the democratic $1/3 : 1/3 : 1/3$. Since the effects of quantum decoherence would alter the flavor mixture to the ratio $1/3 : 1/3 : 1/3$ (regardless of the initial flavor content) and the loss of quantum coherence is weighted by the distance travelled by the (anti) neutrinos, by measuring the $\bar{\nu}$ -Cygnus beam IceCube will be sensitive to the effects of quantum decoherence at a level well beyond current limits [116].

The Lindblad operators of an N -level quantum mechanical system can be expanded in a basis of matrices satisfying standard commutation relations of Lie groups. For a 3-level system, the basis comprises the eight Gell-Mann SU(3) matrices plus the 3×3 identity matrix. As mentioned above, the theoretical approach provided by Lindblad quantum dynamical semi-groups is a very general in the sense that no explicit hypothesis has been made about the actual interactions causing the loss of coherence. In what follows we adopt an expansion in a 3 flavor basis with a diagonal form for the 9×9 decoherence matrix, \mathcal{D} . Note that neutrinos oscillate among flavors separately between particle and antiparticle sectors and so the respective decoherence parameters for antineutrinos can be different from the corresponding ones in the neutrino sector. Upon averaging over the rapid oscillation for propagation between Cygnus OB2 and the Earth, only the diagonal Gell-Mann matrices survive, and so the transition probability for antineutrinos takes the form [117]

$$\begin{aligned} P_{\bar{\nu}_\alpha \rightarrow \bar{\nu}_\beta} = & \frac{1}{3} + \left[\frac{1}{2} e^{-\bar{\gamma}_3 d} (U_{\alpha 1}^2 - U_{\alpha 2}^2)(U_{\beta 1}^2 - U_{\beta 2}^2) \right. \\ & \left. + \frac{1}{6} e^{-\bar{\gamma}_8 d} (U_{\alpha 1}^2 + U_{\alpha 2}^2 - 2U_{\alpha 3}^2)(U_{\beta 1}^2 + U_{\beta 2}^2 - 2U_{\beta 3}^2) \right], \end{aligned} \quad (74)$$

where $\bar{\gamma}_3$ and $\bar{\gamma}_8$ are eigenvalues of the decoherence matrix for antineutrinos. Note that in Eq. (74) we set the CP violating phase to zero, so that all mixing matrix elements become real. Furthermore, under the assumptions that CPT is conserved and that decoherence effects are negligible at present experiments, the values of the mixing angle combinations appearing in Eq. (74) can be well determined by the usual oscillation analysis of solar, atmospheric, long-baseline and reactor data [80]. In what follows, we will assume that CPT is conserved both by neutrino masses and mixing as well as in decoherence effects. Note however that since the decoherence effects in the present study primarily affect antineutrinos, the result will hold for the antineutrino decoherence parameters exclusively if CPT is violated only through quantum-gravity effects.

Now, we require further $\bar{\gamma}_3 = \bar{\gamma}_8 \equiv \bar{\gamma}$ ($= \gamma_3 = \gamma_8$ under CPT conservation) so that Eq. (74) can be rewritten for the case of interest as:

$$\begin{aligned} P_{\bar{\nu}_e \rightarrow \bar{\nu}_\mu} &= P_{\bar{\nu}_\mu \rightarrow \bar{\nu}_e} = P_{\nu_e \rightarrow \nu_\mu} = P_{\nu_\mu \rightarrow \nu_e} = \frac{1}{3} + f_{\nu_e \rightarrow \nu_\mu} e^{-\bar{\gamma}L}, \\ P_{\bar{\nu}_e \rightarrow \bar{\nu}_\tau} &= P_{\bar{\nu}_\tau \rightarrow \bar{\nu}_e} = P_{\nu_e \rightarrow \nu_\tau} = P_{\nu_\tau \rightarrow \nu_e} = \frac{1}{3} + f_{\nu_e \rightarrow \nu_\tau} e^{-\bar{\gamma}L}, \\ P_{\bar{\nu}_\mu \rightarrow \bar{\nu}_\tau} &= P_{\bar{\nu}_\tau \rightarrow \bar{\nu}_\mu} = P_{\nu_\mu \rightarrow \nu_\tau} = P_{\nu_\tau \rightarrow \nu_\mu} = \frac{1}{3} + f_{\nu_\mu \rightarrow \nu_\tau} e^{-\bar{\gamma}L}, \\ P_{\bar{\nu}_e \rightarrow \bar{\nu}_e} &= P_{\nu_e \rightarrow \nu_e} = \frac{1}{3} - (f_{\nu_e \rightarrow \nu_\mu} + f_{\nu_e \rightarrow \nu_\tau}) e^{-\bar{\gamma}L}, \\ P_{\bar{\nu}_\mu \rightarrow \bar{\nu}_\mu} &= P_{\nu_\mu \rightarrow \nu_\mu} = \frac{1}{3} - (f_{\nu_e \rightarrow \nu_\mu} + f_{\nu_\mu \rightarrow \nu_\tau}) e^{-\bar{\gamma}L}, \\ P_{\bar{\nu}_\tau \rightarrow \bar{\nu}_\tau} &= P_{\nu_\tau \rightarrow \nu_\tau} = \frac{1}{3} - (f_{\nu_e \rightarrow \nu_\tau} + f_{\nu_\mu \rightarrow \nu_\tau}) e^{-\bar{\gamma}L}. \end{aligned} \quad (75)$$

We make this simplification only to emphasize the primary signature of quantum decoherence, namely that after travelling a sufficiently long distance the flavor mixture is altered to the ratio $1/3 : 1/3 : 1/3$, regardless of the initial flavor content. Consequently, if a flux of antineutrinos were to be observed from the Cygnus spiral arm with a flavor ratio $\neq 1/3 : 1/3 : 1/3$, strong constraints can be placed on the decoherence parameter $\bar{\gamma}$.

Using the results of the up-to-date 3ν oscillation analysis of solar, atmospheric, long-baseline and reactor data [80] we obtain the following values and 95% confidence ranges [9]

$$\begin{aligned} f_{\nu_e \rightarrow \nu_\mu} &= -0.106^{+0.060}_{-0.082}, \\ f_{\nu_e \rightarrow \nu_\tau} &= -0.128^{+0.089}_{-0.055}, \\ f_{\nu_\mu \rightarrow \nu_\tau} &= 0.057^{+0.011}_{-0.035}. \end{aligned} \quad (76)$$

The numbers given in Eq. (76) are obtained using the same techniques as described in Ref. [80] but including the final SNO salt phase data [118].

Equipped with Eqs. (66), (75), and (76), we now proceed to determine the sensitivity of IceCube to decoherence effects. We estimate the expected number of ν_μ induced tracks from the Cygnus OB2 source antineutrino flux using the semi-analytical calculation discussed in Sec. II A. Namely, we replace the antineutrino flux shown in Fig. 6 into Eq. (6) and obtain, for standard mass-induced oscillations, a total of $212 \times P_{\bar{\nu}_e \rightarrow \bar{\nu}_\mu} = 48$ $\bar{\nu}_\mu$ -induced tracks in 15 years of observation (cluster within 1° of the source direction). For showers, the angular resolution is significantly worse than for muon tracks. Normally, a reduction of the muon bremsstrahlung background is effected by placing a cut of 4×10^4 GeV on the

minimum reconstructed energy [8]. For Cygnus OB2, this strong energy cut is not needed since this background is filtered by the Earth. Thus we account for all events with shower energy $E_{\text{sh}} \geq E_{\text{sh}}^{\text{min}} = 10^3$ GeV, trigger level. The directionality requirement, however, implies that the effective volume for detection of showers is reduced to the instrumented volume of the detector, 1 km^3 , because of the small size of the showers (less than 200 m in radius) in this energy range. Replacing the antineutrino flux shown in Fig. 6 into Eq. (14), within the framework of standard oscillations, one expects 25 showers from the Cygnus OB2 source in 15 years of operation. We now turn to the estimate of the background. There are two different contributions — atmospheric neutrinos and additional fluxes of extraterrestrial neutrinos. We obtain the number of expected track and shower events from atmospheric neutrinos as in Eqs (6), (15), and (16) with $dF_{\text{atm}}^{\nu\alpha}/dE_\nu$ as given in Fig. 6, being the ν_e and ν_μ atmospheric neutrino fluxes integrated over a solid angle of $1^\circ \times 1^\circ$ (for tracks) and $10^\circ \times 10^\circ$ (for showers) width around the direction of the Cygnus OB2 source ($\theta = 131.2^\circ$). We get an expected background of 14 atmospheric tracks and 47 atmospheric showers in 15 years. Of the 47 showers, 16 correspond to ν_e CC interactions while 31 correspond to ν_μ NC interactions. The large yield of NC events is due to the fact that at these energies, the atmospheric flux contains a very unequal mix of neutrino flavors (with ratios $\approx 1/20 : 19/20 : 0$). Interestingly, by increasing the minimum shower energy cut to 5×10^3 GeV, ν_e CC and ν_μ NC contribute in equal amounts to the number of atmospheric showers. This is in agreement with simulations by the AMANDA Collaboration [119]. We turn now to the discussion of background events from other extraterrestrial sources. As discussed in Sec. III C, the TeV γ -ray flux reported by the HEGRA Collaboration [52] in the vicinity of Cygnus OB2 is likely to be due to hadronic processes. For the purposes of setting an upper bound on the neutrino flux we ignore all other sources near J2032+4130 because their steady emission in γ -rays is estimated to be smaller by more over a factor of 5 than the source of interest.⁸ Using the expected flux of neutrinos from J2032+4130 given in Fig. 6 we obtain the corresponding background from neutrinos with flavor ratios $1/3 : 1/3 : 1/3$. As can be seen in Fig. 6, the background is dominated by atmospheric neutrinos. Thus after 15 years of data collection we expect 18 tracks and 1 shower from J2032+4130 for standard oscillations.

We will now discuss how to isolate the possible signal due to decoherence in the antineutrinos from Cygnus OB2 from the atmospheric background and possible fluctuations in the event rate due to unknown diffuse fluxes of extraterrestrial neutrinos. In general, we can predict that the expected number of track and shower events in the direction of the Cygnus OB2 source to be

$$\mathcal{N}_{\text{tr}} = \mathcal{N}_{\text{tr}}^{\text{S}} + \mathcal{N}_{\text{tr}}^{\text{atm}} + \mathcal{N}_{\text{tr}}^{\text{HEGRA}} , \quad (77)$$

$$\mathcal{N}_{\text{sh}} = \mathcal{N}_{\text{sh}}^{\text{S}} + \mathcal{N}_{\text{sh}}^{\text{atm}} + \mathcal{N}_{\text{sh}}^{\text{HEGRA}} . \quad (78)$$

The first term corresponds to antineutrinos from neutron β -decay. In the presence of decoherence effects these event rates can be computed from Eqs. (6), (15) and (16) with flavour transition probabilities given in Eq. (75) with $L = 1.7$ kpc. The second term refers to atmospheric (anti)neutrinos ($\mathcal{N}_{\text{tr}}^{\text{atm}} = 14$, $\mathcal{N}_{\text{sh}}^{\text{atm}} = 47$ for 15 years of exposure). The third term takes into account additional contributions from a diffuse flux of (anti)neutrinos produced

⁸ This includes the famous microquasar Cygnus X-3, for which HEGRA Collaboration reported [52] an upper limit for steady emission of $F_\gamma(E_\gamma > 0.7 \text{ TeV}) = 1.7 \times 10^{-13} \text{ cm}^{-2} \text{ s}^{-1}$.

via charged pion decay. In principle, decoherence effects may also affect the expected number of events from this diffuse flux. However given that the flavour ratios both from oscillation and decoherence are very close to $1/3 : 1/3 : 1/3$ for the case of neutrinos produced via charged pion decay, there is no difference in the sensitivity region if decoherence effects are included or not in the evaluation of $\mathcal{N}_{\text{tr}}^{\text{HEGRA}}$ and $\mathcal{N}_{\text{sh}}^{\text{HEGRA}}$. They are normalized to the maximum expected flux from J2032+4130 by a factor $x = \mathcal{N}_{\text{tr}}^{\text{HEGRA}}/18 = \mathcal{N}_{\text{sh}}^{\text{HEGRA}}/1$.

Altogether, the quantities \mathcal{N}_{tr} and \mathcal{N}_{sh} , as defined in Eqs. (77) and (78), can be regarded as the theoretical expectations of these event rates, corresponding to different points in the $x - \kappa_n$ parameter space. For a given set of observed rates, $\mathcal{N}_{\text{tr}}^{\text{obs}}$ and $\mathcal{N}_{\text{sh}}^{\text{obs}}$, two curves are obtained in the two-dimensional parameter space by setting $\mathcal{N}_{\text{tr}}^{\text{obs}} = \mathcal{N}_{\text{tr}}$ and $\mathcal{N}_{\text{sh}}^{\text{obs}} = \mathcal{N}_{\text{sh}}$. These curves intersect at a point, yielding the most probable values for the flux and decoherence scale for the given observations. Fluctuations about this point define contours of constant χ^2 in an approximation to a multi-Poisson likelihood analysis. These contours can be obtained using Eq. (46) with the identification $i = \text{sh, tr}$. Marginalizing with respect to x , for $n = 2$ we obtain the following 1 degree-of-freedom bound

$$\tilde{\kappa} \left(\frac{M_{\text{QG}}}{\text{GeV}} \right)^{-1} \leq 2.0 \times 10^{-44} \ (5.5 \times 10^{-42}) \text{ GeV}, \quad (79)$$

at the 90% (99%) CL [9]. This corresponds to an improvement of about 17 orders of magnitude over the best existing bounds from the SK and K2K data [107]. Moreover, for $n = 3$, the 1-degree freedom bound is

$$\tilde{\kappa} \left(\frac{M_{\text{QG}}}{\text{GeV}} \right)^{-2} \leq 3.0 \times 10^{-47} \ (2.9 \times 10^{-45}) \text{ GeV} \quad (80)$$

at 90% (99%) CL [9]. For $M_{\text{QG}} = M_{\text{Pl}}$ this corresponds to $\tilde{\kappa} \lesssim 3 \times 10^{-3}$ at the 99% CL, well below the natural expectation.

Finally we note that, for $\bar{\gamma} = \kappa (E_\nu/\text{GeV})^{-1}$, a non-vanishing $\bar{\gamma}$ in Eq. (75) can be related to a finite $\bar{\tau}_{\bar{\nu}_e}$ lifetime in the lab system [120]

$$e^{-\bar{\gamma}L} \equiv e^{-L/\tau_{\text{lab}}} = e^{-L m_{\bar{\nu}_e}/E_{\bar{\nu}} \bar{\tau}_{\bar{\nu}_e}}, \quad (81)$$

where $\bar{\tau}_{\bar{\nu}_e}$ is the antineutrino rest frame lifetime and $m_{\bar{\nu}_e}$ its mass. By duplicating our discussion for $\bar{\gamma} \propto E^{-1}$ we obtain a 90% (99%) CL sensitivity [9]

$$\kappa \leq 1.0 \times 10^{-34} \ (2.3 \times 10^{-31}) \text{ GeV}, \quad (82)$$

which can be translated into

$$\frac{\bar{\tau}_{\bar{\nu}_e}}{m_{\bar{\nu}_e}} > 10^{34} \text{ GeV}^{-2} \equiv 6.5 \text{ s eV}^{-1}. \quad (83)$$

This corresponds to an improvement of about 4 orders of magnitude over the best existing bounds from solar neutrino data [121], and of course gives results comparable to the reach derived for neutrinos decaying over cosmic distances [122]. It should be noted that although the similar algebraic structure of the decoherence term in Eq. (75) and a decaying component in the neutrino beam provide a bound on the neutrino lifetime, these are conceptually two different processes. The decoherence case can be viewed as a successive absorption and re-emission of a neutrino from the quantum foam with change in flavor but no change in the

average energy because of the condition $[H, b_j] = 0$. This contrasts with the decay process which involves the emission of an additional particle.

In summary, IceCube will provide a major improvement in the sensitivity to possible effects of quantum gravity. Because of the increase energy and statistics over present experiments measuring the atmospheric neutrino flux, existing bounds on the violation of the equivalence principle and of Lorentz invariance can be improved by two orders of magnitude. On the other hand, antineutrinos produced in the decays of neutrons from Cygnus OB2 provide an excellent source in which to search for decoherence effects. Although the precise conclusions depend on the model considered, IceCube will improve the sensitivity to decoherence effects of $\mathcal{O}(E^2/M_{\text{Pl}})$ by 17 orders of magnitude over present limits and, moreover, it can probe decoherence effects of $\mathcal{O}(E^3/M_{\text{Pl}}^2)$ which are well beyond the reach of other experiments.

VI. DARK MATTER

Over the past few years, a flood of high-quality data from the Supernova Cosmology Project [123], the Supernova Search Team [124], the Wilkinson Microwave Anisotropy Probe (WMAP) [125], the Two Degree Field Galaxy Redshift Survey (2dFGRS) [126], and the Sloan Digital Sky Survey (SDSS) [127] pin down cosmological parameters to-percent level precision, establishing a new paradigm of cosmology. A surprisingly good fit to the data is provided by a simple geometrically flat Friedman-Robertson-Walker Universe, in which 30% of the energy density is in the form of non-relativistic matter ($\Omega_m = 0.30 \pm 0.04$) and 70% in the form of a new, unknown dark energy component with strongly negative pressure ($\Omega_\Lambda = 0.70 \pm 0.04$) [128]. The matter budget has only 3 free parameters: the Hubble parameter $h = 0.70^{+0.04}_{-0.03}$, the matter density $\Omega_m h^2 = 0.138 \pm 0.012$, and the density in baryons, $\Omega_b h^2 = 0.0230^{+0.0013}_{-0.0012}$.⁹ This implies that the structure of the Universe is dictated by the physics of as-yet-undiscovered cold dark matter ($\Omega_{\text{CDM}} h^2 = 0.115 \pm 0.012$) and the galaxies we see today are the remnants of relatively small overdensities in the nearly uniform distribution of matter in the very early Universe. Overdensity means overpressure that drives an acoustic wave into the other components making up the Universe: the hot gas of nuclei and photons and the neutrinos. These acoustic waves are seen today in the temperature fluctuations of the microwave background as well as in the distribution of galaxies on the sky.

The only dark matter particle which is known to exist from experiment is the neutrino. Neutrinos decouple from thermal equilibrium while still relativistic, and consequently constitute the hot dark matter. With a contribution to the Universe's matter balance similar to that of light, neutrinos play a secondary role. The role is however identifiable: because of their large mean free path, neutrinos prevent the smaller structures in the cold dark matter from fully developing and this is visible in the observed distribution of galaxies, see Fig. 9. Simulations of structure formation with varying amounts of matter in the neutrino component can match to a variety of observations of today's sky, including mea-

⁹ The latter is consistent with the estimate from Big Bang nucleosynthesis, based on measurements of deuterium in high redshift absorption systems, $\Omega_b h^2 = 0.020 \pm 0.002$ [129].

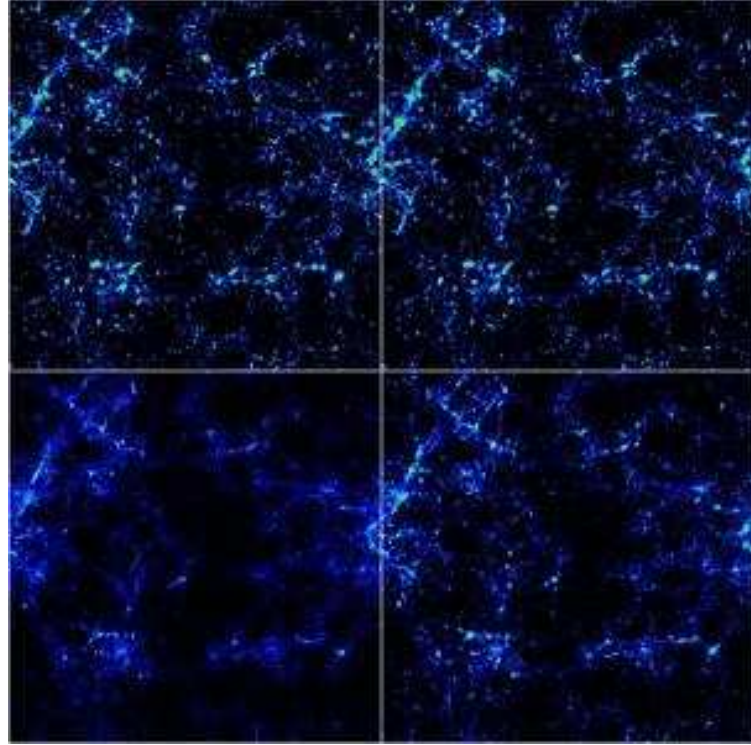


FIG. 9: Simulations of structure formation with varying amounts of matter in the neutrino component, i.e., varying neutrino mass: (top left) massless neutrinos, (top right) $\sum_\alpha m_{\nu_\alpha} = 1$ eV, (bottom left) $\sum_\alpha m_{\nu_\alpha} = 7$ eV, (bottom right) $\sum_\alpha m_{\nu_\alpha} = 4$ eV.

surement of galaxy-galaxy correlations and temperature fluctuations on the surface of last scattering. The results suggest a neutrino mass, summed over the three neutrino flavors, $\sum_\alpha m_{\nu_\alpha} \lesssim 1$ eV [130], a range compatible with the one deduced from oscillations.

The simplest model for cold dark matter consists of WIMP's - weakly interacting massive particles [131]. Generic WIMP's were once in thermal equilibrium, but decoupled while strongly non-relativistic. Many approaches have been developed to attempt to detect dark matter. Such endeavors include direct detection experiments which hope to observe the scattering of dark matter particles with the target material of the detector [132] and indirect detection experiments which are designed to search for the products of WIMP annihilation into gamma-rays, anti-matter and neutrinos [133]. Neutrino telescopes indirectly search for the presence of dark matter by taking advantage of the Sun's ability to capture large numbers of WIMP's over time. Over billions of years, a sufficiently large number of WIMP's can accumulate in the Sun's core to allow for their efficient annihilation. Such annihilations produce a wide range of particles, most of which are quickly absorbed into the solar medium. Neutrinos, on the other hand, may escape the Sun and be detected in experiments on the Earth. The prospects for such experiments detecting dark matter critically depend on the capture rate of WIMP's in the Sun, which in turn depends on the elastic scattering cross section of these particles.

The rate at which WIMP's are captured in the Sun depends on the nature of the interaction the WIMP undergoes with nucleons in the Sun. These elastic scattering processes are often broken into two classifications: *spin dependent* interactions in which cross sections increase with the spin of the target nuclei, and *spin independent* interactions in which

cross sections increase with the total number of nucleons in the target. For spin-dependent interactions, the WIMP capture rate in the Sun is given by [134]

$$C_{\text{SD}}^{\odot} \simeq 3.35 \times 10^{20} \text{ s}^{-1} f(\rho_{\text{local}}, \bar{v}_{\text{local}}, m_{\text{WIMP}}) \left(\frac{\sigma_{\text{H,SD}}}{10^{-6} \text{ pb}} \right), \quad (84)$$

where

$$f(\rho_{\text{local}}, \bar{v}_{\text{local}}, m_{\text{WIMP}}) = \left(\frac{\rho_{\text{local}}}{0.3 \text{ GeV/cm}^3} \right) \left(\frac{\bar{v}_{\text{local}}}{270 \text{ km/s}} \right)^{-3} \left(\frac{m_{\text{WIMP}}}{100 \text{ GeV}} \right)^{-2}, \quad (85)$$

ρ_{local} is the local dark matter density, $\sigma_{\text{H,SD}}$ is the spin-dependent WIMP-on-proton (hydrogen) elastic scattering cross section, \bar{v}_{local} is the local rms velocity of halo dark matter particles, and m_{WIMP} is the dark matter particle's mass. The analogous formula for the capture rate from spin-independent (scalar) scattering is [134]

$$C_{\text{SI}}^{\odot} \simeq 3.35 \times 10^{20} \text{ s}^{-1} f(\rho_{\text{local}}, \bar{v}_{\text{local}}, m_{\text{WIMP}}) \left(\frac{\sigma_{\text{H,SI}} + 0.07 \sigma_{\text{He,SI}}}{10^{-6} \text{ pb}} \right), \quad (86)$$

where $\sigma_{\text{H,SI}}$ is the spin-independent WIMP-on-proton elastic scattering cross section and $\sigma_{\text{He,SI}}$ is the spin-independent WIMP-on-helium, elastic scattering cross section. Typically, $\sigma_{\text{He,SI}} \simeq 16.0 \sigma_{\text{H,SI}}$. The factor of 0.07 reflects the solar abundances of helium relative to hydrogen as well as dynamical factors and form factor suppression. Note that these capture rates are suppressed by two factors of the WIMP mass. One of these is simply the result of the depleted number density of WIMP's ($n \propto m_{\text{WIMP}}^{-1}$) while the second factor is the result of kinematic suppression for the capture of a WIMP much heavier than the target nuclei, in this case hydrogen or helium.

If the capture rate and annihilation cross section is sufficiently high, equilibrium will be reached between these two processes. For N WIMP's in the Sun, the rate of change of this quantity is given by

$$\frac{dN}{dt} = C^{\odot} - A^{\odot} N^2, \quad (87)$$

where $C^{\odot} = C_{\text{SD}}^{\odot} + C_{\text{SI}}^{\odot}$ and $A^{\odot} = \langle \sigma v \rangle / V_{\text{eff}}$. Here, $V_{\text{eff}} = 5.7 \times 10^{27} \text{ cm}^3 (m_{\text{WIMP}}/100 \text{ GeV})^{-3/2}$, is the effective volume of the core of the Sun, which is estimated by matching the core temperature with the gravitational potential energy of a single WIMP at the core radius [135]. The present WIMP annihilation rate is given by

$$\Gamma = \frac{1}{2} A^{\odot} N^2 = \frac{1}{2} C^{\odot} \tanh^2 \left(\sqrt{C^{\odot} A^{\odot}} t_{\odot} \right), \quad (88)$$

where $t_{\odot} \simeq 4.5$ billion years is the age of the solar system. The annihilation rate is maximized when it reaches equilibrium with the capture rate. This occurs when

$$\sqrt{C^{\odot} A^{\odot}} t_{\odot} \gg 1. \quad (89)$$

For many particle dark matter candidates, this condition can be met. If this is the case, the final annihilation rate (and corresponding event rate or neutrino flux) has no further dependence on the dark matter particle's annihilation cross section.

The sensitivity of direct detection experiments has been improving at a steady rate. The Cold Dark Matter Search (CDMS) experiment, operating in the Soudan mine in northern

Minnesota, currently has produced the strongest limits on spin-independent scattering cross sections of WIMP's with nucleons [136], as well as on spin-dependent scattering cross sections of WIMP's with neutrons [137]. CDMS data exclude spin-independent cross sections larger than approximately 2×10^{-7} pb for a 50-100 GeV WIMP or 7×10^{-7} pb ($m_{\text{WIMP}}/500 \text{ GeV}$) for a heavier WIMP [136]. The Zeplin-I [138] and Edelweiss [139] experiments currently have spin-independent bounds that are roughly a factor of 5 weaker over this mass range. The NAIAD experiment [140] has placed the strongest constraints on spin-dependent WIMP-proton scattering. The data limit the spin-dependent cross section with protons to be less than approximately 0.3 pb for a WIMP in the mass range of 50-100 GeV and less than 0.8 pb ($m_{\text{WIMP}}/500 \text{ GeV}$) for a heavier WIMP. The PICASSO [141] and CDMS [137] experiments have placed limits on the spin-dependent WIMP-proton cross section roughly one order of magnitude weaker than the NAIAD bound. All of these results (of course) impact the prospects for detecting neutrinos produced by the annihilation of WIMP's in the Sun [142]. Currently, the SK experiment has placed the strongest bounds on high-energy neutrinos from the direction of the Sun [143]. SK has two primary advantages over other experiments. Firstly, they have analyzed data over a longer period than most of their competitors, a total of nearly 1700 live days. Secondly, SK was designed to be sensitive to low energy ($\sim \text{GeV}$) neutrinos, which gives them an advantage in searching for lighter WIMP's. SK's limit on neutrino-induced muons above 1 GeV from WIMP annihilations in the Sun is approximately 1000 to 2000 per square kilometer per year for WIMP's heavier than 100 GeV, and approximately 2000 to 5000 per square kilometer per year for WIMP's in the 20 to 100 GeV range. The precise value of these limits depends on the WIMP annihilation modes considered. The AMANDA [144] and MACRO [145] collaborations have reported limits on the flux of neutrino-induced muons from the Sun that are only slightly weaker than SK. The limit placed by the AMANDA experiment resulted from only 144 live days of data. Having operated the detector for five years, AMANDA is expected to produce significantly improved bounds in the future.

The supersymmetric extension of the Standard Model is the leading candidate to avoid 't Hooft naturalness problem with the Higgs mass [146]. Supersymmetry (SUSY) posits a "complete democracy" between integral and half-integral spins, implying the existence of many as-yet-undiscovered superpartners. Thus, if SUSY can serve as a theory of low energy interactions, it must be a broken symmetry. The most common assumption is that the minimal low energy effective supersymmetric theory (MSSM) has a breaking scale of order $\Lambda_{\text{SUSY}} \sim 1 \text{ TeV}$. MSSM has a concrete advantage in embedding the Standard Model in a GUT: the supersymmetric beta functions for extrapolating the measured strengths of the strong, electromagnetic, and weak couplings lead to convergence at a unified energy value of the order $M_{\text{GUT}} \sim 10^{16} \text{ GeV}$ [147]. Moreover, by imposing R -parity conservation one obtains as a byproduct the stability of the lightest SUSY particle $\tilde{\chi}$, making it a possible candidate for cold dark matter [148].

The relic abundance of SUSY WIMP's can be found by integrating the Boltzman equation [149],

$$\frac{dn}{dt} + 3Hn = -\langle\sigma v\rangle(n^2 - n_{\text{eq}}^2), \quad (90)$$

where n is the present number density of SUSY WIMP's, $n_{\text{eq}} = g(m_{\tilde{\chi}} T/2\pi)^{3/2} e^{-m_{\tilde{\chi}}/T}$ is the equilibrium number density, H is the expansion rate of the Universe at temperature T , g is the number of internal degrees of freedom of the WIMP, $\langle\sigma v\rangle$ is the thermally averaged annihilation cross section, and $m_{\tilde{\chi}}$ is the neutralino mass. Note that in the very early

Universe, when $n \simeq n_{\text{eq}}$, the right hand side of Eq. (90) is small and the evolution of the density is dominated by Hubble expansion. As the temperature falls below $m_{\tilde{\chi}}$, however, the equilibrium number density becomes suppressed and the annihilation rate increases, rapidly reducing the number density. Finally, when the number density falls enough, the rate of depletion due to expansion becomes greater than the annihilation rate, $H \gtrsim n\langle\sigma v\rangle$, and the neutralinos *freeze out* of thermal equilibrium. The freeze-out temperature T_f depends logarithmically upon $\langle\sigma v\rangle$, but for models with TeV scale SUSY breaking, one finds that $T_f/m_{\tilde{\chi}} \sim 0.05$. SUSY WIMPs are, by far, the favored candidate for cold dark matter, because for masses of order 100 GeV to 10 TeV a present density of $\Omega_{\tilde{\chi}} h^2 \sim 0.1$, comes out fairly naturally [150].¹⁰ In what follows we maintain our discussion as general as possible but keep in mind the specific needs of the MSSM.

As they annihilate, WIMPs can generate neutrinos through a wide range of channels. Annihilations to heavy quarks, tau leptons, gauge bosons and Higgs bosons can all generate neutrinos in the subsequent decay [152]. The total flux of neutrinos emitted by the Sun due to WIMP annihilation is then

$$\left. \frac{dF_{\odot}^{\nu\mu}}{dE_{\nu}} \right|_{\text{source}} = C_{\odot} F_{\text{Eq}} \sum_j \left(\frac{dN_{\nu\mu}}{dE_{\nu}} \right)_j e^{-E_{\nu}/150 \text{ GeV}} , \quad (91)$$

where F_{Eq} is the non-equilibrium suppression factor (≈ 1 for capture-annihilation equilibrium), $(dN_{\nu\mu}/dE_{\nu})_j$ is the ν_{μ} flux produced by the j decay channel per WIMP annihilation [152]. Note that neutrinos produced near the center of the Sun interact with the solar medium [153], yielding a depletion of the emission spectrum by a factor $\sim e^{-E_{\nu}/150 \text{ GeV}}$. Finally, the ν_{μ} flux reaching the Earth is,

$$\phi_{\odot}^{\nu\mu} = \frac{1}{4\pi d^2} \left. \frac{dF_{\odot}^{\nu\mu}}{dE_{\nu}} \right|_{\text{source}} , \quad (92)$$

where $d \approx 1.5 \times 10^8$ km is the Earth-Sun distance.

By replacing this flux in Eq. (6) it is easily seen that the CDMS bound implies that the event rate at IceCube for spin-independent interactions is at the level of the atmospheric neutrino background [154]. Thus, isolating a signal from WIMP's which scatter with nucleons mostly spin-independently in the IceCube data sample would be a challenge. On the other hand, a WIMP with a largely spin-dependent scattering cross section with protons may be capable of generating large event rates at IceCube. For example, a 300 GeV WIMP with a cross section near the experimental limit, leads to rates as high as $\sim 10^6$ per year [154]. The elastic scattering and annihilation cross sections of a neutralino depend on its various couplings and on the mass spectrum of the Higgs bosons and superpartners. The neutralino couplings depend on its composition. Generally, the lightest neutralino can be any mixture of bino, wino and the two CP-even higgsinos, although in most models a largely bino-like neutralino is lightest. Spin dependent, axial-vector, scattering of neutralinos with

¹⁰ An alternative dark matter candidate, which has received quite some attention recently, arises in models where all of the particles of the Standard Models can propagate through the bulk of an extra dimensional space that is compactified on a scale around $\sim \text{TeV}^{-1}$. Within this set up each Standard Model particle is accompanied by a tower of Kaluza Klein states. The lightest KK particle can be naturally stable in a way analogous to how the lightest superpartner is stabilized in R -parity conserving models of SUSY [151].

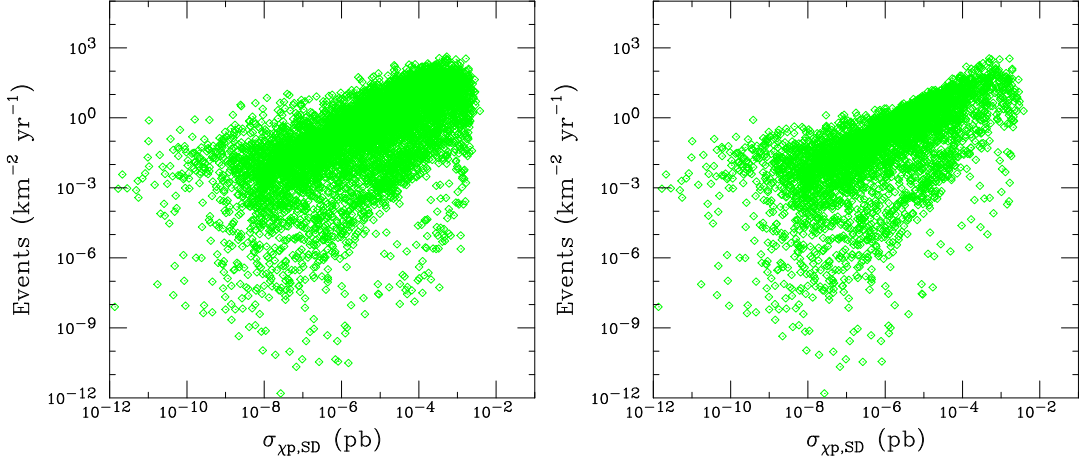


FIG. 10: IceCube event rate from dark matter annihilations in the Sun, as a function of the WIMP’s spin-dependent elastic scattering cross section. In the left frame, no points shown violate the current spin-independent scattering constraints of CDMS. In the right frame, no points would violate the a spin-independent bound 100 times stronger [154].

quarks within a nucleon is made possible through the t-channel exchange of a Z , or the s-channel exchange of a squark. Spin independent scattering occurs at the tree level through s-channel squark exchange and t-channel Higgs exchange, and at the one-loop level through diagrams involving a loop of quarks and/or squarks. For generality, here we do not assume any particular SUSY breaking scenario or unification scheme, and scan the entire MSSM parameter space using the DarkSUSY program [155]. We find that, after applying the cuts to comply with all collider constraints and to produce a thermal relic density that saturates the observational limits [156], very large spin-dependent cross sections ($\sigma_{\text{SD}} \gtrsim 10^{-3} \text{ pb}$) are possible even in models with very small spin-independent scattering rates.

In Fig. 10 we show the event rate at IceCube from WIMP annihilation in the Sun versus the WIMP’s spin-dependent cross section with protons. In the left frame, all points evade current constraints from CDMS. In the right frame we show the same result, but only showing those points which evade a constraint *100 times stronger* than current CDMS bound. We can thus conclude that next generation direct detection experiment will not be able to probe the MSSM parameter space accessible to IceCube.

In summary, direct detection dark matter experiments, lead by the CDMS Collaboration, have placed increasingly stronger constraints on the cross section for elastic scattering of WIMP’s on nucleons. Although these constraints impact the prospects for indirect detection experiments, the latest bounds placed on the scalar WIMP-nucleon cross section by the CDMS experiment do not seriously limit the WIMP parameter space to be probed by IceCube. This is largely due to the fact that the spin-dependent scattering of WIMP’s with protons is the most efficient process for capture in the Sun for many particle dark matter models. The spin-dependent scattering cross section of a WIMP is not nearly as strongly constrained as the spin-independent quantity and large values of spin-dependent cross sections are beyond the reach of any planned direct detection experiments. Thus, IceCube will play an important as well as complementary role in the search for particle dark matter.

VII. TOPOLOGICAL DEFECTS AND SUPERHEAVY RELICS

A plethora of explanations have been proposed to address the production mechanism of ultra-high energy cosmic rays [157]. In the absence of a single model which is consistent with all data, the origin of these particles remains a mystery. Clues to solve the mystery are not immediately forthcoming from the data, particularly since various experiments report mutually inconsistent results.

In recent years, a somewhat confused picture *vis-à-vis* the energy spectrum and arrival direction distribution has been emerging. Since 1998, the AGASA Collaboration has consistently reported [158] a continuation of the spectrum beyond the GZK cutoff [23]. In contrast, the most recent results from HiRes [159] describe a spectrum which is consistent with the expected GZK feature. This situation exposes the challenge posed by systematic errors (predominantly arising from uncertainties in hadronic interaction models [160]) in these types of measurements. Although there seems to be a remarkable agreement among experiments on predictions about isotropy on large scale structure, this is certainly not the case when considering the two-point correlation function on a small angular scale. The AGASA Collaboration reports observations of event clusters which have a chance probability smaller than 1% to arise from a random distribution [161]. Far from confirming the AGASA results, the recent analysis reported by the HiRes Collaboration showed that their data are consistent with no clustering among the highest energy events [162]. The discovery of such clusters would be a tremendous breakthrough for the field, but the case for them is not yet proved. Special care must be taken when computing the statistical significance in such an analysis. In particular, it is important to define the search procedure *a priori* in order to ensure one does not inadvertently perform “trials” by studying the data before deciding upon the cuts. Very recently, with the aim of avoiding accidental bias on the number of trials performed in selecting the angular bin, the original claim of the AGASA Collaboration [161] was re-examined considering only those events observed after the original claim [163]. This study showed that the evidence for clustering in the AGASA data set is weaker than was previously supposed, and is consistent with the hypothesis of isotropically distributed arrival directions.

Further confusing the issue, recent HiRes data have been interpreted as a change in cosmic ray composition, from heavy nuclei to protons, at $\sim 10^9$ GeV [164]. This is an order of magnitude lower in energy than the previous crossover deduced from the Fly’s Eye data [165]. The end-point of the galactic flux is expected to be dominated by iron, as the large charge Ze of heavy nuclei reduces their Larmor radius (containment scales linearly with Z) and facilitates their acceleration to highest energy (again scaling linearly with Z). The dominance of nuclei in the high energy region of the Galactic flux carries the implication that any changeover to protons represents the onset of dominance by an extra-galactic component. The inference from this new HiRes data is therefore that the extra-galactic flux is beginning to dominate the Galactic flux already at $\sim 10^9$ GeV. Significantly, this is well below $E_{\text{GZK}} \sim 10^{10.7}$ GeV [23], and so samples sources even at large redshift.

The Pierre Auger Observatory is confronting the low statistics problem at the highest energies by instrumenting a huge collection area covering 3000 square kilometers on an elevated plane in Western Argentina [3]. The instrumentation consists of 1600 water Čerenkov detectors spaced 1.5 km apart. Showers occurring on clear moonless nights (about 10% of the operational time) are also viewed by four fluorescence detectors, allowing powerful reconstruction and cross-calibration techniques. Simultaneous observations of showers using

two distinct detector methods will help to control the systematic errors that have plagued cosmic ray experiments to date. While no breakthroughs were reported [166], preliminary data forecast rapid progress and imminent results in deciding event rates at the high end of the spectrum.

The difficulties so far encountered in modeling the production of ultra-high energy cosmic rays arise from the need to identify a source capable of launching particles to extreme energy [167]. In contrast to the “bottom-up” acceleration of charged particles, the “top-down” scenario avoids the acceleration problem by assuming that charged and neutral primaries simply arise in the quantum mechanical decay of supermassive elementary X particles [168]. To maintain an appreciable decay rate today, it is necessary to tune the X lifetime to be longer (but not too much longer) than the age of the universe, or else “store” short-lived X particles in topological vestiges of early universe phase transitions.

According to current unified models of high energy interactions, the Universe may have experienced several spontaneous symmetry breakings, where some scalar field, generally referred to as the Higgs field, acquired a non-vanishing expectation value in the new vacuum (ground) state. Quanta associated with these fields are typically of the order of the GUT symmetry-breaking scale. During a phase transition, non-causal regions may evolve towards different states, so that in different domain borders the Higgs field may keep a null expectation value. Energy is then stored in a topological defect whose characteristics depend on the topology of the manifold where the Higgs potential reaches its minimum [169]. The relic defects such as magnetic monopoles [170], cosmic strings [171], superconducting cosmic strings [172], and cosmic necklaces [173] (a possible hybrid topological defect consisting of a closed loop of cosmic string with monopole “beads” on it [174]) are all relatively topologically stable, but can release part of their energy (through radiation, annihilation, or collapse) in the form of X particles that typically decay to quarks and leptons.

The highest energy cosmic rays may also be produced from the decay of some metastable superheavy relic particle with mass $m_X \gtrsim 10^{12}$ GeV and lifetime exceeding the age of the Universe [175]. Discrete gauged symmetries [176] or hidden sectors [177] are generally introduced to stabilize the X particles. Higher dimensional operators, wormholes, and instantons are then invoked to break the new symmetry super-softly to maintain the long lifetime [175] (collisional annihilation has been considered too [178]). Arguably, these metastable superheavy relics may constitute (a fraction of) the dark matter in galactic haloes [179]. If this were the case, due to the non-central position of the Sun in our galaxy the decay or annihilation products of the X particles would have highly anisotropic spectra [180].

The cascade decay to cosmic ray particles is driven by the ratio of the volume density of the X -particle ($n_X = \rho_c \Omega_X / m_X$) to its decay time (τ_X). This is very model dependent, as neither the cosmic average mass density contributed by the relics (Ω_X), nor τ_X is known with any degree of confidence ($\rho_c \approx 1.05 \times 10^{-4} h^2$ GeV cm $^{-3}$). Moreover, the internal mechanisms of the decay and the detailed dynamics of the first secondaries do depend on the exact nature of the particles. Consequently, no firm prediction on the expected flux of cosmic rays can be made. However, if there are no new mass scales between $\Lambda_{\text{SUSY}} \sim 1$ TeV and m_X ,¹¹ the squark and sleptons would behave like their corresponding supersymmetric partners, enabling one to infer from the “known” evolution of quarks and leptons the gross

¹¹ This hypothesis, known as the desert “hypothesis”, is well motivated by the fact that the existence of new physics between the GUT scale and the SUSY breaking scale would destroy the very impressive feature of “natural” unification of the gauge couplings at $M_{\text{GUT}} \sim 10^{16}$ GeV occurring in the MSSM.

features of the X -particle cascade: the quarks hadronize producing jets of hadrons containing mainly pions together with a 3% admixture of nucleons [181]. This implies that the injection spectrum is a rather hard fragmentation-type shape (with an upper limit usually fixed by the GUT scale) and dominated by γ -rays and neutrinos produced via pion decay. Therefore, the photon/proton ratio [182] and the ultra-high energy neutrino flux (which would be beyond the WB-flux of transparent sources) [183] can be used as diagnostic tools to probe top-down models.

In light of the mounting evidence that ultra-high energy cosmic rays are not γ -rays [184], one may try to force a proton dominance at ultra-high energies by postulating efficient absorption of the dominant ultra-high energy photon flux on the universal and/or galactic radio background. According to current estimates of the strengths of the magnetic field and of the radio wave background in our own galaxy, most ultra-high energy photons produced in the halo are expected to reach the Earth. In what follows we assume that the photon interaction length in the galaxy has been greatly over-estimated, and explore this assumption for neutrino signals.

If a top down scenario is to explain the origin of ultra-high energy cosmic rays, the injection spectrum should be normalized to account for the super-GZK events without violating any observational flux measurements or limits at higher or lower energies [185]. In particular, neutrino and γ -ray fluxes depend on the energy released integrated over redshift, and thus on the specific top down model. Note that the electromagnetic energy injected into the Universe above the pair production threshold on the cosmic microwave background is recycled into a generic cascade spectrum below this threshold on a short time scale compared with the Hubble time. Therefore, it can have several potential observable effects, such as modified light element abundances due to ^4He photodisintegration, or induce spectral distortions of universal photon and neutrino backgrounds [186]. Additionally, measurements of the diffuse GeV γ -ray flux [38], to which the generic cascade spectrum would contribute directly, limit significantly the parameter space in which X 's can generate the flux of the ultra-high energy cosmic rays [187].

A point worth noting at this juncture: as we discussed in the previous section, the cold dark matter hunt traditionally concentrates on WIMP's that were once in thermal equilibrium in the early Universe. Its present abundance is determined by the self-annihilation cross section. Since the largest annihilation cross section at early times is expected to be $\propto m_{\text{WIMP}}^{-2}$, heavy WIMP's would have such a small cross section that their present abundance would be too large. Consequently, the mass of a thermal WIMP is found to be less than about 500 TeV. Then, in associating metastable superheavy relics with cold dark matter we assume that the X -particles have never experienced thermal equilibrium. Moreover, since the density of thermal WIMP's saturates the WMAP limit [156], the contribution from superheavy relics to the cold dark matter density must be much less than that of the relic neutralinos. As noted above the cosmic ray flux resulting from X -particle decays depends on the dimensionless parameter $r_X \equiv \xi_X t_0 / \tau_X$, where $\xi_X = \Omega_X / \Omega_{\text{CDM}}$, and t_0 is the age of the universe. Scenarios which include in the rate normalization photon flux from X -particles clustered in the halo lead to a value $r_X \sim 5 \times 10^{-11}$ [175]. Omission of the photon channel in the normalization increases r_X by a factor of about 10. Since models of X -production and decay typically lead to exponential dependence of both ξ_X and τ_X on a reheating temperature T_R and a quantum mechanical tunneling action, respectively; there is no impediment on accommodating this change in r_X while maintaining $\Omega_X \ll \Omega_{\text{CDM}}$. For example, assuming a relic overdensity of 10^5 in the vicinity of our galaxy, as expected for X particles that move

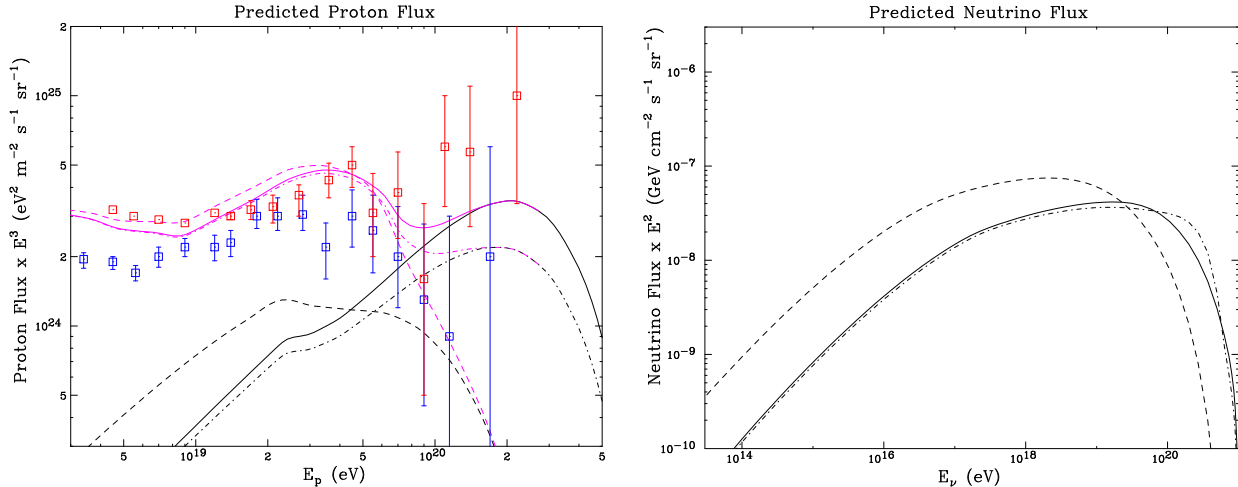


FIG. 11: Right: The ultra-high energy cosmic ray flux predicted for the decay of superheavy particles with mass $m_X = 2 \times 10^{12}$ GeV is compared to the HiReS and AGASA cosmic ray data. The distribution of jets used includes an overdensity factor of 10^5 within 20 kpc of the galaxy. Spectra are shown for quark+antiquark (solid), quark+squark (dot-dash) and 5 quarks + 5 squarks (dashes) initial states. Dark lines are from top-down origin alone whereas lighter lines are top-down plus contributions from an homogeneous population of astrophysical sources. Left: The neutrino plus antineutrino flux corresponding to the cosmic ray spectra from decay of superheavy particles [189].

freely under the influence of gravity [175], an Earthly proton dominated spectrum requires $\xi_X \propto e^{-2m_X/T_R} \sim 10^{-4} - 10^{-8}$ [188].

In Fig. 11 we show the neutrino spectra produced in top-down models for a variety of X -decay channels. We have assumed that X particles have an overdensity of 10^5 in the vicinity of our galaxy. The exact profile of the halo of X particles does not affect the results as long as most ultra-high energy cosmic ray events originate at distances well below one GZK interaction length. The spectra of stable particles (protons, photons, neutralino, electrons and neutrinos of the three species) have been computed using the SH-decay program [190]. At the energies under consideration, it is necessary to take into account all the gauge couplings of the MSSM; indeed, at the scale of unification, they are all of the same strength, so that electroweak (and some Yukawa) interactions can be as relevant as the QCD ones. The perturbative part of the shower was computed by solving numerically the complete set of evolution equations for the relevant fragmentation functions of the MSSM. We carefully modeled the decays of unstable particles with mass near $\Lambda_{\text{SUSY}} \sim 1$ TeV, as well as the hadronization process at the GeV scale for light quarks and gluons.¹² The normalization is determined by matching the X -particle baryon flux to the difference between the observed cosmic ray spectrum at $E \sim 10^{11}$ GeV and contributions from a homogeneous population of astrophysical sources. All fluxes shown in Fig. 11 are consistent with current measurements of the diffuse GeV γ -ray background.

The event rates at AMANDA-II and IceCube are given in Table II [189]. They are

¹² The primary 10-body decay $X \rightarrow 5q5\bar{q}$ has been modeled using phase space only, i.e. ignoring any possible dependence of the matrix element on external momenta.

X -decay channel	AMANDA-II	IceCube
$q\bar{q}$	0.39 yr^{-1}	12.2 yr^{-1}
$q\tilde{q}$	0.36 yr^{-1}	11.4 yr^{-1}
$5 \times q\tilde{q}$	1.40 yr^{-1}	44.6 yr^{-1}

TABLE II: Neutrino event rates at AMANDA-II and IceCube for various X -decay channels.

estimated using Eqs. (6) and (14) with a threshold energy 10^5 GeV for showers and muons. This energy cut effectively removes any background from atmospheric neutrino events. For simplicity, the muon effective area and shower effective volume of the AMANDA-II detector are taken to be uniform: $A_{\text{eff}}^0 \sim 0.05 \text{ km}^2$, [57] and $\mathcal{V}_{\text{eff}} \sim 0.008 \text{ km}^3$ [8], respectively.

In summary, IceCube can test the viability of top-down models. If a signal is found, future high statistics experiments should be able to map out the neutrino spectrum, thereby allowing us experimental access to physics at energy scales many order of magnitude beyond the scope of any conceivable particle collider on Earth.

On a separate track, the cubic kilometer of ice provides a large detector area for direct search of fast magnetic monopoles. This topological defect appears in phase transitions which leave an unbroken $U(1)$ symmetry group. A symmetry-breaking temperature $T_c \sim \langle H \rangle$ at which the order parameter $\langle H \rangle$ turns on, leads to a monopole mass $m_{X_m} \sim T_c/\alpha$, where α is the fine structure constant at scale T_c . To avoid violations of Standard Model physics the value of $\langle H \rangle$ should be at or above the electroweak scale, yielding a lower limit on the monopole mass for $m_{X_m} \gtrsim 40 \text{ TeV}$.

The number density and therefore the flux of monopoles emerging from a phase transition are determined by the Kibble mechanism [169]. At the time of the phase transition, roughly one monopole or antimonopole is produced per correlated volume. The resulting monopole number density today is

$$n_{X_m} \sim 10^{-19} (T_c/10^{11} \text{ GeV})^3 (l_H/\xi_c)^3 \text{ cm}^{-3}, \quad (93)$$

where ξ_c is the phase transition correlation length, bounded from above by the horizon size l_H at the time when the system relaxes to the true broken-symmetry vacuum. In a second order or weakly first order phase transition, the correlation length is comparable to the horizon size. In a strongly first order transition, the correlation length is considerably smaller than the horizon size.

These monopoles easily pick up energy from the magnetic fields permeating the Universe and can traverse unscathed through the primeval radiation. The kinetic energy imparted to a magnetic monopole on traversing a magnetic field along a particular path is [191]

$$E = g \int_{\text{path}} \vec{B} \cdot d\vec{l} \sim g B \xi \sqrt{n}, \quad (94)$$

where $g = e/2\alpha = 3.3 \times 10^{-8}$ dynes/G is the magnetic charge according to the Dirac quantization [192], B is the magnetic field strength, ξ specifies the field's coherence length, and \sqrt{n} is a factor to approximate the random-walk through the n domains of coherent fields traversed by the path. From Eq. (93) then, the general expression for the relativistic monopole flux may be written as

$$\phi_{X_m} = c n_{X_m} / 4\pi \sim 2 \times 10^{-4} \left(\frac{m_{X_m}}{10^{15} \text{ GeV}} \right)^3 \left(\frac{l_H}{\xi_c} \right)^3 \text{ cm}^{-2} \text{ sec}^{-1} \text{ sr}^{-1}. \quad (95)$$

Phenomenologically, the monopole flux is constrained by cosmology and by astrophysics. Cosmology requires that the monopole energy density Ω_{X_m} not be so large as to add observable curvature to the Universe. From Eq. (93) comes a constraint $\Omega_{X_m} \sim 0.1 (m_{X_m}/10^{13} \text{GeV})^4 (l_H/\xi_c)^3$, which implies that monopoles with $m_{X_m} \lesssim 10^{13} (\xi_c/l_H)^{3/4} \text{GeV}$ do not over-curve the Universe. Astrophysics requires that there not be so many monopoles around as to effectively “short out” the Galactic magnetic field, $\phi_{X_m} < 10^{-15} \text{ cm}^{-2} \text{ s}^{-1} \text{ sr}^{-1}$ [193]. To satisfy this constraint, the Kibble flux in Eq. (95) requires $m_{X_m} \lesssim 10^{11} (\xi_c/l_H) \text{GeV}$. Note that with the usual GUT scale, the fractional monopole mass density $\Omega_{X_m} \sim 10^{16}$ overcloses the Universe by sixteen orders of magnitude. However, to dilute the monopole density inflation can be invoked after the phase transition [194], or else the $U(1)$ group can be broken temporarily so as to create cosmic string defects which connect monopoles to anti-monopoles pairwise, which then annihilate [195].

A magnetic monopole with velocity $v \rightarrow c$ would emit Čerenkov radiation along its path. The total power emitted per unit frequency ν and per unit length l

$$\frac{d^2W}{d\nu dl} = \frac{\pi n_r^2 \nu}{4\alpha} \left[1 - \frac{c^2}{v^2 n_r^2} \right], \quad (96)$$

exceeds that of a bare relativistic muon by $n_r^2/4\alpha$, where n_r is the refractive index of the medium [196]. This corresponds to an enhancement factor of 4700 for monopoles interacting in vacuum and 8300 for monopole interactions in ice. Clearly, the large light output of a monopole track would be a rather unique signal at IceCube [197]. The non-observation of monopoles signals at the large Čerenkov detector in the lake Baikal leads to a 90% CL upper limit $\phi_{X_m}^{\max} = 0.5 - 0.7 - 1.9 \times 10^{-16} \text{ cm}^{-2} \text{ s}^{-1} \text{ sr}^{-1}$ for $\beta = 1.0 c - 0.9 c - 0.8 c$, respectively [198]. The AMANDA (data taken during 1997) [199] and MACRO [200] collaborations reported slightly weaker flux limits. Since the muon effective area of IceCube is about a factor of 20 larger than that of AMANDA, in 5 years of operation the kilometer scale telescope will reach a sensitivity nearly two orders of magnitude below existing limits.

VIII. OUTLOOK

Today, precision data from man-made accelerators can, without exception, be accommodated by the Standard Model of particle physics. Whenever the experimental precision increases, the higher precision measurements invariably collapse into Standard Model values. Nevertheless, since all the big questions remain unanswered, there is no feeling that we are now dotting the i’s and crossing the t’s of a mature theory. Worse, the theory has its own demise built into its radiative corrections.

Led by a string of fundamental experimental measurements that unmasked the leptonic flavor mixing, neutrino physics has wounded the Standard Model. The hope is that at this point the glass is half full and that high-precision high-statistics IceCube data will continue the process and pierce the Standard Model’s resistant armor.

Acknowledgments

We have benefited from discussions with Felix Aharonian, Markus Ahlers, Jaime Alvarez Muñiz, George Alverson, Cyrille Barbot, Vernon Barger, John Beacom, Tere Dova, Manuel Drees, Luis Epele, Jonathan Feng, Tom Gaisser, Haim Goldberg, Concha Gonzalez Garcia,

Tao Han, Dan Hooper, Chung Kao, Mitja Khangulyan, Michele Maltoni, Alan Martin, Tom McCauley, Teresa Montaruli, Pran Nath, Charly Nuñez, Tom Paul, Steve Reucroft, Andreas Ringwald, David Saltzberg, Subir Sarkar, Sergio Scutto, Al Shapere, Guenter Sigl, Todor Stanev, Floyd Stecker, Ed Stoeffhaas, John Swain, Lucas Taylor, Diego Torres, Huitzu Tu, Ricardo Vazquez, Alan Watson, Tom Weiler, Enrique Zas, and the AMANDA and IceCube collaborations. This work has been partially supported by the US National Science Foundation (NSF Grants Nos. PHY-0457004 and OPP- 0236449), the US Department of Energy (DoE Grant No. DE-FG02-95ER40896), and the University of Wisconsin Research Committee with funds granted by the Wisconsin Alumni Research Foundation.

- [1] E. Andres *et al.*, *Astropart. Phys.* **13**, 1 (2000) [arXiv:astro-ph/9906203].
- [2] J. Ahrens *et al.* [IceCube Collaboration], *Nucl. Phys. Proc. Suppl.* **118**, 388 (2003) [arXiv:astro-ph/0209556].
- [3] J. Abraham *et al.* [Auger Collaboration], *Nucl. Instrum. Meth. A* **523**, 50 (2004).
- [4] S. Eidelman *et al.* [Particle Data Group], *Phys. Lett. B* **592**, 1 (2004).
- [5] M. C. Gonzalez-Garcia, F. Halzen and M. Maltoni, *Phys. Rev. D* **71**, 093010 (2005) [arXiv:hep-ph/0502223].
- [6] J. Ahrens *et al.* [IceCube Collaboration], *Astropart. Phys.* **20**, 507 (2004) [arXiv:astro-ph/0305196].
- [7] J. Ahrens *et al.* [The AMANDA Collaboration], *Nucl. Phys. Proc. Suppl.* **143**, 343 (2005) [arXiv:astro-ph/0409423].
- [8] M. Ackermann [AMANDA Collaboration], *Astropart. Phys.* **22**, 127 (2004) [arXiv:astro-ph/0405218].
- [9] L. A. Anchordoqui, H. Goldberg, M. C. Gonzalez-Garcia, F. Halzen, D. Hooper, S. Sarkar and T. J. Weiler, *Phys. Rev. D* **72**, 065019 (2005) [arXiv:hep-ph/0506168].
- [10] F. Halzen and A. D. Martin, “Quarks And Leptons: An Introductory Course In Modern Particle Physics,” (John Wiley & Sons, New York, 1984).
- [11] F. Becattini and S. Bottai, *Astropart. Phys.* **15**, 323 (2001) [arXiv:astro-ph/0003179].
- [12] See e.g., T. K. Gaisser, F. Halzen and T. Stanev, *Phys. Rept.* **258**, 173 (1995) [Erratum-*ibid.* **271**, 355 (1996)] [arXiv:hep-ph/9410384]; J. G. Learned and K. Mannheim, *Ann. Rev. Nucl. Part. Sci.* **50**, 679 (2000); F. Halzen and D. Hooper, *Rept. Prog. Phys.* **65**, 1025 (2002) [arXiv:astro-ph/0204527].
- [13] T. K. Gaisser and M. Honda, *Ann. Rev. Nucl. Part. Sci.* **52**, 153 (2002) [arXiv:hep-ph/0203272].
- [14] P. Lipari, *Astropart. Phys.* **1**, 195 (1993).
- [15] M. Ribordy *et al.* [IceCube Collaboration], arXiv:astro-ph/0509322.
- [16] K. Daum [Frejus Collaboration.], *Z. Phys. C* **66**, 417 (1995).
- [17] L. V. Volkova, *Sov. J. Nucl. Phys.* **31**, 784 (1980) [*Yad. Fiz.* **31** (1980) 1510].
- [18] E. Zas, F. Halzen and R. A. Vazquez, *Astropart. Phys.* **1**, 297 (1993); P. Gondolo, G. Ingelman and M. Thunman, *Astropart. Phys.* **5**, 309 (1996) [arXiv:hep-ph/9505417].
- [19] J. F. Beacom and J. Candia, *JCAP* **0411**, 009 (2004) [arXiv:hep-ph/0409046].
- [20] M. Honda, T. Kajita, K. Kasahara and S. Midorikawa, *Phys. Rev. D* **70**, 043008 (2004) [arXiv:astro-ph/0404457].
- [21] E. V. Bugaev, A. Misaki, V. A. Naumov, T. S. Sinegovskaya, S. I. Sinegovsky and N. Taka-

hashi, Phys. Rev. D **58**, 054001 (1998) [arXiv:hep-ph/9803488].

[22] V. S. Berezinsky and G. T. Zatsepin, Phys. Lett. B **28** 423 (1969); V. S. Berezinsky and A. Y. Smirnov, Phys. Lett. B **48**, 269 (1974); F. W. Stecker, Astrophys. J. **228** (1979) 919.

[23] K. Greisen, Phys. Rev. Lett. **16**, 748 (1966); G. T. Zatsepin and V. A. Kuzmin, JETP Lett. **4**, 78 (1966) [Pisma Zh. Eksp. Teor. Fiz. **4**, 114 (1966)].

[24] S. Yoshida and M. Teshima, Prog. Theor. Phys. **89**, 833 (1993); R. J. Protheroe and P. A. Johnson, Astropart. Phys. **4** (1996) 253.

[25] R. Engel, D. Seckel and T. Stanev, Phys. Rev. D **64**, 093010 (2001).

[26] C. T. Hill and D. N. Schramm, Phys. Rev. D **31**, 564 (1985).

[27] Z. Fodor, S. D. Katz, A. Ringwald and H. Tu, JCAP **0311**, 015 (2003).

[28] D. Hooper, A. Taylor and S. Sarkar, Astropart. Phys. **23**, 11 (2005); M. Ave, N. Busca, A. V. Olinto, A. A. Watson and T. Yamamoto, Astropart. Phys. **23**, 19 (2005).

[29] E. Waxman and J. N. Bahcall, Phys. Rev. D **59**, 023002 (1999) [arXiv:hep-ph/9807282].

[30] E. Waxman, Astrophys. J. **452**, L1 (1995).

[31] T. K. Gaisser, arXiv:astro-ph/9707283.

[32] M. Ahlers, L. A. Anchordoqui, H. Goldberg, F. Halzen, A. Ringwald and T. J. Weiler, Phys. Rev. D **72**, 023001 (2005).

[33] J. Ahrens *et al.* [AMANDA Collaboration], Nucl. Phys. Proc. Suppl. **138**, 167 (2005).

[34] J. Ahrens *et al.*, Phys. Rev. Lett. **90**, 251101 (2003) [arXiv:astro-ph/0303218].

[35] F. W. Stecker, C. Done, M. H. Salamon and P. Sommers, Phys. Rev. Lett. **66**, 2697 (1991) [Erratum-ibid. **69**, 2738 (1992)]; F. W. Stecker, arXiv:astro-ph/0510537; O. E. Kalashev, V. A. Kuzmin, D. V. Semikoz and G. Sigl, Phys. Rev. D **66**, 063004 (2002) [arXiv:hep-ph/0205050]; A. Neronov, D. Semikoz, F. Aharonian and O. Kalashev, Phys. Rev. Lett. **89**, 051101 (2002) [arXiv:astro-ph/0201410].

[36] M. Ackermann *et al.*, Astropart. Phys. **22**, 339 (2005).

[37] K. Mannheim, R. J. Protheroe and J. P. Rachen, Phys. Rev. D **63**, 023003 (2001) [arXiv:astro-ph/9812398].

[38] P. Sreekumar *et al.*, Astrophys. J. **494**, 523 (1998) [arXiv:astro-ph/9709257].

[39] A. W. Strong, I. V. Moskalenko and O. Reimer, arXiv:astro-ph/0306345; U. Keshet, E. Waxman and A. Loeb, JCAP **0404**, 006 (2004) [arXiv:astro-ph/0306442].

[40] L. Anchordoqui, H. Goldberg and C. Nunez, Phys. Rev. D **71**, 065014 (2005) [arXiv:hep-ph/0408284].

[41] Y. Fukuda *et al.* [Super-Kamiokande Collaboration], Phys. Rev. Lett. **81**, 1158 (1998) [Erratum-ibid. **81**, 4279 (1998)] [arXiv:hep-ex/9805021]. Y. Fukuda *et al.* [Super-Kamiokande Collaboration], Phys. Rev. Lett. **82**, 1810 (1999) [arXiv:hep-ex/9812009]. Y. Fukuda *et al.* [Super-Kamiokande Collaboration], Phys. Rev. Lett. **82**, 2430 (1999) [arXiv:hep-ex/9812011]; S. Fukuda *et al.* [Super-Kamiokande Collaboration], Phys. Rev. Lett. **86**, 5651 (2001) [arXiv:hep-ex/0103032]. S. Fukuda *et al.* [Super-Kamiokande Collaboration], Phys. Rev. Lett. **86**, 5656 (2001) [arXiv:hep-ex/0103033]; S. Fukuda *et al.* [Super-Kamiokande Collaboration], Phys. Lett. B **539**, 179 (2002) [arXiv:hep-ex/0205075].

[42] K. Hirata *et al.* [KAMIOKANDE-II Collaboration], Phys. Rev. Lett. **58**, 1490 (1987); R. M. Bionta *et al.*, Phys. Rev. Lett. **58**, 1494 (1987).

[43] L. A. Anchordoqui, H. Goldberg, F. Halzen and T. J. Weiler, Phys. Lett. B **621**, 18 (2005) [arXiv:hep-ph/0410003].

[44] J. Alvarez-Muniz and F. Halzen, Astrophys. J. **576**, L33 (2002) [arXiv:astro-ph/0205408]; L. A. Anchordoqui, H. Goldberg, F. Halzen and T. J. Weiler, Phys. Lett. B **600**, 202

(2004) [arXiv:astro-ph/0404387]; L. O'C. Drury, F. A. Aharonian, H. J. Voelk, *Astron. Astrophys.* **287**, 959 (1994); L. A. Anchordoqui, *Acta Phys. Polon. B* **36**, 495 (2005) [arXiv:astro-ph/0410087].

[45] F. A. Aharonian *et al.* [HEGRA Collaboration], *Astrophys. J.* **539**, 317 (2000) [arXiv:astro-ph/0003182].

[46] F. A. Aharonian *et al.* [HESS Collaboration], *Nature* **432** (2004) 75 [arXiv:astro-ph/0411533].

[47] F. Aharonian *et al.* [HESS Collaboration], arXiv:astro-ph/0505380.

[48] F. Aharonian *et al.* [HEGRA Collaboration], arXiv:astro-ph/0401301.

[49] F. A. Aharonian, L. A. Anchordoqui, D. Khangulyan and T. Montaruli, arXiv:astro-ph/0508658.

[50] D. J. Bird *et al.* [Fly's Eye Collaboration], *Astrophys. J.* **511**, 739 (1999) [arXiv:astro-ph/9806096]; N. Hayashida *et al.* [AGASA Collaboration], *Astropart. Phys.* **10**, 303 (1999) [arXiv:astro-ph/9807045].

[51] M. Teshima *et al.*, Proc. 27th International Cosmic Ray Conference, (Copernicus Gesellschaft, 2001) p.341; G. L. Cassiday *et al.*, *Phys. Rev. Lett.* **62**, 383 (1989); M. Teshima *et al.*, *Phys. Rev. Lett.* **64**, 1628 (1990).

[52] F. A. Aharonian *et al.* [HEGRA Collaboration], *Astron. Astrophys.* **393**, L37 (2002) [arXiv:astro-ph/0207528]; F. Aharonian *et al.* [HEGRA Collaboration], arXiv:astro-ph/0501667.

[53] Y. Butt *et al.*, *Astrophys. J.* **597**, 494 (2003) [arXiv:astro-ph/0302342].

[54] J. Knodlseder, astro-ph/0007442.

[55] M. Nagano *et al.*, *J. Phys. G* **18**, 423 (1992).

[56] L. A. Anchordoqui, H. Goldberg, F. Halzen and T. J. Weiler, *Phys. Lett. B* **593**, 42 (2004) [arXiv:astro-ph/0311002].

[57] J. Ahrens [AMANDA Collaboration], *Phys. Rev. Lett.* **92**, 071102 (2004) [arXiv:astro-ph/0309585].

[58] S. Weinberg, *Eur. Phys. J. C* **34**, 5 (2004) [arXiv:hep-ph/0401010].

[59] E. Fermi, *Z. Phys.* **88**, 161 (1934); E. Fermi, *Nuovo Cim.* **11**, 1 (1934).

[60] See e.g., J. A. Casas, J. R. Espinosa and I. Hidalgo, *JHEP* **0411**, 057 (2004) [arXiv:hep-ph/0410298].

[61] A. Kusenko and T. J. Weiler, *Phys. Rev. Lett.* **88**, 161101 (2002) [arXiv:hep-ph/0106071].

[62] L. A. Anchordoqui, J. L. Feng, H. Goldberg and A. D. Shapere, *Phys. Rev. D* **65**, 124027 (2002) [hep-ph/0112247].

[63] L. A. Anchordoqui, J. L. Feng and H. Goldberg, *Phys. Rev. Lett.* (to be published) [arXiv:hep-ph/0504228].

[64] H. Abramowicz and A. Caldwell, *Rev. Mod. Phys.* **71**, 1275 (1999) [arXiv:hep-ex/9903037].

[65] R. Gandhi, C. Quigg, M. H. Reno and I. Sarcevic, *Phys. Rev. D* **58**, 093009 (1998) [arXiv:hep-ph/9807264].

[66] H. L. Lai *et al.*, *Phys. Rev. D* **55**, 1280 (1997) [arXiv:hep-ph/9606399].

[67] L. V. Gribov, E. M. Levin and M. G. Ryskin, *Phys. Rept.* **100**, 1 (1983); A. H. Mueller and J. w. Qiu, *Nucl. Phys. B* **268**, 427 (1986).

[68] K. Kutak and J. Kwiecinski, *Eur. Phys. J. C* **29**, 521 (2003) [arXiv:hep-ph/0303209].

[69] J. Kwiecinski and A. D. Martin, *Phys. Rev. D* **43**, 1560 (1991).

[70] N. Arkani-Hamed, S. Dimopoulos and G. R. Dvali, *Phys. Lett. B* **429**, 263 (1998) [arXiv:hep-ph/9803315]; I. Antoniadis, N. Arkani-Hamed, S. Dimopoulos and G. R. Dvali, *Phys. Lett. B* **436**, 257 (1998) [arXiv:hep-ph/9804398]; L. Randall and R. Sundrum, *Phys.*

Rev. Lett. **83**, 3370 (1999) [arXiv:hep-ph/9905221].

[71] S. Nussinov and R. Shrock, Phys. Rev. D **59**, 105002 (1999) [hep-ph/9811323]; P. Jain, D. W. McKay, S. Panda and J. P. Ralston, Phys. Lett. B **484**, 267 (2000) [hep-ph/0001031]. The sensitivity of IceCube has been estimated by, J. Alvarez-Muniz, F. Halzen, T. Han and D. Hooper, Phys. Rev. Lett. **88**, 021301 (2002) [hep-ph/0107057]; J. I. Illana, M. Masip and D. Meloni, Phys. Rev. D **72**, 024003 (2005) [arXiv:hep-ph/0504234].

[72] J. L. Feng and A. D. Shapere, Phys. Rev. Lett. **88**, 021303 (2002) [arXiv:hep-ph/0109106]; L. Anchordoqui and H. Goldberg, Phys. Rev. D **65**, 047502 (2002) [arXiv:hep-ph/0109242]. The sensitivity of IceCube has been estimated by M. Kowalski, A. Ringwald and H. Tu, Phys. Lett. B **529**, 1 (2002) [hep-ph/0201139]; J. Alvarez-Muniz, J. L. Feng, F. Halzen, T. Han and D. Hooper, Phys. Rev. D **65**, 124015 (2002) [hep-ph/0202081].

[73] G. Domokos and S. Kovesi-Domokos, Phys. Rev. Lett. **82**, 1366 (1999) [hep-ph/9812260]; F. Cornet, J. I. Illana and M. Masip, Phys. Rev. Lett. **86**, 4235 (2001) [hep-ph/0102065]. The sensitivity of IceCube has been estimated by J. J. Friess, T. Han and D. Hooper, Phys. Lett. B **547**, 31 (2002) [hep-ph/0204112].

[74] Z. Fodor, S. D. Katz, A. Ringwald and H. Tu, Phys. Lett. B **561**, 191 (2003) [arXiv:hep-ph/0303080]. The sensitivity of IceCube has been estimated by T. Han and D. Hooper, Phys. Lett. B **582**, 21 (2004) [arXiv:hep-ph/0307120];

[75] M. Carena, D. Choudhury, S. Lola and C. Quigg, Phys. Rev. D **58**, 095003 (1998) [arXiv:hep-ph/9804380]; I. Albuquerque, G. Burdman and Z. Chacko, Phys. Rev. Lett. **92**, 221802 (2004) [arXiv:hep-ph/0312197].

[76] F. Halzen and D. Saltzberg, Phys. Rev. Lett. **81**, 4305 (1998) [arXiv:hep-ph/9804354]; X. Bertou, P. Billoir, O. Deligny, C. Lachaud and A. Letessier-Selvon, Astropart. Phys. **17**, 183 (2002) [arXiv:astro-ph/0104452]; J. L. Feng, P. Fisher, F. Wilczek and T. M. Yu, Phys. Rev. Lett. **88**, 161102 (2002) [arXiv:hep-ph/0105067]; J. J. Tseng, T. W. Yeh, H. Athar, M. A. Huang, F. F. Lee and G. L. Lin, Phys. Rev. D **68**, 063003 (2003) [arXiv:astro-ph/0305507]; J. Jones, I. Mocioiu, M. H. Reno and I. Sarcevic, Phys. Rev. D **69**, 033004 (2004) [arXiv:hep-ph/0308042].

[77] S. I. Dutta, Y. Huang and M. H. Reno, Phys. Rev. D **72**, 013005 (2005) [arXiv:hep-ph/0504208].

[78] S. Baker and R. D. Cousins, Nucl. Instrum. Meth. A **221**, 437 (1984).

[79] R. Gandhi, C. Quigg, M. H. Reno and I. Sarcevic, arXiv:hep-ph/9510295.

[80] M. C. Gonzalez-Garcia, arXiv:hep-ph/0410030.

[81] Y. Fukuda *et al.* [Super-Kamiokande Collaboration], Phys. Lett. B **433**, 9 (1998) [arXiv:hep-ex/9803006]; Y. Fukuda *et al.* [Super-Kamiokande Collaboration], Phys. Lett. B **436**, 33 (1998) [arXiv:hep-ex/9805006]; Y. Fukuda *et al.* [Super-Kamiokande Collaboration], Phys. Rev. Lett. **81**, 1562 (1998) [arXiv:hep-ex/9807003]; Y. Fukuda *et al.* [Super-Kamiokande Collaboration], Phys. Lett. B **467**, 185 (1999) [arXiv:hep-ex/9908049]; Y. Fukuda *et al.* [Super-Kamiokande Collaboration], Phys. Rev. Lett. **82**, 2644 (1999) [arXiv:hep-ex/9812014]; S. Fukuda *et al.* [Super-Kamiokande Collaboration], Phys. Rev. Lett. **85**, 3999 (2000) [arXiv:hep-ex/0009001]; Y. Ashie *et al.* [Super-Kamiokande Collaboration], Phys. Rev. D **71**, 112005 (2005) [arXiv:hep-ex/0501064].

[82] S. H. Ahn *et al.* [K2K Collaboration], Phys. Lett. B **511**, 178 (2001) [arXiv:hep-ex/0103001]; M. H. Ahn *et al.* [K2K Collaboration], Phys. Rev. Lett. **90**, 041801 (2003) [arXiv:hep-ex/0212007]; M. H. Ahn *et al.* [K2K Collaboration], Phys. Rev. Lett. **93**, 051801 (2004) [arXiv:hep-ex/0402017].

[83] M. Apollonio *et al.* [CHOOZ Collaboration], *Phys. Lett. B* **466**, 415 (1999) [arXiv:hep-ex/9907037]; S. M. Bilenky, D. Nicolo and S. T. Petcov, *Phys. Lett. B* **538**, 77 (2002) [arXiv:hep-ph/0112216].

[84] S. N. Ahmed *et al.* [SNO Collaboration], *Phys. Rev. Lett.* **92**, 181301 (2004) [arXiv:nucl-ex/0309004].

[85] T. Araki *et al.* [KamLAND Collaboration], *Phys. Rev. Lett.* **94**, 081801 (2005) [arXiv:hep-ex/0406035].

[86] J. N. Bahcall, M. C. Gonzalez-Garcia and C. Pena-Garay, *JHEP* **0408**, 016 (2004) [arXiv:hep-ph/0406294].

[87] M. C. Gonzalez-Garcia and Y. Nir, *Rev. Mod. Phys.* **75**, 345 (2003) [arXiv:hep-ph/0202058].

[88] M. Gasperini, *Phys. Rev. D* **38**, 2635 (1988).

[89] M. J. Longo, *Phys. Rev. Lett.* **60**, 173 (1988). L. M. Krauss and S. Tremaine, *Phys. Rev. Lett.* **60**, 176 (1988).

[90] J. M. LoSecco, *Phys. Rev. D* **39**, 1013 (1989).

[91] S. R. Coleman and S. L. Glashow, *Phys. Lett. B* **405**, 249 (1997) [arXiv:hep-ph/9703240]; S. L. Glashow, A. Halprin, P. I. Krastev, C. N. Leung and J. T. Pantaleone, *Phys. Rev. D* **56**, 2433 (1997) [arXiv:hep-ph/9703454]; S. R. Coleman and S. L. Glashow, *Phys. Rev. D* **59**, 116008 (1999) [arXiv:hep-ph/9812418].

[92] V. De Sabbata and M. Gasperini, *Nuovo Cim. A* **65**, 479 (1981).

[93] D. Colladay and V. A. Kostelecky, *Phys. Rev. D* **55**, 6760 (1997) [arXiv:hep-ph/9703464]; V. D. Barger, S. Pakvasa, T. J. Weiler and K. Whisnant, *Phys. Rev. Lett.* **85**, 5055 (2000) [arXiv:hep-ph/0005197].

[94] M. Gasperini, *Phys. Rev. D* **39**, 3606 (1989).

[95] M. C. Gonzalez-Garcia and M. Maltoni, *Phys. Rev. D* **70**, 033010 (2004) [arXiv:hep-ph/0404085].

[96] T. K. Gaisser, “Cosmic Rays and Particle Physics,” (Cambridge University Press, 1990).

[97] J. A. Wheeler, *Annals Phys.* **2**, 604 (1957); S. W. Hawking, *Nucl. Phys. B* **144**, 349 (1978).

[98] S. W. Hawking, *Phys. Rev. D* **53**, 3099 (1996) [arXiv:hep-th/9510029].

[99] S. W. Hawking, *Phys. Rev. D* **14** (1976) 2460. S. W. Hawking, *Commun. Math. Phys.* **87**, 395 (1982).

[100] See however, S. W. Hawking, arXiv:hep-th/0507171.

[101] F. C. Adams, G. L. Kane, M. Mbonye and M. J. Perry, *Int. J. Mod. Phys. A* **16**, 2399 (2001) [arXiv:hep-ph/0009154].

[102] M. Shiozawa *et al.* [Super-Kamiokande Collaboration], *Phys. Rev. Lett.* **81**, 3319 (1998) [arXiv:hep-ex/9806014]; Y. Hayato *et al.* [Super-Kamiokande Collaboration], *Phys. Rev. Lett.* **83**, 1529 (1999) [arXiv:hep-ex/9904020].

[103] N. Arkani-Hamed and M. Schmaltz, *Phys. Rev. D* **61**, 033005 (2000) [arXiv:hep-ph/9903417].

[104] G. Lindblad, *Commun. Math. Phys.* **48**, 119 (1976).

[105] F. Benatti and H. Narnhofer, *Lett. Math. Phys.* **15**, 325 (1988).

[106] T. Banks, L. Susskind and M. E. Peskin, *Nucl. Phys. B* **244**, 125 (1984). J. Liu, arXiv:hep-th/9301082.

[107] E. Lisi, A. Marrone and D. Montanino, *Phys. Rev. Lett.* **85**, 1166 (2000) [arXiv:hep-ph/0002053].

[108] F. Benatti and R. Floreanini, *JHEP* **0002**, 032 (2000) [arXiv:hep-ph/0002221].

[109] See Eq. (41) in, D. Hooper, D. Morgan and E. Winstanley, *Phys. Rev. D* **72**, 065009 (2005) [arXiv:hep-ph/0506091].

[110] J. R. Ellis, N. E. Mavromatos, D. V. Nanopoulos and E. Winstanley, *Mod. Phys. Lett. A* **12**, 243 (1997) [arXiv:gr-qc/9602011]; J. R. Ellis, N. E. Mavromatos and D. V. Nanopoulos, *Mod. Phys. Lett. A* **12**, 1759 (1997) [arXiv:hep-th/9704169].

[111] A. Romosan *et al.* [CCFR/NuTeV Collaboration], *Phys. Rev. Lett.* **78**, 2912 (1997) [arXiv:hep-ex/9611013].

[112] D. Naples *et al.* [CCFR/NuTeV Collaboration], *Phys. Rev. D* **59**, 031101 (1999) [arXiv:hep-ex/9809023].

[113] A. M. Gago, E. M. Santos, W. J. C. Teves and R. Zukanovich Funchal, *Phys. Rev. D* **63**, 073001 (2001) [arXiv:hep-ph/0009222].

[114] See e.g., L. M. Krauss and F. Wilczek, *Phys. Rev. Lett.* **62**, 1221 (1989).

[115] J. G. Learned and S. Pakvasa, *Astropart. Phys.* **3**, 267 (1995) [arXiv:hep-ph/9405296].

[116] D. Hooper, D. Morgan and E. Winstanley, *Phys. Lett. B* **609**, 206 (2005) [arXiv:hep-ph/0410094].

[117] A. M. Gago, E. M. Santos, W. J. C. Teves and R. Zukanovich Funchal, arXiv:hep-ph/0208166.

[118] K. Miknaitis [the SNO Collaboration], arXiv:hep-ex/0505071.

[119] J. Ahrens *et al.* [AMANDA Collaboration], *Phys. Rev. D* **67**, 012003 (2003) [arXiv:astro-ph/0206487].

[120] V. D. Barger, J. G. Learned, S. Pakvasa and T. J. Weiler, *Phys. Rev. Lett.* **82**, 2640 (1999) [arXiv:astro-ph/9810121].

[121] J. N. Bahcall, S. T. Petcov, S. Toshev and J. W. F. Valle, *Phys. Lett. B* **181**, 369 (1986); J. F. Beacom and N. F. Bell, *Phys. Rev. D* **65**, 113009 (2002) [arXiv:hep-ph/0204111].

[122] J. F. Beacom, N. F. Bell, D. Hooper, S. Pakvasa and T. J. Weiler, *Phys. Rev. Lett.* **90**, 181301 (2003) [arXiv:hep-ph/0211305].

[123] A. G. Riess *et al.* [Supernova Search Team Collaboration], *Astron. J.* **116**, 1009 (1998) [arXiv:astro-ph/9805201].

[124] S. Perlmutter *et al.* [Supernova Cosmology Project Collaboration], *Astrophys. J.* **517**, 565 (1999) [arXiv:astro-ph/9812133].

[125] D. N. Spergel *et al.* [WMAP Collaboration], *Astrophys. J. Suppl.* **148**, 175 (2003) [arXiv:astro-ph/0302209].

[126] M. Colless *et al.*, arXiv:astro-ph/0306581.

[127] M. Tegmark *et al.* [SDSS Collaboration], *Astrophys. J.* **606**, 702 (2004) [arXiv:astro-ph/0310725].

[128] M. Tegmark *et al.* [SDSS Collaboration], *Phys. Rev. D* **69**, 103501 (2004) [arXiv:astro-ph/0310723].

[129] S. Burles, K. M. Nollett and M. S. Turner, *Astrophys. J.* **552**, L1 (2001) [arXiv:astro-ph/0010171]; R. H. Cyburt, B. D. Fields and K. A. Olive, *Phys. Lett. B* **567**, 227 (2003) [arXiv:astro-ph/0302431].

[130] S. Hannestad, arXiv:astro-ph/0505551.

[131] See e.g., L. Bergstrom, *Rept. Prog. Phys.* **63**, 793 (2000) [arXiv:hep-ph/0002126]; G. Bertone, D. Hooper and J. Silk, *Phys. Rept.* **405**, 279 (2005) [arXiv:hep-ph/0404175]; J. L. Feng, arXiv:astro-ph/0511043.

[132] M. W. Goodman and E. Witten, *Phys. Rev. D* **31**, 3059 (1985).

[133] J. Silk, K. A. Olive and M. Srednicki, *Phys. Rev. Lett.* **55**, 257 (1985); M. Srednicki, K. A. Olive and J. Silk, *Nucl. Phys. B* **279**, 804 (1987); K. W. Ng, K. A. Olive and M. Srednicki, *Phys. Lett. B* **188**, 138 (1987); L. Bergstrom, J. Edsjo and P. Gondolo, *Phys. Rev. D* **58**, 103519 (1998) [arXiv:hep-ph/9806293]; J. L. Feng, K. T. Matchev and F. Wilczek, *Phys.*

Rev. D **63**, 045024 (2001) [arXiv:astro-ph/0008115]; V. D. Barger, F. Halzen, D. Hooper and C. Kao, Phys. Rev. D **65**, 075022 (2002) [arXiv:hep-ph/0105182].

[134] G. Jungman, M. Kamionkowski and K. Griest, Phys. Rept. **267**, 195 (1996) [arXiv:hep-ph/9506380].

[135] K. Griest and D. Seckel, Nucl. Phys. B **283**, 681 (1987) [Erratum-ibid. B **296**, 1034 (1988)]. A. Gould, Astrophys. J. **321**, 560 (1987).

[136] D. S. Akerib *et al.* [CDMS Collaboration], arXiv:astro-ph/0509259.

[137] D. S. Akerib *et al.* [CDMS Collaboration], arXiv:astro-ph/0509269.

[138] G. J. Alner *et al.* [UK Dark Matter Collaboration], Astropart. Phys. **23** (2005) 444.

[139] V. Sanglard *et al.* [The EDELWEISS Collaboration], Phys. Rev. D **71**, 122002 (2005) [arXiv:astro-ph/0503265].

[140] G. J. Alner *et al.* [UK Dark Matter Collaboration], Phys. Lett. B **616**, 17 (2005) [arXiv:hep-ex/0504031].

[141] M. Barnabe-Heider *et al.* [PICASSO Collaboration], arXiv:hep-ex/0502028.

[142] M. Kamionkowski, K. Griest, G. Jungman and B. Sadoulet, Phys. Rev. Lett. **74**, 5174 (1995) [arXiv:hep-ph/9412213].

[143] S. Desai *et al.* [Super-Kamiokande Collaboration], Phys. Rev. D **70**, 083523 (2004) [Erratum-ibid. D **70**, 109901 (2004)] [arXiv:hep-ex/0404025].

[144] M. Ackermann *et al.* [AMANDA Collaboration], arXiv:astro-ph/0508518.

[145] M. Ambrosio *et al.* [MACRO Collaboration], Phys. Rev. D **60**, 082002 (1999) [arXiv:hep-ex/9812020].

[146] S. Dimopoulos and H. Georgi, Nucl. Phys. B **193**, 150 (1981).

[147] S. Dimopoulos, S. Raby and F. Wilczek, Phys. Rev. D **24**, 1681 (1981).

[148] H. Goldberg, Phys. Rev. Lett. **50**, 1419 (1983); J. R. Ellis, J. S. Hagelin, D. V. Nanopoulos, K. A. Olive and M. Srednicki, Nucl. Phys. B **238**, 453 (1984).

[149] R. J. Scherrer and M. S. Turner, Phys. Rev. D **33**, 1585 (1986) [Erratum-ibid. D **34**, 3263 (1986)].

[150] K. Griest, M. Kamionkowski and M. S. Turner, Phys. Rev. D **41**, 3565 (1990); M. Drees and M. M. Nojiri, Phys. Rev. D **47**, 376 (1993) [arXiv:hep-ph/9207234]; A. Birkedal-Hansen and E. h. Jeong, JHEP **0302**, 047 (2003) [arXiv:hep-ph/0210041].

[151] G. Servant and T. M. P. Tait, Nucl. Phys. B **650**, 391 (2003) [arXiv:hep-ph/0206071]; H. C. Cheng, J. L. Feng and K. T. Matchev, Phys. Rev. Lett. **89**, 211301 (2002) [arXiv:hep-ph/0207125].

[152] G. Jungman and M. Kamionkowski, Phys. Rev. D **51**, 328 (1995) [arXiv:hep-ph/9407351].

[153] P. Crotty, Phys. Rev. D **66**, 063504 (2002) [arXiv:hep-ph/0205116].

[154] F. Halzen and D. Hooper, arXiv:hep-ph/0510048.

[155] P. Gondolo, J. Edsjo, L. Bergstrom, P. Ullio and E. A. Baltz, arXiv:astro-ph/0012234; P. Gondolo, J. Edsjo, P. Ullio, L. Bergstrom, M. Schelke and E. A. Baltz, JCAP **0407**, 008 (2004) [arXiv:astro-ph/0406204].

[156] J. R. Ellis, K. A. Olive, Y. Santoso and V. C. Spanos, Phys. Lett. B **565**, 176 (2003) [arXiv:hep-ph/0303043]; A. B. Lahanas and D. V. Nanopoulos, Phys. Lett. B **568**, 55 (2003) [arXiv:hep-ph/0303130]; U. Chattopadhyay, A. Corsetti and P. Nath, Phys. Rev. D **68**, 035005 (2003) [arXiv:hep-ph/0303201].

[157] See *e.g.*, L. Anchordoqui, T. Paul, S. Reucroft and J. Swain, Int. J. Mod. Phys. A **18**, 2229 (2003) [arXiv:hep-ph/0206072].

[158] M. Takeda *et al.*, Phys. Rev. Lett. **81**, 1163 (1998) [arXiv:astro-ph/9807193]; M. Takeda *et*

al., Astropart. Phys. **19**, 447 (2003) [arXiv:astro-ph/0209422].

[159] T. Abu-Zayyad *et al.* [HiRes Collaboration], arXiv:astro-ph/0208301.

[160] L. A. Anchordoqui, M. T. Dova, L. N. Epele and S. J. Sciutto, Phys. Rev. D **59**, 094003 (1999) [arXiv:hep-ph/9810384].

[161] N. Hayashida *et al.* [AGASA Collaboration], Phys. Rev. Lett. **77**, 1000 (1996); N. Hayashida *et. al.* [AGASA Collaboration], arXiv:astro-ph/0008102.

[162] R. U. Abbasi *et al.* [HiRes Collaboration], arXiv:astro-ph/0404137; R. U. Abbasi *et al.* [HiRes Collaboration], arXiv:astro-ph/0404366. R. U. Abbasi *et al.* [HiRes Collaboration], arXiv:astro-ph/0412617.

[163] C. B. Finley and S. Westerhoff, Astropart. Phys. **21**, 359 (2004) [arXiv:astro-ph/0309159].

[164] D. R. Bergman [HiRes Collaboration], arXiv:astro-ph/0407244.

[165] D. J. Bird *et al.* [Fly's Eye Collaboration], Phys. Rev. Lett. **71** (1993) 3401.

[166] P. Sommers *et al.* [Auger Collaboration], arXiv:astro-ph/0507150; M. Risse *et al* [Auger Collaboration], arXiv:astro-ph/0507402; A. Letessier-Selvon *et al.* [Auger Collaboration], arXiv:astro-ph/0507331; B. Revenu *et al.* [Auger Collaboration], arXiv:astro-ph/0507600.

[167] See e.g., D. F. Torres and L. A. Anchordoqui, Rept. Prog. Phys. **67**, 1663 (2004) [arXiv:astro-ph/0402371].

[168] See e.g., P. Bhattacharjee and G. Sigl, Phys. Rept. **327**, 109 (2000) [arXiv:astro-ph/9811011].

[169] T. W. Kibble, J. Phys. A **9**, 1387 (1976); A. Vilenkin, Phys. Rept. **121**, 263 (1985); M. B. Hindmarsh and T. W. Kibble, Rept. Prog. Phys. **58**, 477 (1995) [arXiv:hep-ph/9411342].

[170] C. T. Hill, Nucl. Phys. B **224**, 469 (1983); P. Bhattacharjee and G. Sigl, Phys. Rev. D **51**, 4079 (1995) [arXiv:astro-ph/9412053].

[171] P. Bhattacharjee, Phys. Rev. D **40**, 3968 (1989); P. Bhattacharjee and N. C. Rana, Phys. Lett. B **246**, 365 (1990).

[172] C. T. Hill, D. N. Schramm and T. P. Walker, Phys. Rev. D **36**, 1007 (1987).

[173] V. Berezinsky and A. Vilenkin, Phys. Rev. Lett. **79**, 5202 (1997) [arXiv:astro-ph/9704257].

[174] M. Hindmarsh and T. W. Kibble, Phys. Rev. Lett. **55**, 2398 (1985).

[175] M. Birkel and S. Sarkar, Astropart. Phys. **9**, 297 (1998) [arXiv:hep-ph/9804285]; V. Berezinsky, M. Kachelriess and A. Vilenkin, Phys. Rev. Lett. **79**, 4302 (1997) [arXiv:astro-ph/9708217]; V. A. Kuzmin and V. A. Rubakov, Phys. Atom. Nucl. **61**, 1028 (1998) [Yad. Fiz. **61**, 1122 (1998)] [arXiv:astro-ph/9709187]; V. Kuzmin and I. Tkachev, JETP Lett. **68**, 271 (1998) [arXiv:hep-ph/9802304]; Z. Fodor and S. D. Katz, Phys. Rev. Lett. **86**, 3224 (2001) [arXiv:hep-ph/0008204].

[176] K. Hamaguchi, Y. Nomura and T. Yanagida, Phys. Rev. D **58**, 103503 (1998) [arXiv:hep-ph/9805346]; K. Hamaguchi, Y. Nomura and T. Yanagida, Phys. Rev. D **59**, 063507 (1999) [arXiv:hep-ph/9809426]; K. Hamaguchi, K. I. Izawa, Y. Nomura and T. Yanagida, Phys. Rev. D **60**, 125009 (1999) [arXiv:hep-ph/9903207].

[177] J. R. Ellis, J. L. Lopez and D. V. Nanopoulos, Phys. Lett. B **247**, 257 (1990); K. Benakli, J. R. Ellis and D. V. Nanopoulos, Phys. Rev. D **59**, 047301 (1999) [arXiv:hep-ph/9803333].

[178] P. Blasi, R. Dick and E. W. Kolb, Astropart. Phys. **18**, 57 (2002) [arXiv:astro-ph/0105232].

[179] S. Sarkar and R. Toldra, Nucl. Phys. B **621**, 495 (2002) [arXiv:hep-ph/0108098].

[180] S. L. Dubovsky and P. G. Tinyakov, JETP Lett. **68**, 107 (1998) [arXiv:hep-ph/9802382]; V. Berezinsky, P. Blasi and A. Vilenkin, Phys. Rev. D **58**, 103515 (1998) [arXiv:astro-ph/9803271]; V. Berezinsky and A. A. Mikhailov, Phys. Lett. B **449**, 237 (1999) [arXiv:astro-ph/9810277]; G. A. Medina-Tanco and A. A. Watson, Astropart. Phys. **12**, 25

(1999) [arXiv:astro-ph/9903182]; N. W. Evans, F. Ferrer and S. Sarkar, *Astropart. Phys.* **17**, 319 (2002) [arXiv:astro-ph/0103085].

[181] C. Coriano and A. E. Faraggi, *Phys. Rev. D* **65**, 075001 (2002) [arXiv:hep-ph/0106326]; C. Barbot and M. Drees, *Astropart. Phys.* **20**, 5 (2003) [arXiv:hep-ph/0211406].

[182] F. A. Aharonian, P. Bhattacharjee and D. N. Schramm, *Phys. Rev. D* **46**, 4188 (1992).

[183] P. Gondolo, G. Gelmini and S. Sarkar, *Nucl. Phys. B* **392**, 111 (1993) [arXiv:hep-ph/9209236].

[184] M. Ave, J. A. Hinton, R. A. Vazquez, A. A. Watson and E. Zas, *Phys. Rev. Lett.* **85**, 2244 (2000) [arXiv:astro-ph/0007386]; M. Risse *et al.*, arXiv:astro-ph/0502418.

[185] G. Sigl, S. Lee, P. Bhattacharjee and S. Yoshida, *Phys. Rev. D* **59**, 043504 (1999) [arXiv:hep-ph/9809242].

[186] G. Sigl, K. Jedamzik, D. N. Schramm and V. S. Berezinsky, *Phys. Rev. D* **52**, 6682 (1995) [arXiv:astro-ph/9503094]; G. Sigl, S. Lee, D. N. Schramm and P. Coppi, *Phys. Lett. B* **392**, 129 (1997) [arXiv:astro-ph/9610221].

[187] G. Sigl, S. Lee and P. Coppi, arXiv:astro-ph/9604093. R. J. Protheroe and T. Stanev, *Phys. Rev. Lett.* **77**, 3708 (1996) [Erratum-ibid. **78**, 3420 (1997)] [arXiv:astro-ph/9605036]; D. V. Semikoz and G. Sigl, *JCAP* **0404**, 003 (2004) [arXiv:hep-ph/0309328].

[188] L. Anchordoqui, H. Goldberg and P. Nath, *Phys. Rev. D* **70**, 025014 (2004) [arXiv:hep-ph/0403115].

[189] C. Barbot, M. Drees, F. Halzen and D. Hooper, *Phys. Lett. B* **555**, 22 (2003) [arXiv:hep-ph/0205230].

[190] C. Barbot, *Comput. Phys. Commun.* **157**, 63 (2004) [arXiv:hep-ph/0306303].

[191] T. W. Kephart and T. J. Weiler, *Astropart. Phys.* **4**, 271 (1996) [arXiv:astro-ph/9505134].

[192] P. A. M. Dirac, *Proc. Roy. Soc. Lond. A* **133**, 60 (1931).

[193] M. S. Turner, E. N. Parker and T. J. Bogdan, *Phys. Rev. D* **26**, 1296 (1982).

[194] A. H. Guth, *Phys. Rev. D* **23**, 347 (1981).

[195] P. Langacker and S. Y. Pi, *Phys. Rev. Lett.* **45**, 1 (1980); T. H. Farris, T. W. Kephart, T. J. Weiler and T. C. Yuan, *Phys. Rev. Lett.* **68**, 564 (1992); V. V. Dixit and M. Sher, *Phys. Rev. Lett.* **68**, 560 (1992).

[196] D. R. Tompkins, *Phys. Rev.* **138**, B248 (1965).

[197] See e.g., S. D. Wick, T. W. Kephart, T. J. Weiler and P. L. Biermann, *Astropart. Phys.* **18**, 663 (2003) [arXiv:astro-ph/0001233].

[198] V. Aynutdinov *et al.* [Baikal Collaboration], arXiv:astro-ph/0507713.

[199] P. Niessen *et al.* [AMANDA Collaboration], Proc. 27th International Cosmic Ray Conference, (Copernicus Gesellschaft, 2001) p.1496

[200] M. Ambrosio *et al.* [MACRO Collaboration], *Eur. Phys. J. C* **25**, 511 (2002) [arXiv:hep-ex/0207020].